# *Shewanella loihica PV-4* electroactive biofilms (EABs) grown in potentiostat-controlled electrochemical cells

**Monica Epifanio**, M.Sc.

Ph.D. Thesis

December, 2015

School of Biotechnology

Dublin City University

Under the supervision of Dr. Brendan O'Connor (DCU) and Dr. Enrico Marsili (NTU).

**DECLARATION**

I hereby certify that this material, which I now submit for assessment on the program of study leading to the award of Ph.D. is entirely my own work, that I have exercised reasonable care to ensure that the work is original, and does not to the best of my knowledge breach any law of copyright, and has not been taken from the work of others save and to the extent that such work has been cited and acknowledged within the text of my work.

ID No.: 11212059

Date: 7th December, 2015

Signed: 

**ACKNOWLEDGEMENTS**

I would like to extend my sincerest gratitude to the all the School of Biotechnology in Dublin City University and especially to the technician staff, in particular I would like to thank David Cunningham who has taught me how to use many machineries which I need for my experiments, and how to deal with students during the demonstration classes. I would also like to thank Allison Tipping who patiently helped me to manage many, many orders and to deal with suppliers at the beginning of my staying in DCU when my level English was still elementary. I would also like to thank the other member of the Microbial Bioelectrochemistry Group, my colleague Michael Kitching for his moral and technical support over the three years spent together in the laboratory, and all the students who I have supervised and who have helped me in many ways during my PhD, for this I would like to thank Fintan Diarmuide Burke, Caille Morgan, Felix Medina Manjon, Sarah Gapin and Lucinda Doyle. I would like to thank my external supervisor, Dr. Enrico Marsili, for his guidance in the field of electrochemistry and for his support during the writing of our last publication. Special thank goes also to my primary supervisor Dr. Brendan O' Connor and to Dr. Ciaran Fagan, for their patience in correcting my thesis and their moral support. I am also, extremely grateful to my current supervisor of the Marie Curie project Dr. Emanuele Barborini, who kindly allowed me to travel very often back to Dublin to finalize important experiments for my PhD, and also to all the Marie Curie project staff, Prof. Marc Bauman and Dr. Alexander Yavorskyy for sharing their knowledge with me and their sense of humor every day. I must also thank the secretaries of the School of Biotechnology, Deidre Donnelly and Hilary Coates who did not do just the administrative job for me but who were great support during the three years of PhD. As last but not the least, huge thanks go to my family who have supported me morally and economically in accomplishing my Bachelor and Master degree and to my sister too who shook me up when the fears of going abroad came to my mind. Very special thanks to Triona O'Connell who has shown me more the once to be more than a simple colleague to whom ask for scientific advices, but who has rather been a very good and supportive friend.

**GLOSSARY**

**ABBREVIATIONS**

**BES**= Bioelectrochemical system

**CF=** Carbon felt

**$CH_3$-ITO**= Trichloro(propyl)silane

**$CH_3$-ITO**= Trichloro(propyl)silane

**CNTs**= Carbon nanotubes

**DM**= Defined medium

**EAM=** Electroactive microorganism

**ECs**= Electrochemical cells

**EET** =Extracellular electron transfer

**LB**= Luria Bertani

**MECs=** Microbial electrolysis cells

**MFCs**= Microbial Fuel Cells

**NMP**= N-methyl-2-pyrrolidone

**P240=** Grit diameter 58.5 μm

**P400=** Grit diameter 35 μm

**P600=** Grit diameter 25.8 μm

**SH-ITO=** (3-mercaptopropyl) trimethoxysilane

## PUBLICATIONS

### Articles in refereed journals

**Monica Epifanio**, Saikumar Inguva , Michael Kitching , Jean-Paul Mosnier, Enrico Marsili (2015) Effects of atmospheric air plasma treatment of graphite and carbon felt electrodes on the anodic current from *Shewanella* attached cells. Bioelectrochemistry

Zhang Xiaoming, **Epifanio Monica,** Marsili Enrico (2013) Electrochemical characteristics of Shewanella loihica on carbon nanotubes-modified graphite surfaces. Electrochimica Acta 102, 252-258.

### Conference presentations

### Oral talks

- *Shewanella loihica PV-4* electroactive biofilms (EABs) grown in potentiostat-controlled electrochemical cells - Research day at **Dublin City University;** Dublin; Ireland (February 2013)

- *Shewanella loihica PV-4* electroactive biofilms (EABs) grown in potentiostat-controlled electrochemical cells **-** Biotechnology Industrial Research Society meeting at **University of Palermo;** Palermo; Italy (December 2013)

- Microbial Fuel Cells (MFCs) for primary wastewater treatment in Northern Ireland Water treatment plants - Questor meeting at **Queen's University Belfast;** Belfast; Northern Ireland (May 2014)

### Poster presentations

- Microbial Fuel Cells (MFCs) for primary wastewater treatment at Northern Ireland (NI) Water treatment plants - Questor meeting **Cranfield University,** Cranfield, England (May 2012)

- *Shewanella loihica PV-4* electroactive biofilms (EABs) grown in potentiostat-controlled electrochemical cells - Research day at **Dublin City University;** Dublin; Ireland (February 2013)

  Surface roughness and atmospheric plasma pre-treatment determine the anodic current of *Shewanella loihica* PV-4 – Society For Industrial Microbiology and Biotechnology annual meeting at Missouri, **St. Louis**; USA (July 2014)

**ABSTRACT**

*S.loihica PV-4* is a biofilm forming bacterium with an incredible respiratory versatility under anoxic conditions. It can indeed use various number of electron acceptors, such as heavy metals and solid substrates like an electrode surface., thus finding its application in diverse field like bioremediation and bio-energy production.

*S.loihica PV*-4 can form electro-active biofilms on solid electrodes, an dthe electron transfer between the electrode surface and the m.o. can occur through two main mechanism. One, called direct electron transfer (DET), involves a network of c-type cytochromes localized in the periplasm and outer membrane of *Shewanella* sp. The other, named mediated electron transfer (MET), involves the release of soluble redox-active electron shuttles that transfer electrons from cell-associated reductases to the electron acceptor.

Despite all members of the *Shewenella spp.* genus have the presence of c-type cytochromes, the number and the order of their genes varies, and this might affect their ability to reduce external insoluble substrates.

In this study, improved electron transfer rate characterization in *S. loihica PV-4* biofilms in potentiostat-controlled three-electrode cells was achieved. Different electrode materials were used, as well as chemical (carbon nanotube coating and atmospheric air plasma treatments) and physical (surface abrasion) treatment of the electrode, under various growth and inoculum conditions.

Results confirm that carbon nanotube surface-modified electrodes improve the electron transfer rate in thin biofilms (<5 μm), but are not feasible for power production in microbial fuel cells, where the biofilm thickness is much greater. Atmospheric air plasma treatment is a feasible option to increase power output in bioelectrochemical systems. However, the effects of plasma pre-treatment are mixed, and the interplay between DET and MET must be considered when designing optimal electrode pre-treatment.

# CHAPTER 1

# OVERVIEW OF ELECTRO-ACTIVE BIOFILMS AND ELECTROCHEMISTRY

## 1.1 Introduction

Scientists have recently realized that microbial life often exists in highly complex and interactive communities called biofilms. For many microorganisms, being part of a microbial biofilm is the default mode of life. In general, biofilms form in presence of mechanical and chemical stress, lack of nutrient, exposure to antibiotics, etc. (Flemming & Wingender, 2010).

Carpentier and Cerf were the first to use and define the word biofilm in 1993 (Carpentier *et al.*, 1993) describing it as a community of microbes embedded in an organic polymer matrix, adhering to a surface. Costerton *et al*. in 1999 adjusted the concept of polymeric matrix as something that bacteria self-produced and adheres to an inert or living surface (Costerton *et al*., 1999). Clearly, this is an oversimplification of a complex process that does not take into account the species of microorganism, the composition of the surface, or the influences of environmental factors. Virtually any kind of surface or live cell (e.g. animal or plant cells) can be colonized by biofilms.

Biofilms are essential for our environment and health, they are important component of food chain and ocean and freshwater ecosystems and for a large extended responsible of for the recycle of our resources. On the other hand however, biofilm might cause problems for the human society, for example by forming in water pipes a process called bio-fouling (Block *et al.,* 1993*)* or by harboring pathogenic microorganisms that facilitating the spread of chronic infection in humans (Parsek & Singh, 2003). We are now witnessing a serious breakthrough of understanding biofilms thanks to new technologies that allow us to understand the power of biofilms and their impact in our life. Indeed, if we learn how to predict and regulate the activity of biofilm we can improve the structure for maximum efficiency and optimize a beneficial system while controlling the harmful ones.

There could be so much possible outcomes from this biofilm revolution. For instance, rapid remediation of polluted environments, or the advantage of human health that will come from preventing pathogens to proliferate in our environment and spreading diseases in humans, or waste water treatment plans that generate energy rather than consuming it. There is then an urgent need to better understand the biological and ecological processes and the development of a new bio-engineering platform which can allow us to better manage the environment and efficiency utilize our limited natural resources. With this in mind it will be possible ensure secure water quality, sustain a healthy environment, and protect our natural resources.

The finding of electro-active biofilms (EABs) forming bacteria with the ability to oxidise organic compounds whilst exchanging electrons with external solid surfaces has opened a wide spectrum of possibilities to exploit bacterial metabolic capabilities, such electricity production biosensing, nanoparticles production, rapid remediation of polluted environments by controlling that external electron transfer and developing new interface between bacteria and solid surfaces (Landoulsi *et al*., 2008; Parot *et al*., 2011; Tian *et al*., 2007). Several genera and families have been investigated as EABs: like *Clostridium* (Park *et al*., 2001), *Aeromonas* (Pham *et al*., 2003), *Geobacter* (Lovley, 1991) and *Shewanella* (Nealson & Saffarini, 1994,). This research project will particularly focuses on the electrochemical characterization of an electroactive biofilm forming model bacterium called *S. loihica PV-4* by electrochemical techniques as chronoamperometry (CA), differential pulse voltammetry (DPV), cyclic voltammetry (CV) and electrochemical impedance spectroscopy.

### 1.2 *Shewanella sp.*

The first Shewanella was isolated in 1931 as one of several contaminating microorganisms responsible for butter putrefaction (Derby & Hammer, 1931). Members of the Shewanella genus are facultative anaerobes, Gramnegative, biofilm-forming soil gamma-proteobacteria, typically encountered in aquatic environments, though may also be found as part of intestinal microflora of some marine life (Satomi *et al*., 2003). Most Shewanella strains are psychrotolerant, and they are so capable to grow at low temperatures (< 5°C), but their temperature optimum is above 16°C. Shewanellae are the most diverse respiratory organisms described so far, indeed they grow in widely disparate environments and play key roles in elemental cycling, especially in environments with varied redox conditions. Members of the Shewanellaceae family have a unique respiratory versatility (Venkateswaran *et al*., 1999), as they are able to couple the oxidation of organic substrates or hydrogen to the reduction of a wide variety of insoluble external electron acceptors by Extracellular Electron Transfer (**EET**) as a part of their energy conservation strategy. Electron transfer is one of the most important chemical process in nature and it plays a central role in many biological, physical and chemical systems.

In the case of *S.loihica PV-4* the greatest energy yield can be gained with oxygen as terminal electron acceptor, but in its absence or limiting condition, like the anoxic zones of lakes or in sediments, or fecal pellets, Shewanella species can exploit a wide range of alternative electron

acceptors, including Fe(III) and Mn(IV) (Roden & Zachara, 1996, Myers & Nealson, 1988, D. Lovley, 2000). With respect to other well-known EAB-forming bacteria, such as *Geobacter sp*., *Shewanella sp*. have a more adaptable metabolism and versatility in living in extreme and varied environments. Yet, these organisms are easy to grow robustly in the lab and are amenable to genetic manipulation. Thus they are relevant to carbon cycling and have considerable potential for the remediation of contaminated environments and use in microbial fuel cells (Hau & Gralnick, 2007) where their metabolism is harnessed to make electricity (Logan & Regan, 2006). *Shewanella sp.* express numerous multi-heme cytochromes on the outer membrane (Xiong *et al*., 2006, Richardson, 2000), and also secrete flavins, extracellular redox mediators which are involved in the electron transfer (Marsili *et al.*, 2008).

Electrons require a discrete patway to traverse distance > 0.01 μm, in addition bacteria such Shewanella demonstrate an ability to transfer electrons to metal located > 50 μm from cell surfaces. According to the **Marcus theory**, the probability that an electron will be transfered from an electron donor to an electron acceptor during a transition state decreases by increasing the distance between the donor and acceptor. Indeed the kinetics of electron transfer between two redox species is determined by the distance between the two redox centers, the driving force (e.g., the potential difference) and the reorganizational energy (which qualitatively reflects the structural rigidity of the redox species). Moreover, the electron donor must have an appropriate orientation, which also should facilitate communication between its active center and electron acceptor such as an electrode surface.

One approach to optimize direct electron transfer is the design of suitable surfaces to enable the right orientation of the catalytic site of the electron donor (e.g., cytochrome c proteins).

For instance, it was demonstrated that ***Shewanella alga BrY*** reduced iron oxides trapped within porous alginate beads without any close physical contact (Nevin *et al*, 2002). Another great example is provided by Lies *et al*. in 2005 where they established that ***Shewanella oneidensis MR-1*** was able to reduce at distance Fe (III) oxides precipitated within nano porous glass beads. Different hypothesis were given to explain these observations. Newman & Kolter, in 2000 already talked about the role of excreted molecoles called quinones been involved in the external electron transfer, yet Gorby *et al*., 2006 talked about external electron transfer through electrically conductive pili or “nanowires”, and Richardson in 2000 talked about multi-heme cytochromes on the outer membrane of Shewanella and other electroactive bacteria which couple electrons from the bacterium outer membrane to the electron acceptor.

### 1.3 *Shewanella loihica PV-4*

*Shewanella loihica PV-4* is a strain derived from an iron-rich mat located at the Loihi seamount off the coast of Hawai'I (Fredrickson *et al*., 2008). It is a rod-shaped, motile, Gram negative bacterium which is facultatively anaerobic and psychrotolerant (Gao *et al.* 2006). Due to its status as a dissimilatory metal reducing bacterium (DMRB), the species is of interest to electrochemists by virtue of the fact that it is capable of forming electroactive biofilms on solid electrodes. Its electroactivity is due to the ability of the organism to reduce a solid external electron acceptor, a task achieved through three main mechanisms common to the *Shewanella* genus; direct contact, use of nanowires and secretion of electron shuttles (indirect contact) (Liang *et al.* 2009; Gorby *et al.* 2006; Marsili *et al*. 2008).
Although all members of the genus have the presence of c-type cytochromes, the number and order of their genes varies and this might affect their ability to reduce external insoluble substrates.

In an early comparative test with other electroactive microrganisms, it measured the highest open circuit voltage, however it shown the poorest generators of power and current density (Boukhalfa *et al*., 2007). Nonetheless, when *S. loihica PV-4* was grown over approximately 30-day alongside *S. oneidensis MR-1*, it produced higher current density, and eventually surpassed that of *S. oneiensis MR- 1* and it also possessed a superior coulombic efficiency, 26% in PV-4 versus 16% in MR-1 (Newton *et al.*, 2009).

Furthermore, the biofilm growth on the electrochemical cell's anode showed a sevenfold increase in current to that of planktonic growth, with a deletion mutant of the MR-1 homologue of MtrC almost completely ceasing PV-4's current generation; thus one may conclude biofilm formation to be of vital importance in PV-4's ability to generate current. (Newton *et al.*, 2009).

### 1.4 Extracellular electron transfer mediated by the electro-active bacteria

Effective extracellular electron transfer is one of the physiological features of *Shewanella spp.* Research efforts have largely focused on the model *S. oneidensis* MR-1 to describe the external electron transfer. The three most commonly considered mechanisms for electron transfer to extracellular electron acceptors are (**i**) direct contact between redox-active proteins on the outer surfaces of the cells (c-type cytochromes) and the electron acceptor, (**ii**) electron transfer via soluble electron shuttling molecules, and (**iii**) the conduction of electrons along pili or other filamentous structures. (**Figure 1.1**).

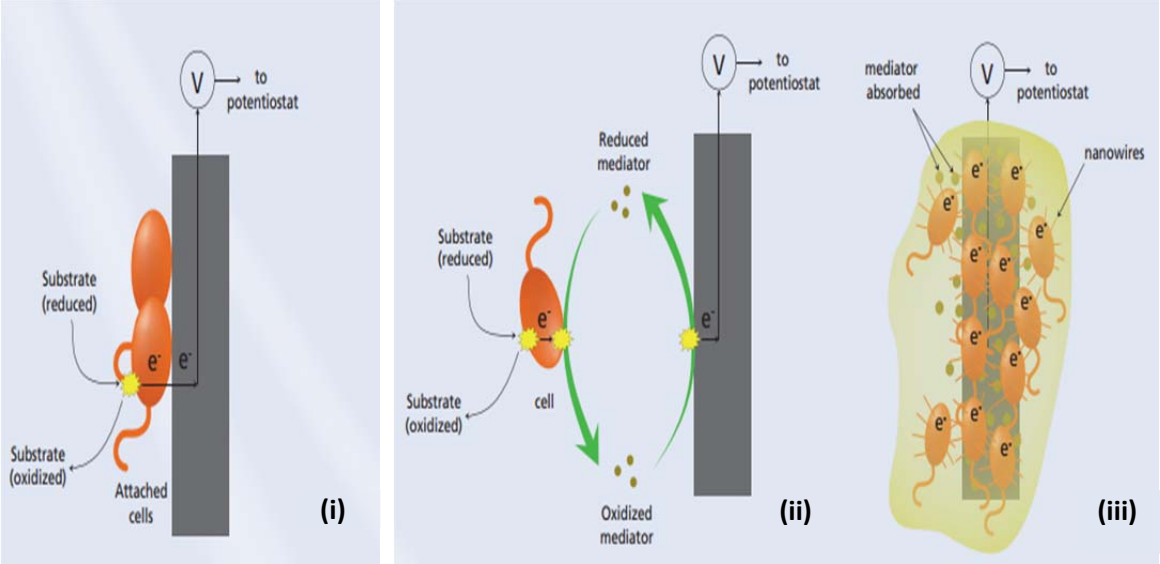


**Figure 1.1**: External electron transfer in EABs (Borole *et al.*, 2011). (**i**) Direct ET to electrodes involves outer membrane c-type cytochromes. (**ii**) Indirect mechanisms can involve redox-active molecules, such as flavins, which can be secreted by the electrogenic cells at a distance from the electrode or attached to it. (**iii**) Biofilm matrix composed of nanowires and matrix-associated c-type cytochromes also can mediate indirect ET, with the electrode-associated cells catalyzing the last step of ET via a direct mechanism.

Most of the metal oxides (electron acceptors) that can be reduced by *Shewanella sp.* are unable to cross the bacterial outer-membrane (OM), due to their insolubility in water. In order then to cross the periplasm and the cytoplasmic or inner-membrane where the bacterial terminal reductases are usually located, *S. oneidensis MR-1* and other metal-reducing bacteria have developed the ability to transfer electrons from the inner-membrane (IM), where electrons are accumulated from bacterial metabolic activity to the bacterial cell surface where reduction of Fe(III) oxides occurs. Indeed, the oxidation of organic molecules releases

electrons to the IM. From the IM electrons may pass to soluble terminal electron acceptors (**Figure 1.2**) that enter the periplasm. Alternatively, the electrons may cross the periplasm and the OM to be delivered to extracellular terminal electron acceptors. Electron transfer from the cell surface may be mediated either by flavin (F) (**Figure 1.2a**), or occur directly from an extracellular cytochrome (**Figure 1.2b**) or involve cellular appendages called nanowires (**Figure 1.2c**). So, while organic molecules are taken inside the cytoplasm compartment, the reduction of terminal electron acceptors occurs outside the bacterium or within the periplasm maintaining the cytoplasm separated from the cell exterior.

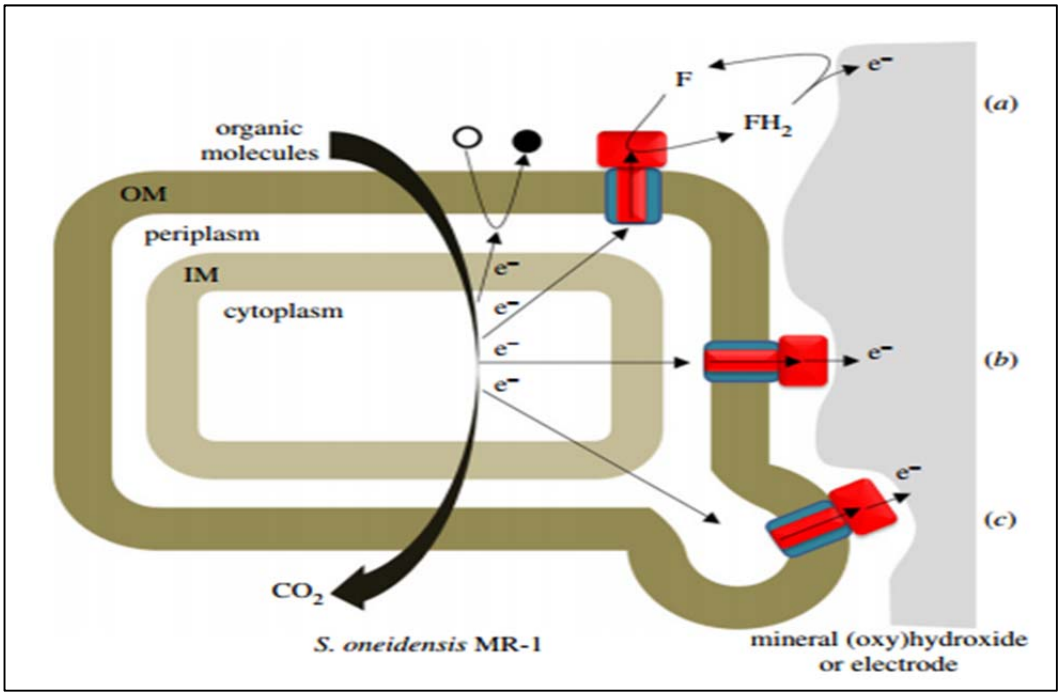


**Figure 1.2**: Overview of strategies for respiratory electron transport during the anaerobic growth in *S. oneidensis MR-1* (Breuer *et al*., 2015). Electron transfer from the cell surface to the electron acceptor is either mediated by soluble flavins (**a**), or outer membrane c-type cytochromes (**b**) or nanowires and matrix-associated c-type cytochromes (**c**).

### 1.4.1 Direct electron transfer from cells to electrode

Direct electron transfer is thought to involve a network of c-type cytochromes recently identified in the genome of *Shewanella oneidensis MR-1* (Heidelberg *et al*., 2002) and shown in several studies to be localized in the periplasm (Schwalb, Chapman, & Reid, 2002), in the outer membranes of Shewanella species (Beliaev *et al*., 2001, Dichristina *et al*., 2002, Myers

& Myers, 1992) and in pilus-like assemblages (Gorby *et al*., 2006). The most spectacular utilization of these proteins is in the reduction of extracellular solid substrates, including electrodes and insoluble mineral oxides of Fe(III) and Mn(III/IV). The mechanism by which *Shewanella* donates electrons to the electrode surface or to the surface of metal oxides is still far from being completely understood, however it seems that different outer membrane cytochromes are required to interact with different extracellular substrate such as insoluble metal and/or electrode surfaces.

These cytochromes are lipoproteins that are associated with the outer membrane (Charles R. Myers & Myers, 2004) and are translocated across the outer membrane by the type II protein-secretion pathway (Shi *et al.*, 2008), where they are exposed to the extracellular environment (C.R. Myers & Myers, 2003) where they can interact with mineral or electrode surfaces. All these protein form a pathway where electrons move from the inner membrane through the periplasm and across the outer-membrane to the surface of insoluble electron acceptor (e.g., Fe (III) oxides, electrode surface).

In particular, **CymA** (**21 KDa**) is a quinol dehydrogenase, anchored to the IM by a single α-helix as a tetraheme c-type cytochrome which catalyses quinols (**$QH_2$**) oxidation which are IM soluble electron carriers, in quinones (**Q**) and to present the resulting electrons to **MtrA (**35KDa**)** which is a decaheme *c*-Cyt that is embedded in the trans outer-membrane and forms a complex with the 28 strand β- barrel porin called **MtrB** (85KDa) . Together, MtrAB deliver the electrons through the outer-membrane to the **MtrC** (75KDa) and **OmcA** (85KDa) on the bacterial surface, where they are found in a 2:1 stochiometry (**Figure 1.3**).

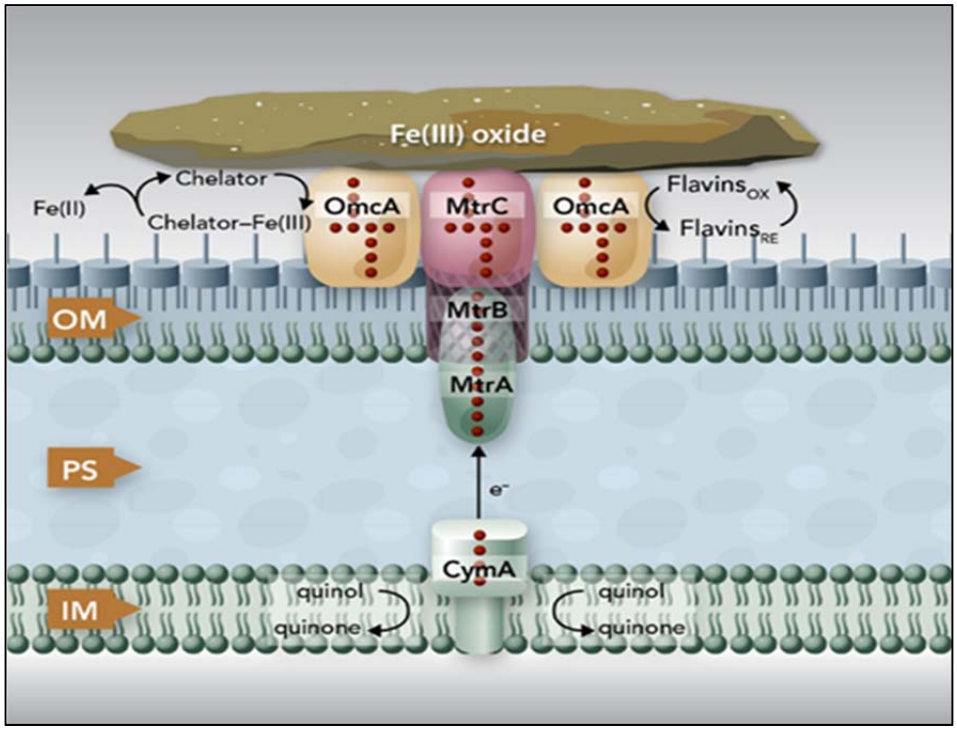


**Figure 1.3:** Proposed model depicting electron transfer pathway of *S. oneidensis* MR-1 during dissimilatory reduction of solid metal oxide. The protein components identified to date for the Mtr pathway include CymA, MtrA, MtrB, MtrC, and OmcA. CymA oxidizes quinol in the IM and transfers the released electrons to MtrA in the outer-membrane (OM).The dimer MtrA-MtrB, together helps the electron transfer across the OM to the protein complex MtrC-OmcA on the bacterial surface. The complex MtrC-OmcA is the terminal reductase that binds the surface of Fe (III) oxides (in the picture) or other electron acceptors (i.e.,electrode surface) through their solvent-exposed hemes. To improve the electron transfer yield, MtrC and OmcA use flavins secreted by the *Shewanella sp*. cells as diffusible co-factors or shuttles for electron acceptor reductions (Shi *et al*., 2012)**.**

Different studies have been carried out to better understand the correlation of this patway with the current production in *Shewanella sp.* Deletions in the periplasmic MtrA c-type cytochrome and the MtrB b-barrel porin abolished the reduction of both metal oxides and electrodes (O. Bretschger *et al*., 2007). Yet, it was noticed that mutants for both MtrC and OmcA had a severe defect in current production, and poor attachment on the electrode surface, suggesting that the current production is mostly driven by indirect EET (Bretschger *et al*., 2007). Indeed, another study where a nanoelectrode arrays was designed to prevent physical contact between *S. onedensis MR-1* cells and the electrode (X. Jiang *et al,* 2010) showed that similar current profiles were obtained when either the cell membrane established

direct physical contact with the electrode surface or when current was recorded before cell-electrode contact. These results suggested that mediated mechanisms drive current generation by *S. oneidensis* even when cells are in physical contact with the electrode.

Baron *et al*., (2009) gave a deeper description of that mechanism by immobilizing single cells of *S. oneidensis* on the electrode surface with optical tweezer. They noticed that MtrC and OmcA outer membrane c-type cytochromes were required for direct ET by cell monolayers, but evidences supported a transition from a direct contact to a mediator mechanism via secreted flavins as a function of the applied potential. Although these results supported a direct contact mechanism via outer membrane c-type cytochromes in Shewanella, the direct pathway was slow compared to a mediator mechanism, especially at low potentials. In addition, the type of electrode used in these systems (Liu *et al*., 2010) is likely to have selected for the most efficient electron transfer mechanism (direct or mediated), suggesting that a different potential applied as well as different electrode materials may affect the orientations of the heme groups of outer membrane c-type cytochromes and so the tunneling rates.

### 1.4.2 Indirect mechanism via soluble electron carriers

The transfer of electrons between the outer membrane, redox-active proteins, and the electrode surface is limited by the maximum distance (14 Å) for tunnel effect (Leys *et al*., 2004). As the biofilm grows, more electroactive cells are positioned further away from the electrode surface, thereby limiting ET toward the electrode surface unless indirect mechanisms are involved. Many bacteria overcome this distance limitation by secreting endogenous soluble redox mediators. Indeed, in addition to the heme redox centers in OM c-Cyts, cell-secreted flavin molecules such as riboflavin (RF) and flavin mononucleotide (FMN) seem to be the major electron carriers that terminate EET processes at the interface between cells and electrodes by obviating the need for direct contact (L. S. Pierson and E. A. Pierson, 2010). Flavins, including flavin adenine dinucleotide (FAD), FMN and RF, are known to be electron transport cofactors in all organisms (Juárez & Barquera, 2012). Shewanella spp. has long been known to reduce insoluble metals at a distance and without the need to physically contact the insoluble electron acceptor (Lies *et al*., 2005; Nevin *et al*., 2002). Nonetheless, the mechanism by which multiple EET-related proteins integrated at the cell outer-membrane (OM) accomplish electronic connections with such diverse solid subsurface conditions remains difficult to ascertain. Recent data has demonstrated that flavin

compounds are excreted by Shewanella species in nanomolar concentrations (Von Canstein *et al*., 2008).

Work by Marsili *et al.* in 2008 shown the importance of soluble mediator in the ET. Culture of *S. oneidensis MR- 1 and MR-4* grown on a non-porous carbon electrode in single chamber electrochemical cells, shown that the removal of the culture medium and so the removal of electron shuttles (i.e.riboflavin) resulted in the loss of more than 70% of the current production. Replacement of the filtered medium completely restored the current production to its previous value, proving the major role of riboflavin (MET) in ET.
In addition, Okamoto *et al.* in 2014 demonstrated the mechanism with which secreted soluble redox molecules can interact with OM c-Cyts. Indeed, *S.onedensis MR-1* grown on ITO electrode in the presence of either nanomolar concentration of FMN or RF shown a bifurcated direct electron transport process via one-electron redox cycling in which FMN and RF are bound to the MtrC and OmcA proteins, respectively, enhancing the electron delivery to the electrode surface. The binding of FMN to MtrC and of RF to OmcA led to a more positive redox potential (Ep), from -260 mV (free FMN) to -150 mV (MtrC-bound FMN) and from - 450 mV (free RF) to - 110 mV (OmcA-bound RF), clearly providing much more thermodynamically favorable ET kinetic to the electrode poised at +0.2V.

#### 1.4.2.1 Flavins: Riboflavin, flavin adenine dinucleotide and flavin mononucleotide

Riboflavin (**RF**) commonly called vitamin B2, flavin adenine dinucleotide (**FAD**) and flavin mononucleotide (**FMN**) are the main representatives of the group of substances known as "flavins." Flavins work as co-factors and form an integral part of the redox active sites of many different enzymes involved in dehydrogenation reactions, dioxygen activation, and electron transfer reactions (M. A. Phelps *et al*., 2004).
The flavins have in common the iso-alloxazine ring system (**Figure 1.4**; **red box**) where the redox processes occur. (**Figure 1.4**).

The flavin molecules (Fl) can exist in three different redox states: oxidized, one-electron reduced (flavin free radical or semiquinone, HFl•) and two-electron reduced states (dihydroflavin, H2Flred). The redox process of the flavins is thermodynamically reversible, irrespective of whether one or two electrons per flavin molecule are being transferred,which

means that their redox states (quinone state,semiquinone state, hydroquinone state) must be considered.

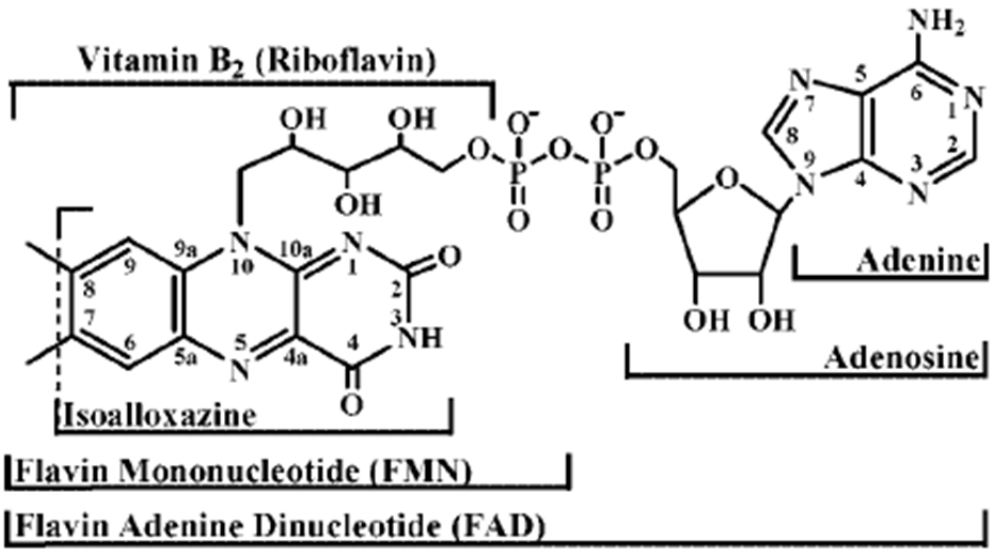


**Figure 1.4:** Chemical structure of flavins

Flavin exhibits light absorbance and intense fluorescence, therefore these properties have been utilized conveniently in their assays to their determination and interaction.
They fluoresce in the green spectral region ant their fluorescence strongly depends on the surrounding environment such as solvent polarity. In contrast to oxidized flavin, the flavin in the reduced state is hardly fluorescent. As consequence of this behavior, fluorescence studies are usually restricted to oxidized flavins.

The excitation and emission spectra of RF are shown in **Figure 1.5.** The excitation spectrum is structured and shows the bands at 270 nm, 375 nm and 445 nm. The emission spectrum is well structured and peaking at 524 nm. In an acid medium, flavin nucleotides are hydrolyzed to free RF. Flavin molecules possess amphoteric properties. Optimal fluorescence occurs at pH 3 to 8. The molecular coefficients of RF and FMN fluorescence are very close, whereas that of FAD is much lower (20% of the molar fluorescence of RF and FMN) due to fluorescence quenching by the adenylic group.

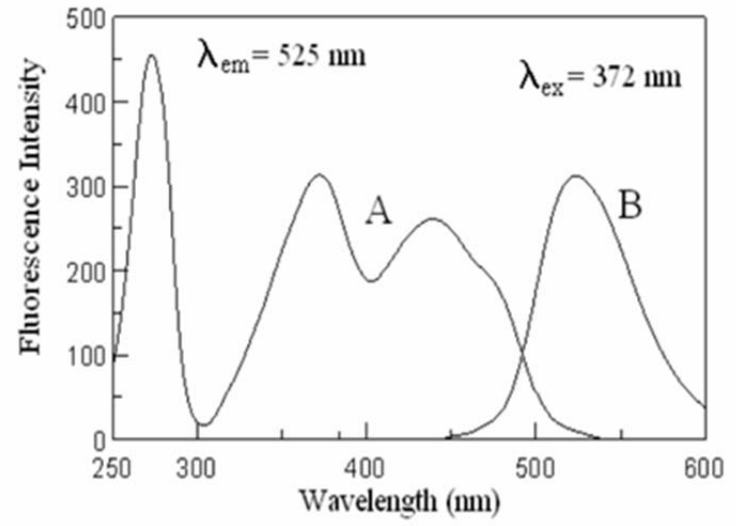


**Figure 1.5**: Excitation **(A)** and emission **(B)** spectra of riboflavin.

### 1.4.2.2 Indirect mechanism via immobile components of the biofilm matrix

When an electroactive bacterium forms a highly structured, multilayer biofilms on the anode surface of a bioelectrochemical system (BES), the mechanical stability of the biofilm is provided by the biofilm matrix, which is a hydrated extracellular polymeric matrix that encases the biofilm cells (Flemming *et al*., 2010). The biofilm matrix adds an electrical resistance to EET unless bacteria develop strategies to increase its conductivity. One of the strategy that EAB use to overcame this issue is represented by bacterial (or microbial) nanowires, which are electrically extensions of the outer membrane and periplasm (**Figure 1.6 A**) and they are challenged to mediate long-range electron transfer across biofilms formed on the electrode surface (Reguera *et al*., 2006).

They have been observed in diverse species of microbes most notably from (but not exclusive to) the *Geobacter* and *Shewanella* genera (Reguera *et al*., 2006). They may provide a "conductive matrix" that makes possible the sustained growth of bacteria far from the charge sink (Polizzi *et al*., 2012) or they may constitute a conductive pathway for long range cell-to-cell communication by electron transfer within microbial communities (Polizzi *et al*., 2012).

c-Type cytochromes have been strongly implicated as the charge carriers along bacterial ‘‘nanowires’’(Polizzi *et al*., 2012). Indeed, a c-type cytochrome was recently shown via transmission electron microscopy to be aligned along the conductive pili of *Geobacter sulfurreducens*, otherwise separated by distances prohibitive for interprotein charge transfer (>20 nm). Fluorescence measurements, immunolabeling, and quantitative gene expression analysis demonstrated that the outer membrane multiheme cytochromes MtrC and OmcA localize to the *S. oneidensis MR-1* nanowires, (Pirbadian *et al*., 2014) and they are involved in the electron transfer since the mutants lacking OmcA and MtrC produce only non-conductive wires (Leung *et al*., 2013) (**Figure 1.6 B**).

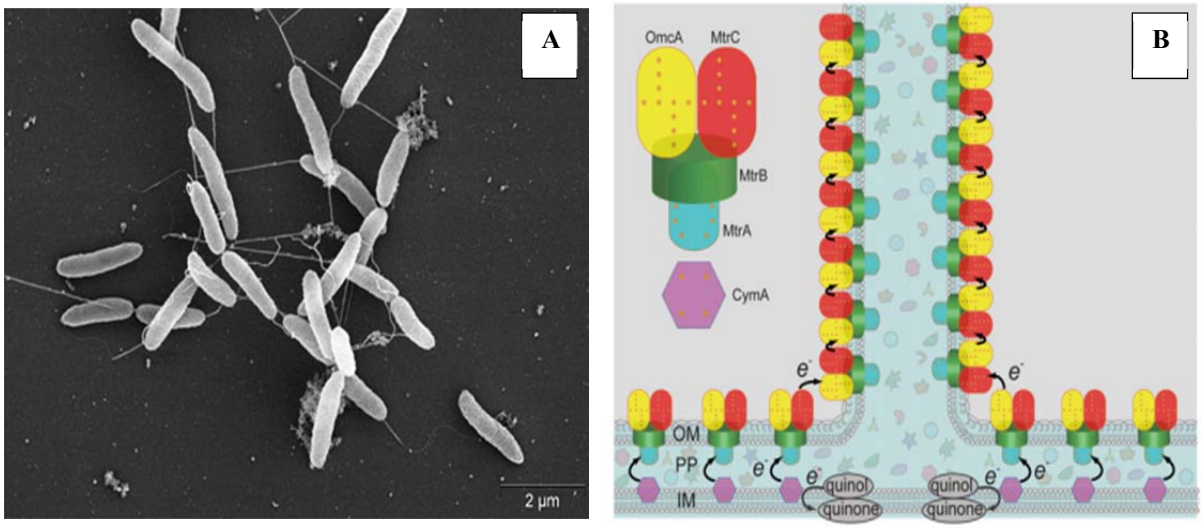


**Figure 1.6:** (**A**) SEM images of *S. onedensis MR-1* nanowires, (**B**) Proposed structural model for Shewanella oneidensis MR-1 nanowires, which are outer membrane (OM) and periplasmic (PP) extensions that includes the multiheme cytochromes involved in the electron transport (Pirbadian *et al*., 2014).

Even though the relation between current production and nanowires has been proved, the contribution of these conductive appendages to current production in MFCs is still highly debated based on the fact that *Shewanella sp.* electron transfer predominantly occurred via mediators (Jain *et al*., 2013).

### 1.5 Electrochemistry: a tool to investigate the behavior of electroactive biofilms

Electrochemical techniques can provide fundamental insights into the microbial electron transfer thermodynamics. The metabolism ability can be investigated electrochemically by providing an electrode of an appropriate potential as the sole electron acceptor, which allows the capture of metabolic electrons and reversible tuning of the electron energy level of the solid-state electron acceptor. BESs aimed at the production of electricity, fuel, and chemicals have received significant attention over the past three decades. A BES consists of a biological anode and/or a biological cathode, where microorganisms function as catalysts. In these systems the microorganisms can be present as planktonic cells and/or biofilms.

This thesis describes the use of a three electrode electrochemical cell configuration used to study the electron transfer properties of *S. loihica PV-4* biofilms.

#### 1.5.1 Three electrodes electrochemical cells

A three electrodes system consists of three different electrodes (reference, working and counter electrode) into a cell connected with an electronic control hardware, called potentiostat, which controls the electric potential at the electrode of interest (working electrode).

The **reference electrode** usually takes the form of a piece of silver wire coated with a thin coat of silver chloride, which is insoluble in water, and the reaction which occurs consists in the oxidation and reduction of the silver:

*Silver-silver chloride electrode (E=+0.225 V saturated)* $AgCl\ (s) + e^- \Leftrightarrow Ag(s) + Cl^-(aq)$

However, several other types of reference electrodes exist as listed below:

Standard hydrogen electrode (SHE) (E=0.000 V) $H_2 \Leftrightarrow 2e^- + 2H^+$
Saturated calomel electrode (SCE) (E=+0.242 V saturated) $Hg_2Cl_2 + 2e^- \Leftrightarrow 2Hg + 2Cl^-$
Copper-copper (II) sulfate electrode (*E=-0.314 V)* $CuSO_4 \Leftrightarrow Cu_2^+ + SO_4^-$

The electric potential of the reference electrode is determined by the Nernst equation (**Equation 1**), and is continuously used by the potentiostat as a constant standard to maintain

a constant potential across an electrochemical cell (EC), by relating the reduction potential of half-cell at any point in time to the standard electrode potential.

This allows studying the mechanisms by which microbes transfer electrons to the **working electrode.** Then, the electrons generated by microbial metabolism flow to the **counter electrode** which closes the circuit.

$$E = E^0 - \frac{RT}{nF} ln \frac{c_R^0}{c_O^0}$$

**Equation 1**

**E**= cell potential at the temperature of interest

**E$^0$**= *standard* cell potential

***R*** = gas constant (8.314 472 J K$^{-1}$ mol$^{-1}$)

***F*** = Faraday constant, so the number of coulombs per mole of electrons (9.6×10$^4$ C mol$^{-1}$)

**n**= number of moles of electrons transferred

**C**= reducing agent and oxidizing agent

A schematic representation of the experimental set up and the schematic representation of a three electrodes potentiostat electrochemical cell (EC) configuration is shown in **Figure 1.7.** Further details about electrodes used are found in the material and methods section.

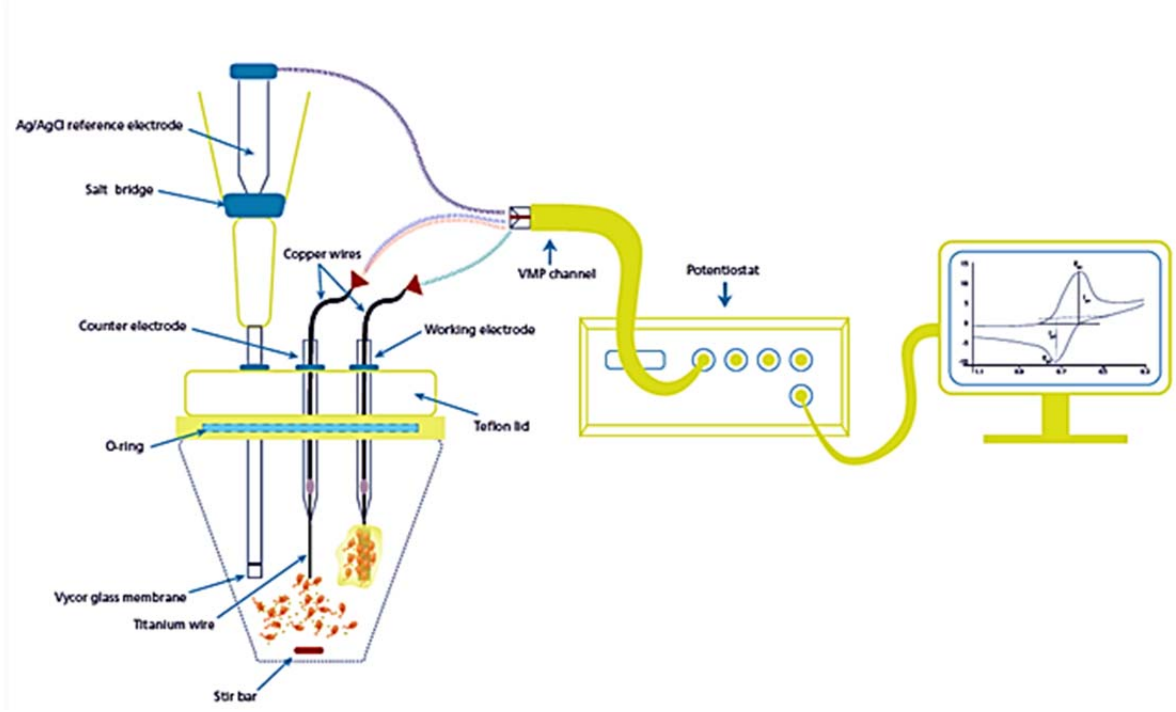


**Figure 1.7**: Scheme of the electrochemical cell used in the *S.loihica PV-4* characterization. Modified from Marsili *et al*., 2008.

### 1.5.2 Chronoamperometry (CA)

CA allows monitoring of the current production by quantifying the net flow of electrons in or out of a working electrode while that electrode is established at a constant electric potential. This is based on the principle that when a species is oxidized or reduced at an electrode, the resulting current is directly proportional to the concentration of the species. The electron flow (current) passes through the working electrode and it is measured as function of the time.

### 1.5.3 Voltammetric techniques: Cyclic voltammetry (CV) and Differential Pulse voltammetry (DPV)

Voltammetry is an analytic method based on electrochemistry. The current-potential-curve gives information about the amount and identity of the substances in the measured solution. Oxidations as well as reductions can be observed and characterised. The current-potential-curve shows the measured current against the applied potential difference between the working electrode and the counter electrode. CV and DPV both enable to study the EET of the electro-active bacteria.

In the cyclicvoltammetry the potential is continuously changed until a previously defined potential is reached. Then the potential is changed in the other direction, until the starting potential is reached again (**Figure 1.8**). Instead of changing the potential and measuring the current continuously, in differential pulse-voltammetry a rectangular pulse potential is applied and the current is measured only shortly before the pulse and at the end of the pulse (**Figure 1.9**).

A useful characteristic of cyclic voltammetry is that an analyte can be shown to be capable of being reversibly oxidized and reduced if both forward and the reverse potential sweeps exhibit a wave or peak with midpoint no more than 60 mV in difference. If a redox system remains in equilibrium throughout the potential scan, the electrochemical reaction is reversible (Armstrong *et al*., 2000). Peaks generated by a reversibly oxidized and reduced analyte (n=1) are separated by approximately 60 mV on a cyclic voltammogram (Léger *et al*., 2003).

Thus, the data analysis of the CVs provides information about the thermodynamics of the microbial electron transfer and allows the formal potential of possible and actual extracellular electron transfer side to be determined.

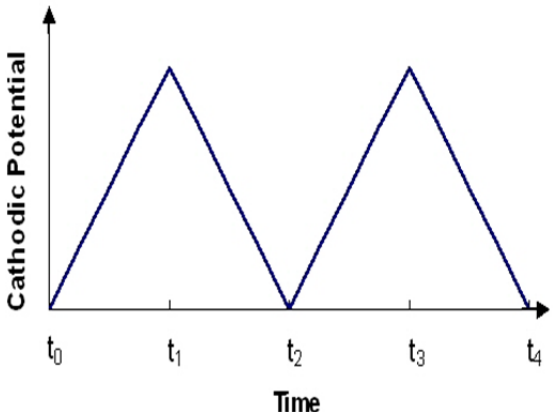


**Figure 1.8:** CV potential waveform

DPV is a more sensitive technique. Indeed, the advantages of DPV are particularly noteworthy when the quantity of bound reactant is small. In addition, there is a dependency between peak currents and the amount of reactant. This provides an approximate method for determining the concentration of the attached reactant(Brown & Anson, 1977; Farahi *et al*., 2014)

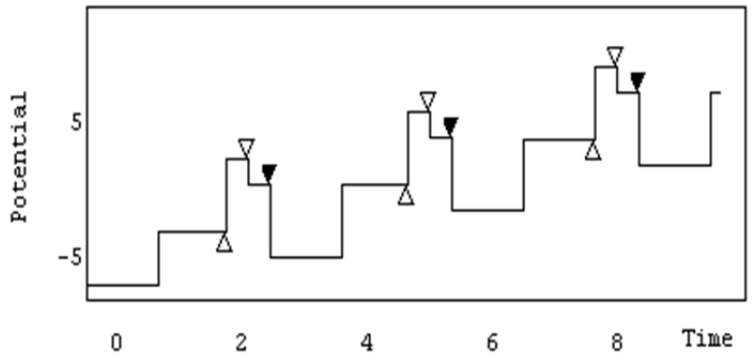


**Figure 1.9**: DPV potential waveform

### 1.6 Electrochemical Impedance Spectroscopy (EIS)

Electrochemical impedance spectroscopy (**EIS**) is a powerful technique for the characterization of electrochemical systems. In recent years, impedance spectroscopy has found widespread applications in the field of characterization of materials. It is routinely used in the characterization of coatings, batteries, fuel cells,*etc*.

The fundamental approach of the EIS is to apply a small amplitude sinusoidal excitation signal to the system under investigation and measure the response which could be either current or voltage or another signal of interest.

The classical electrochemical techniques present measurements of currents, electrical charges or electrode potentials as functions of time. In contrast, EIS presents the signal as a function of frequency at a constant potential.

In EIS a potential perturbation is applied (usually a sine wave) and the current response is observed, which is a sine wave at the same frequency, but with a different amplitude and phase than potential signal.

Impedance (**Z**) can be defined as a measure of the ability of a circuit to resist the flow of electrical current. Per definition a resistance is the ability of a circuit element to resist the flow of electrical current. Ohm's law (**Equation 1**) defines resistance in terms of the ratio between voltage, E, and current, I.

$$R = E/I \quad (1)$$

The use of the above equation is limited to only one circuit element a so called ideal resistor. An ideal resistor follows few properties:

- It follows Ohm's Law at all current and voltage levels.
- Its resistance value is independent of frequency.

Yet the above equation holds for a resistor at a constant potential. But when the EIS analysis is made, a sinusoidally, varying potential is applied (**v**) which is calculated by the follow equation (**Equation 2**).

$$v = V \sin wt \quad (2)$$

Where v is the potential difference at any time (**t**), **w** is the angular frequency of the sine wave, and **V** is the amplitude. Now, if such a potential waveform is applied to a circuit containing only a resistor (**R**), the potential (v) and the current (i) will be in phase and will be oscillate with the same frequency. If the same sine potential is applied to a circuit with only a capacitor (**c**), current only flow when potential is changing, and the potential and the current will still have the same frequency, but they are not in phase (90 phase shift "**j**") (**Figure 10)**.

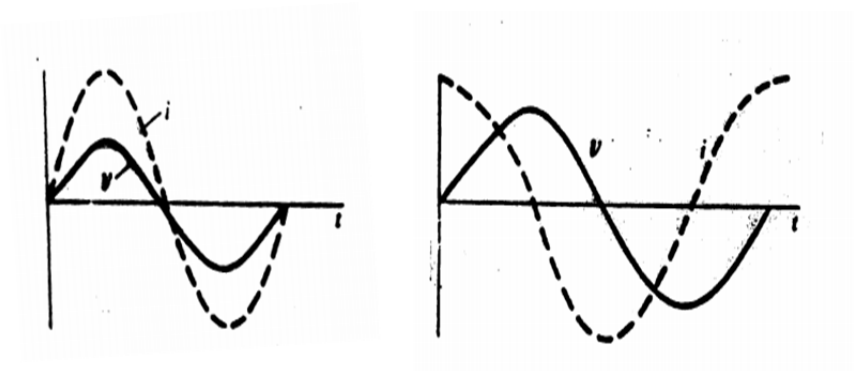


**Figure 10**: Potential (v) and current (i) trend in the case of a circuit containing only a resistor (**left panel**) or capacitor (**right panel**).

Impedance can so be defined as described in **Equation 3**. Thus for a resistor and a capacitor the impedance is defined as in equation 4 and 5 respectively.

$$Z(w) = v(w) / i(w) \quad (3)$$

$$Z(w) = 1/jwc \quad (4)$$

$$Z(w) = R \quad (5)$$

Therefore, for a resistor and capacitor in series will be characterized by the sum of equation 4 and 5 (**Equation 6a**), contrarily if they were in parallel, impedance would be given by the sum of the inverse of Equation 6a (**Equation 6b**).

$$Z(w) = R + 1/jwc \quad (6a)$$

$$Z(w) = 1/R + jwc \quad (6b)$$

By considering a typical electrode-solution interface in a cell, the capacitance is due to charging/discharging the electrochemical double layer ($\mathbf{c_{dl}}$). In a parallel circuit with this double layer, a faradaic reaction can occur at some potential-dependent rate, resulting to a resistant called "$\mathbf{R_{ct}}$". On the contrary, in a series circuit a resistant is ever present and it is called "$\mathbf{R_s}$" Thus the impedance will be expressed by the **Equation 7.**

$$\mathbf{Z= R_s + R_{ct}/\ 1+w^2{}_{cdl}R^2{}_{ct} - j\ (wc_{dl}R^2{}_{ct}/1+\ w^2c^2{}_{dl}R^2{}_{ct})} \qquad \mathbf{(7)}$$

Different graphs can be done by plotting the Equation 7. The most used ones are called "Nyquist plot" and "Bode plot" (**Figure 1.11**).

The Nyquist plot traces a semicircle with a diameter $R_{ct}$ and makes it easy to determine it. The disadvantages of this plot are that the information about the angular frequency of the sine wave (w) are lost, and that the plot looks the same for any capacitor. In the case of the Bode plot it is possible to get the value of the capacitor from the value of the module of Z and the frequency is not lost.

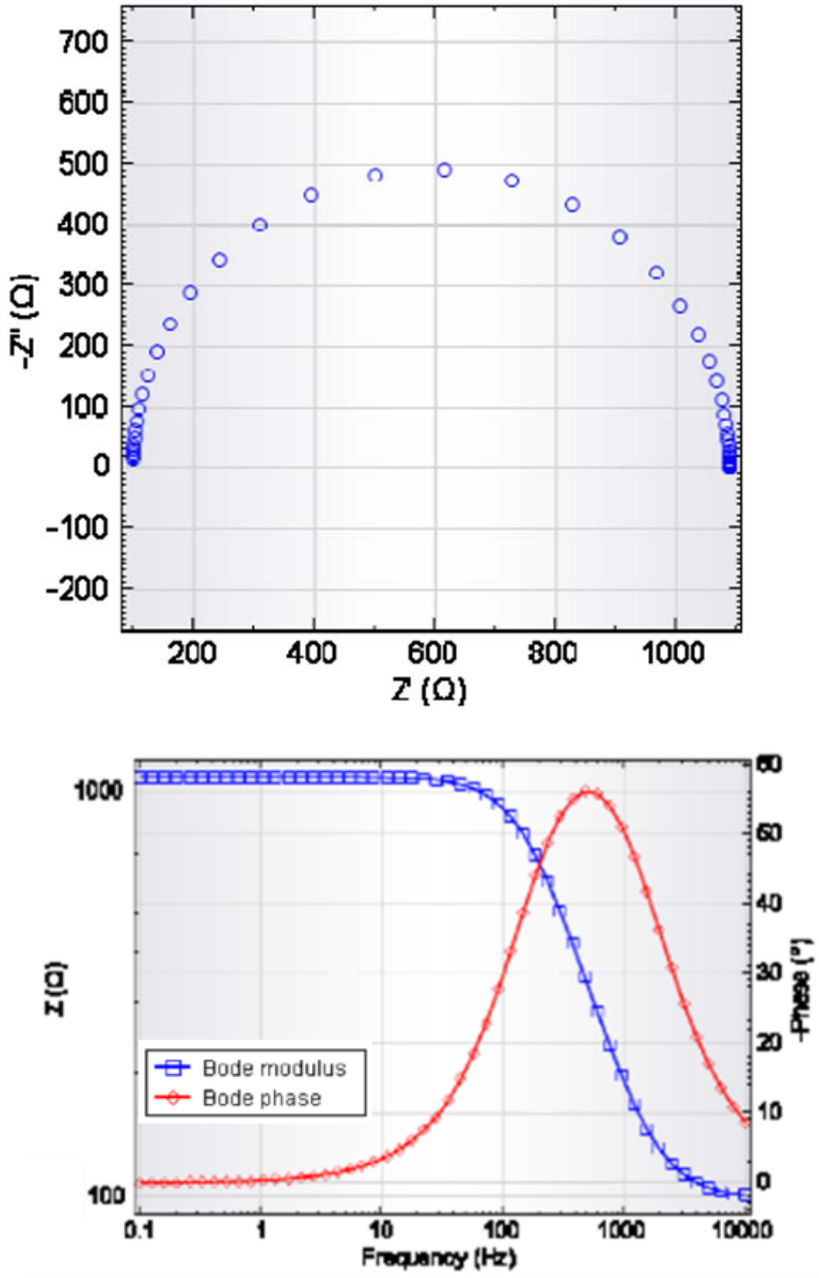


**Figure 1.11 :** Nyquist plot **(**Top graph), Bode plot (Bottom graph).

## 1.7 Parameters that affect current output in bio-electrochemical systems (BESs)

BESs which aim to the production of electricity, have received particular attention over the past decade. They can be classified in two main categories, as Microbial Fuel Cells (MFCs) and Microbial electrolysis cells (MECs). The former convert the chemical energy of organic wastes (i.e. wastewater, lignocellulosic biomass) into electricity, while the second into hydrogen/chemical products. In general, a BES consists of a biological anode and/or a biological cathode, where microorganisms function as catalysts. In these systems the microorganisms can be present as planktonic cells and/or biofilms.

So far, a number of potential rate limiting parameters have been described to affect the performances of BESs. These parameters can mainly be grouped in three categories: 1) **biological parameters** such as the microorganisms used and their capability to form biofilm on the electrode surface, the growth condition of the same (presence or absence of oxygen, nutrient concentration, etc.), 2) **system design parameters** such as electrode surfaces and chemistry, and 3) **operating parameters** at which the BES is kept**,** like temperature and pH, presence or absence of oxygen and the use of a batch or continuous flow reactor (**Figure 1.12**).

For instance, Biffinger *et al*., (2009) shown how operating parameters such as the oxygen concentration can positively affect the current output in *S. oneidensis* biofilms. Indeed, when *S. oneidensis* was cultured with different concentrations of dissolved oxygen, this resulted in different electrode coverage and thickness. Also, a much thicker and robust biofilm was formed under air-exposed conditions compared to strictly anaerobic conditions (Biffinger *et al*., 2009).

For what concern the biological parameters, Srikanth *et al,* (2008) and then Marsili *et al*., (2010) have reported how the ability to form biofilm on an electrode surface can favour higher current production. Indeed, DET resulted in higher kinetic rates of electron transfer than the release of electron shuttles by the planktonic cells (MET). However, it has been proved that this is not a common rule amongst the EABs, but it true just for those which require direct electrical contact with the electrode to transfer electrons (*G. sulfurreducens*). In fact, in *S. oneidensis,* biofilm and planktonic cells can co-exist and synergistically produce current (Biffinger *et al*., 2007).

For what concern the system design parameters, Brutinel *et al*., 2012 showed that in *S. loihica PV-4* (which utilizes both MET and DET) the relative contribution of each route depends on the surface chemistry and topography of the electrode material and yet this determines the EET rate at the biofilm/electrode interface. In addition, the use of rougher electrode surfaces resulted in higher current output in *G. sulfurreducens* (Marsili *et al*., 2008). However, it wasn't proved whether the higher current output at rough electrode surfaces was due to the thicker biofilm or to the high concentration of adsorbed flavins.

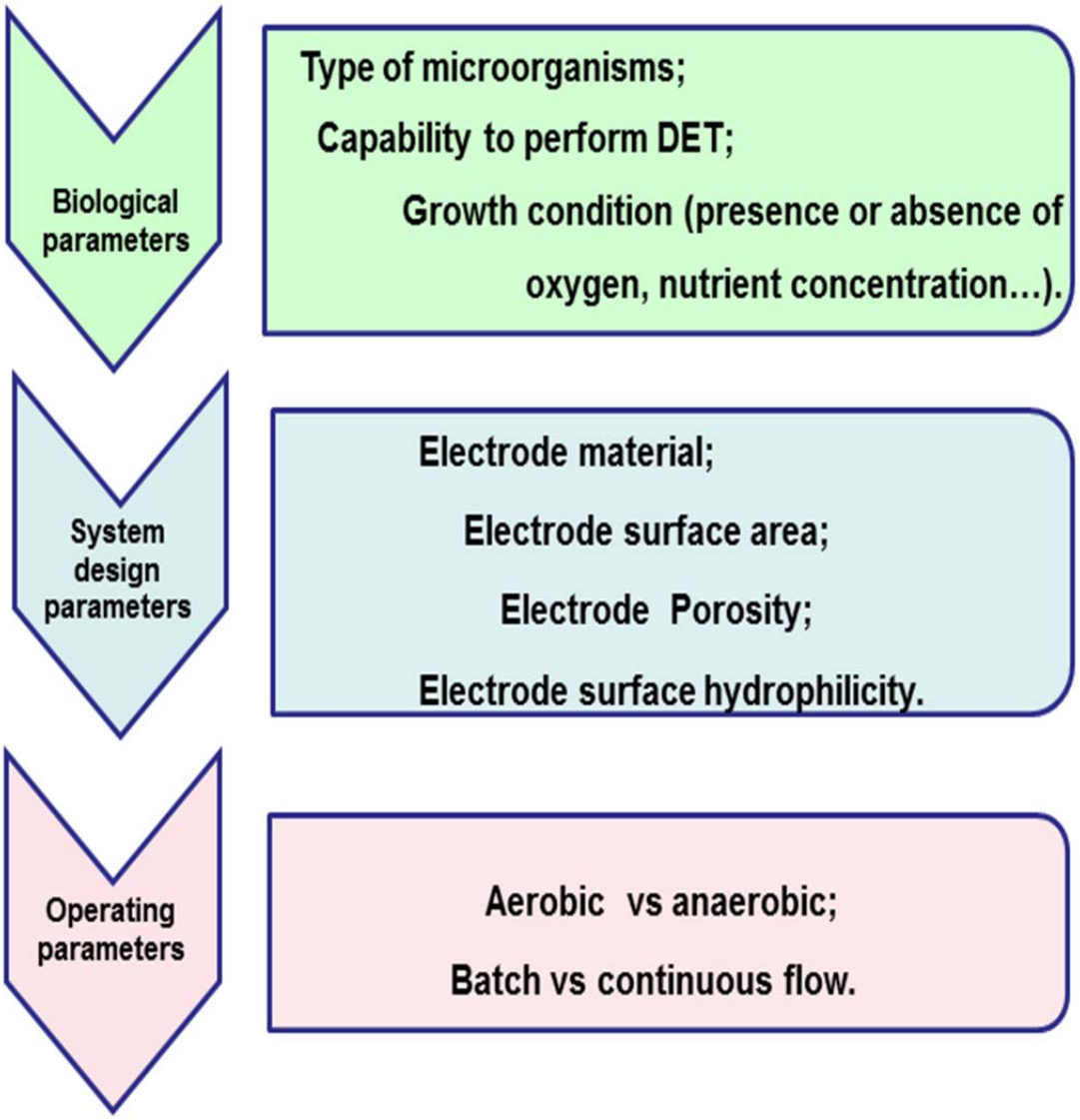


**Figure 1.12:** Schematic representation of the parameters that affect current output in BESs. Green box includes the biological parameters; Blue box illustrates the system design paramaters and the pink box shows the operating parameters.

In general, to support biofilm growth and enable facile electron transfer, the ideal anode should have low resistance, high surface, biocompatibility, and chemical stability at circumneutral pH and ambient temperature.

The aim of this study is to improve the electron transfer rate in *S. loihica PV-4* biofilms in potentiostat-controlled three electrodes ECs. The objectives of this study are:

a) **Investigation of biological parameters** such as the effect of lactate concentration on *S. loihica PV-4* electroactivity and effect of different electron acceptors during *S. loihica PV*-4 growth on its electroactivity.
b) **Investigation of system design parameters** such as effect of electrode surface abrasion and functionalization on *S. loihica PV-4* electroactivity and effect of electrode surface coating on *S. loihica PV-4* electroactivity.

# CHAPTER 2

# INVESTIGATION OF BIOLOGICAL PARAMETERS

**Abstract**

It has been suggested that when nutrients are abundant current production is facilitated by the cycling process of soluble mediators. These enable bacteria to reduce the metal oxide minerals at a distance, while under nutrient poor conditions, cells rely on direct electron transfer (Lies *et al*., 2005). Also, the choice of the right concentration of electron donor (Biffinger *et al*., 2009; Kim *et al*., 1999; Justin *et al*., 2009) and the type of electron acceptor during the growth such Oxygen (aerobic growth) or fumarate or iron citrate (anaerobic growth) play a role in the external electron transfer (EET) mechanism and thus in current production (Biffinger *et al*., 2009; Mao & Verwoerd, 2014). Thus, understand how *S. loihica PV-4* utilizes its resources, different concentration of lactate as carbon source were supplied during the electrochemical experiments, and different electron acceptors were used during the anaerobic growth. Results suggest that the concentration of lactate has an important role in electrochemical performances of bioelectrochemical systems (BESs). The optimal lactate concentration was found to be 20 mM, giving higher current output (82% more than with 40 mM lactate) by a greater production of electron shuttles (riboflavin). Doubling this concentration (40 mM lactate) affected the growth of *S. loihica PV-4* toward the formation of more biofilm rather than planktonic cells, switching the external electron transfer (EET) mechanism more into direct electron transfer through cells attached on the electrode surface as biofilm. Thus, 20 mM concentration of lactate was chosen for further studies of *S. loihica PV-4* EET. Cyclic voltamogrammes (CVs) of S.*loihica PV-4* indicate that the main role of EET is maintained through the release of flavins (MET) and that DET start to play a role only later when the carbon source probably became limiting for an active secretion of electron shuttles (Richter *et al*.,2012). Anaerobic growth with iron citrate as electron acceptor gave a similar current output to the aerobic growth prior to inoculation into EC with 110.49 $\mu Acm^{-2}$ and 106 ± 5 $\mu Acm^{-2}$ respectively. Comparison between two different electron acceptors used during the anaerobic growth showed that, *S. loihica PV-4* cultures previously grown under anaerobic condition with 40 mM iron citrate and 20 mM lactate yielded 57% more current than the other anaerobic culture counterpart with 20 mM fumarate and 20 mM lactate. This was due to a greater production of electron shuttles (flavins) as confirmed by DPV analysis. In all the conditions, it seems that MET play a main role in the EET, however a better understand of the interplay between DET and MET has yet to be clarified.

## 2.1 Introduction

Changes in metabolism and cellular physiology of EABs during exposure to different environmental conditions (temperature, pH, nutrients concentration) can be substantial for enanching current production in BESs. Microorganisms such as *Shewanella sp.* and *Geobacter sp*. are able to catalyze chemical reactions in order to obtain energy for metabolic growth from their environment.

In the past few years, more and more compounds were revealed to be reduced at the surface of the outer membrane of Gram-negative bacteria. *Shewanella* strains are good candidate organisms to discover the biochemistry that enables the dissimilatory reduction of extracellular electron acceptors (Richter *et al*.,2012).

*Shewanella spp.* have diverse capabilities in their use of various forms of electron acceptors ($O_2$, nitrate, sulfate, ferric iron [$Fe^{3+}$] oxide, heavy metals) as well as of electron donors (organic compounds, ferrous iron [$Fe^{2+}$] oxide, $H_2S$, $H_2$) to ‘‘make a living’’ in their natural habitats. Due to the wide electron donors/acceptors that *Shewanella spp.* can use, it needs to adapt quickly to changes in electron donor/acceptor type and availability; hence, the ability to compete and thrive in such environments must ultimately be reflected in the organization and utilization of electron transfer networks, as well as central and peripheral carbon metabolism.

For instance, in response to multiple lactate feedings, ***S. oneidensis* MR-1** generates higher current and ticker biofilm under air-exposed conditions compared to strictly anaerobic conditions (Biffinger *et al*.,2009). In addition, Kim *et al*., (1999), found that the current generation in ***S.oneidensis* MR-1** was in proportion with lactate concentration up to 30 mM. Another correlation between current production and lactate feeding was made by Justin *et al*., (2009). Indeed, they compared aerobic and anaerobic current production of ***S. oneidensis* MR-1** showing that additions of lactate to air-exposed MR-1 culture doubled current output, whereas current output under anaerobic condition was eight-fold less than air-exposed MR-1. However, there were rapid current responses (<4 min) from lactate additions for anaerobic cells.

In addition, it has been proved that, also the electron acceptor used during the growth of EABs might have a role in the EET mechanism used, thus in the current output. For instance, it has been proved that ***S.oneidensis* MR-1** adjusts its membrane transport and its specific

metabolic pathways in response to the use of different electron acceptors as fumarate and iron citrate (Mao & Verwoerd, 2014).

According to the above mentioned results, EABs such as *Shewanella spp.* can direct the reduction of an electron acceptor either through DET, MET or through the synergic cooperation of both mechanisms, depending on the carbon source (electron donor) at which the m.o. is exposed. Thus affecting the current output in BESs.

Therefore, this chapter will focus on the understanding whether ***S.lohica PV-4*** utilizes its resources similarly to the other electroactive model bacteria *S.oneidensis MR-1*.

To do so, **(i)**, different electron acceptors such as fumarate and iron citrate were used during the anaerobic growth prior inoculum into the electrochemical cells (ECs) and **(ii)** different concentration of lactate were supplied during the electrochemical experiments.

Yet, in an effort to develop a novel inoculum-preparation protocol which maximised *S. loihica*'s electroactivity, the organism's growth characteristics were examined under both aerobic and anaerobic conditions.

The hypothesis behind that, was based on the fact that *S. loihica PV-4* grown in anaerobic conditions prior to inoculation into an electrochemical system would be more electro-active than its aerobically-grown counterparts. This theory was based on the probability that the necessary cellular machinery required for extracellular electron transfer would already be established, thus shortening any lag phase associated with a change in environmental conditions, allowing for a more timely delivery of current.

## 2.2 Materials and Methods

### 2.2.1 Organism

*Shewanella loihica PV- 4* (DSM 17748) strain was purchased from the German microbial bank DSMZ. To ensure the culture maintenance -80 °C stock cultures were prepared transferring 1mL of actively growing culture to a cryo-tube containing 0.5 mL v/v of 50 % DMSO.

### 2.2.2 Autoclaving procedure

All media, both solid and liquid, were sterilized by autoclaving at 121 ° C for 15 min in a Tomy SS-325 autoclave (Tomy Seiko Co., Ltd., Japan)

### 2.2.3 Media Preparation

#### 2.2.3.1 Luria Bertani broth (LB)

The Luria Bertani broth contains the components listed in table 2.1, resuspended in deionised water and the pH adjusted to 7.4 using 1 M NaOH. After autoclaving , 2mL of 1M $MgSO_4$ and 0.1mL of 1M $CaCl_2$ were added.

**Table 2.1-** LB medium formulation

| Constituents | Concentration (g/L) |
|---|---|
| $Na_2HPO_4$ | 6 |
| $KH_2PO_4$ | 3 |
| NaCl | 20 |
| $NH_4Cl$ | 1 |
| Peptone | 1 |
| Yeast extract | 0.5 |
| Fe (iii) Citrate | 0.1 |

### 2.2.3.2 Luria Bertani agar

This medium was as listed in table 2.1, along with the addition of 1.5 g/L of Technical Agar

### 2.2.3.3 Defined medium (DM) for aerobic growth conditions

The defined medium contains the components listed in table 2.2, resuspended in deionised water and the pH adjust to 7.6 using 1 M NaOH. After autoclaving, 5 g/L of filter sterilized casamino acids were added.

**Table 2.2-** DM medium formulation. All the concentrations are meant in 1 liter solution.

| Constituents | Concentration |
|---|---|
| $NaHCO_3$ | 2 g |
| $CaCl_2$ H2O | 0.08 g |
| $NH_4Cl$ | 1 g |
| $MgCl_2$ $_6H_2O$ | 0.02 g |
| NaCl | 10 g |
| HEPES | 7 g |
| Trace Minerals * | 10 mL |
| Vitamin Solution * | 1 mL |
| Lactic acid | 10/20/40 mM |

* See composition in Appendix section, Table A2 and A3

### 2.2.3.4 Defined medium (DM) for anaerobic growth conditions

This medium was as listed in table 2.2, along with the addition of either 20 mM of fumarate with 20 mM lactate or 40 mM iron citrate with 20 mM lactate as electron acceptor instead of oxygen. Before autoclaving 100 mL of media was transferred into the anaerobic bottles.

These were then flushed with nitrogen gas for 30 min to remove all traces of oxygen. All the anaerobic bottles where then sealed by using a butyl stopper with aluminum crimp.

#### 2.2.3.5 DM medium for electrochemical cell (EC)

This medium was as listed in table 2.2, along with the transfer of 100 mL of it into the anaerobic bottles prior to autoclaving. These were then flush with nitrogen gas for 30 min to remove all traces of oxygen. All the anaerobic bottles where then sealed by using a butyl stopper with aluminum crimp.

### 2.2.4 Bacteria and growth media

*S.loihica PV-4* was cultured on LB agar plates on a weekly basis to ensure viable cultures. A loop full of cells from a single colony was taken from a stock plate and streaked on to a fresh LB agar plate. Plates were incubated at 30 °C. *S.loihica PV-4* cultures were grown in 50 mL flasks containing 10 mL of LB broth. A loopful of cells from a single colony was transferred to the flask and the flask was incubated at 30 °C on an orbital shaker (150 rpm) for 24 h Afterwards, 1 mL of culture with an optical density of 1 was transferred to a 50 mL flask containing 10 mL of DM. The flask was then incubated for 24 h at 30 °C on an orbital shaker (150 rpm) for 24 h.

In an effort to develop a novel inoculum-preparation protocol which maximised *S. loihica*'s electroactivity, the organism's growth characteristics were examined in DM medium under both aerobic and anaerobic conditions. In the case of anaerobic growth, two alternative terminal electron acceptors (20 mM fumarate [E0= +0.31V] and 40 mM iron citrate [+0.32V]) were used instead of oxygen.

Also in this case a loop full of cells from a single colony was transferred to a 50 ml flask containing LB broth and incubated at 30 °C on an orbital shaker (150 rpm) for 24 h. Afterwards, 1 mL of culture with an optical density of 1 was transferred to a 50 mL flask containing 10 mL of DM with either fumarate or iron citrate.

In all the cases, bacterial growth was determined via optical density using a spectrophotometer and the optical density injected in the electrochemical cells (ECs) was of $OD_{600}$ nm= 2.5 ± 0.2.

However, every time a lower biomass was collected from the 50 ml flask containing anaerobic DM, hence rising the need of mixing more than one anaerobic flask together to achieve the same optical density of the aerobic counterpart prior inoculum into the ECs.

This surely results into a more laborious protocol which also includes the use of an anaerobic chamber and the related cost of the gases use to ensure an anoxic environment.

### 2.2.5 Operation of the anaerobic bioelectrochemical cells

Sheets of graphite (Tokai Co, Japan) were chosen as the working electrode material due to graphite's high surface roughness, conductivity and modest price. The sheets were cut into dimensions of 2 cm x 1 cm x 0.2 cm, yielding electrodes with surface area 5.2 $cm^2$. The electrode was then polished with sandpaper P240 (grit diameter 58.5 μm). Residual graphite dust was removed by sonication in a water bath for 5 min. The electrodes were then soaked overnight in 1 M HCl (to remove all possible contaminants), washed twice with deionized water (to remove organic substances), and then stored in deionized water.

Single chamber electrochemical cells (ECs) with a working volume of 10 mL were operated in a three electrode configuration under the control of a five channel potentiostat (VSP Bio-Logic, USA). ECs were assembled in a similar manner to that described by Marsili *et al.* (2008, **see figure 7, chapter 1)**. The counter electrode was a 0.25 mm Ti wire (Goodfellow, England) which was inserted into glass capillaries and soldered to copper wires. In a similar fashion, the graphite working electrode was attached to the potentiostat via Ti wire, a nylon screw and a nut (Small Part, USA). An Ag/AgCl reference electrode (E = +0.225 V vs. SHE; Fisher Scientific, Ireland) was connected to a 3 mm Vycor glass membrane (Bio-analytical Systems, UK) via a salt bridge consisting of 0.1 M $Na_2SO_4$ in 1% agar which was added after ECs had been autoclaved for 15 min. The resistance of each electrode assembly did not exceed 0.5 ohm in any experiment. Anaerobic conditions were maintained in the ECs by operating under a flow of sterile humidified $N_2$ which had been passed over a heated copper column to remove trace oxygen. The $N_2$ was first humidified by pumping the gas into 100 mL room temperature deionized water in a sealed serum bottle. The gas in the headspace of the serum bottle was then directed to the EC. ECs were maintained at 30°C by the passage of heated water through the cell jacket. Mixing of 150 rpm was achieved via a magnetic stirrer, which was switched off for CV and DPV analysis to allow diffusion-controlled peaks. CV,

CA and DPV experiments (procedures which will be fully explained in next section) were performed on the electrochemical cells to confirm proper setup and obtain baseline data, by using DM medium. To inoculate the electrochemical cells, 5 mL of the minimal media used for recording blank data was first slowly removed from the main chamber using a 3 inches long sterile 24 gauge needle and syringe. The chamber was then filled with 5 mL of aerobic or anaerobic *S.loihica PV-4* culture.

After the inoculation of the electrochemical cell, planktonic *Shewanella* cells were allowed to colonize the poised graphite working electrode over the course of the h. The increase in current density output was measured until a plateau current was reached.

### 2.2.6 Chronoamperometry and Electrochemistry Measurment

The electrical current produced by cells colonizing the working electrode was measured measured until a plateau current was reached on a Bio-Logic VMPR Multichannel Potentiostat. Measurements were performed via an electrochemical procedure known as Chroamperometry (CA). CA is the quantification of the net flow of electrons in or out of a working electrode while that electrode is maintained at a constant electric potential. During all CA experiments the working electrode was poised at a +0.2 V vs. Ag/AgCl reference lectrode and electrical current was measured every 900 s. The chamber was stirred continuously to reduce the mass transfer limitation of lactate in the biofilm and on the electrode surface. Once current reached the plateau, CA was stopped, and CV and DPV were performed.

### 2.2.7 Detection of Adsorbed Redox Species with Voltammetry

Differential pulse voltammetry (DPV) and cyclic voltammetry (CV) were used to analyze *S. loihica PV-4* biofilms for reversible and irreversible redox reactions and other features that would indicate catalytic reaction (unlimited substrate concentration) at the working electrode. Both DPV and CV were performed immediately after the inoculation and again once current had stabilized.

CV was carried out from Ei= –0.8 V vs. Ag/AgCl to $E_f$=0.2 V vs. Ag/AgCl. The scan direction was then reversed and the potential was swept back to the original E value of -0.8 V vsAg/AgCl. CV was performed at a scan rate of 1.0 mV/s. CV was always followed by DPV. DPV was begun from an Ei of –0.8 V vs. Ag/AgCl and ended at an Ev of 0.2 V vsAg/AgCl. DPV scan rate was 4 mV/s. DPV and CV were always performed without stirring to allow visualization of diffusion-limited reactions as peaks and to minimize electrochemical noise.

### 2.2.8. Effect of lactate concentration on EET in *Shewanella loihica PV-4*

The same amount of bacteria (OD600nm= 2.5) were inoculated in all the ECs with different lactate concentrations commonly used in literature (10, 20, 40 mM lactate) after growth in DM medium for 24 h with a residual lactate concentration of 1.9 ± 0.8 mM.

### 2.2.9 Interplay between Direct Electron Transfer and Mediated Electron Transfer

CV was performed every 3 h until current stabilized in the ECs injected with 20 mM lactate as carbon source. This was undertaken in order to clarify the kinetic between direct electron transfer and mediated electron transfer.

### 2.2.10 Kinetic of flavin secretion in short term experiments: Detection by Fluorescence Spectroscopy

Standard solutions of riboflavin (Fisher Science, Ireland) in concentration range from 0 to 5 µM were prepared in DM medium and analysis by spectrofluorometer (JASCO FP FP-8300, USA). The resulting peaks and their intensity were linearly fitted . The corresponding fitting parameters (**see Appendix, Figure A2**) were used to determine the approximate concentration of flavins in the cell free supernatant. In brief, the supernatant was centrifuged at 13,500 rpm for 10 min and then residual cells were removed through filtration on 0.22 µm filters (Millipore, USA). The emission (450-700 nm) at excitation wavelength of 372 nm and the excitation spectra (250-530 nm) at emission wavelength of 540 nm were recorded every 3 h on the spent medium until current stabilized.

### 2.2.11 Relationship between the use of different electron acceptor during *S. loihica PV-4* growth on its electroactivity

The organism was anaerobic cultured with either 40 mM iron citrate or 20 mM of fumarate as described in section 2.4. Then prior to injection into the ECs, 5 mL of the bacterial suspension was centrifuged for 10 min at 3354 g, and the bacterial pellet was resuspended in 10 mL of fresh defined medium with 20 mM lactate and no added riboflavin. This washing procedure ensures removal of microbially-produced soluble redox mediators. The EET after the growth of *S.loihica PV-4* in presence of two alternative electron acceptors was studied by CA, CV and DPV.

### 2.2.12 High-performance liquid chromatography

Lactate concentration of the DM spent media (cells free) from the ECs using different concentration of lactate was quantified by HPLC (Varian Device – Inert 9012) with a Supelcogel C-610H column (Sigma-Aldrich, St. Louis, USA) equipped with a guard column and using a 0.027 % v/v $H_2SO_4$ mobile phase for isocratic elution. Calibration curves for each component were prepared for each run using six synthetic standards of appropriate concentration range.

## 2.3 Results

### 2.3.1 Bacteria and growth media

A bacterial growth curves allows to follow the change in the number of microbial cells over a period of time. Common bacterial growth curves show an exponential trend rather than a linear fitting, with four different distinguishable phases. A **lag phase** where the bacteria do not show any growth, but they are somewhat in a quiescent state. An **exponential or logarithmic (log) phase** where the microorganisms are in a rapidly growing and dividing state. Then, as the bacterial population continues to grow, all the nutrients in the growth medium are used up by the microorganism for their rapid multiplication. This result in the accumulation of waste materials, toxic metabolites This shifts the conditions of the medium such as pH and temperature, thereby creating an unfavorable environment for the bacterial growth. Such phase is called **stationary phase**. Subsequentialy, the depletion of nutrients thus the accumulation of metabolic waste products and other toxic materials in the media will facilitates the bacterium to move on to the **Death phase**. The death phase was never reached in the following experiment because the cultures needed to be alive prior inoculation into the ECs.

In this paragraph *S.loihica PV-4* colonies were previously enriched using LB broth under aerobic condition. Then two different growth conditions were investigated. The first occurs under aerobic condition ($O_2$ as e- acceptor) the second under an anoxic environment (either iron citrate or fumarate as e- acceptor).

**Figure 2.1** depicts the *S.loihica PV-4* growth curves generated from different media and growth conditions. One single colony was picked up from an agar LB plate not older than a week. Then, in all the media and conditions the initial optical density was adjusted to $OD_{600nm}$=0.03 ± 0.001 by using LB fresh medium.

The bacteria from the aerobic condition grown initially in LB aerobic were transferred after 7 h ($OD_{600Nm}$=0.2) in DM medium before they reached the stationary phase (**Figure 2.1 A)**. Due to its lower strength, DM medium result in lower stationary OD and slower growth rate (**Figure 2.1 A)**. The growth rate under aerobic conditions was however, faster than under anaerobic ones. In the latter conditions, the bacteria reach stationary phase after 5 h

($OD_{600nm}$= -0.5), while under aerobic conditions, growth was prolonged up to 24 h ($OD_{600nm}$=0.2).

The only difference between the anaerobic conditions in DM medium using the two different electron acceptors is that bacteria reached a higher plateau when grown in presence of fumarate. The optical density was indeed 0.3 in the case of bacteria grown in presence of fumarate, and 0.23 in presence of iron citrate. (**Figure 2.1 B).**

The bacteria grown either under aerobic condition or anaerobic where then injected into the ECs to study *S.loihica PV-4* electrochemical behavior.

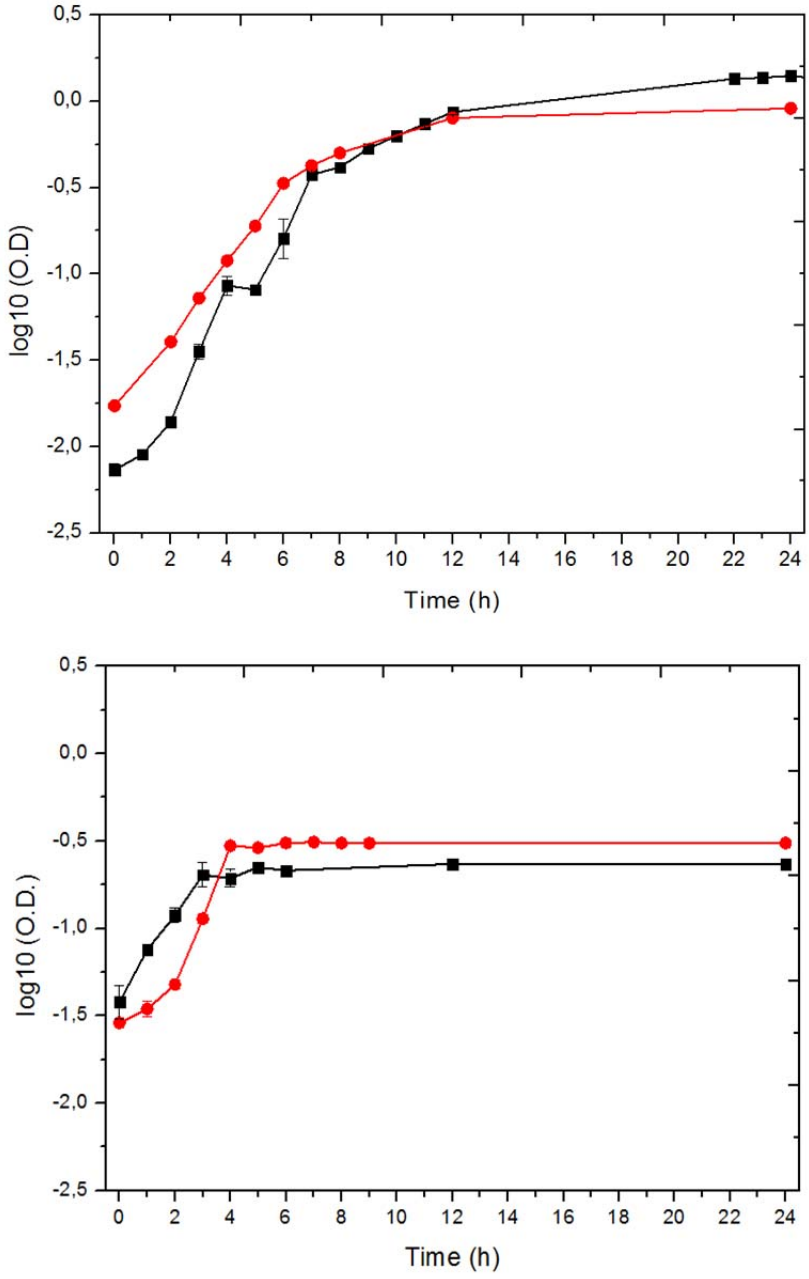


**Figure 2.1:** Growth curves of *S.loihica PV-4.* (**A**) Comparison between LB (red line) and DM (black line) aerobic growth. (**B**) Comparison between DM anaerobic with fumarate (red line) and iron citrate (black line) growth curve.

### 2.3.2 Relationship between the use of different electron acceptor during *S. loihica PV-4* growth on its electroactivity

**Figure 2.2** depicts that bacteria previously grown with iron citrate as electron acceptor were more electro-active than those grown with fumarate. Indeed, the inoculum grown in presence of 40 mM iron citrate produced 110.49± 7 μA/cm$^2$ while 47.7 ± 5 μA/cm$^2$ were produced when 20 mM fumarate was used as electron acceptor.

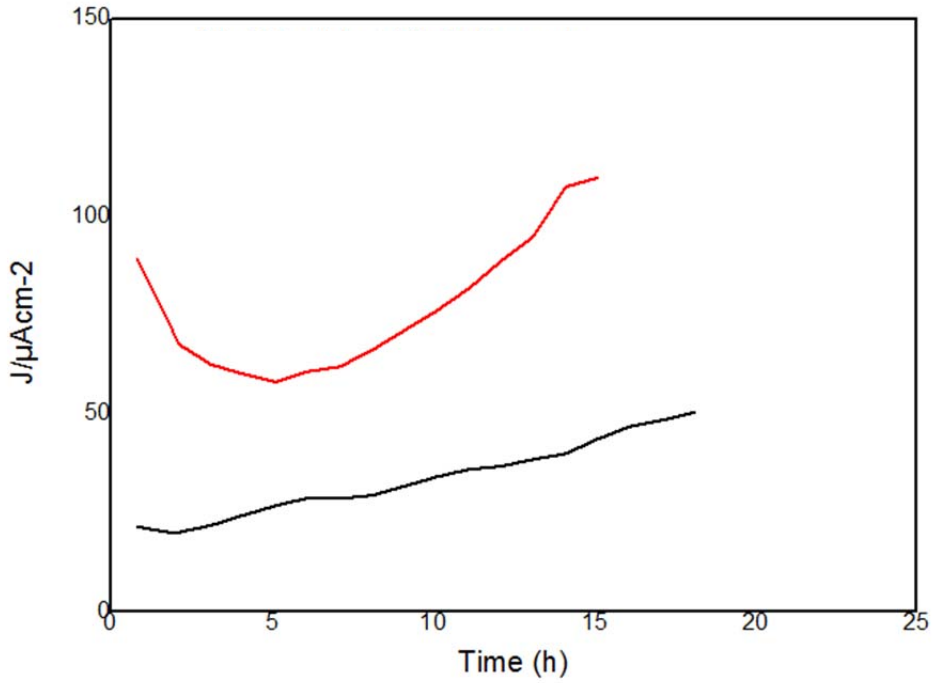


**Figure 2.2:** Chronoamperometry comparison of *S.loihica PV-4* on graphite electrode P240 in presence of different electron acceptors during growth curve in DM medium under anaerobic conditions. **(Red line)** *S.loihica* growth with 40 mM iron citrate, (**Black line**) *S.loihica* growth with 20 mM fumarate. **N=3**

In both conditions 96± 3% of lactate was depleted and converted in pyruvate and/or succinate (**see equation 1 and 2**), with 1.6 ± 3 mM of lactate left in the medium once the current stabilized. Higher electric charge was recorded when iron citrate was used as electron acceptor during the cell growth, with 6.31 C, while 2.7 C in the case of fumarate.

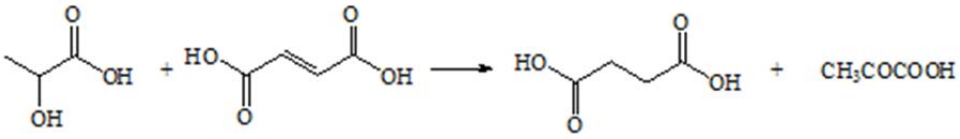

(1)

LACTATE FUMARATE SUCCINATE PYRUVATE

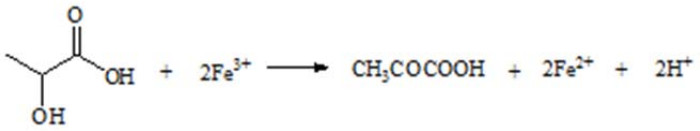

(2)

LACTATE IRON (III) PYRUVATE IRON (II) HYDROGEN $^{+}$

Differential pulse voltammetry in **Figure 2.3** has shown a higher riboflavin (peak centered at -0.44V ± 0.04V) concentration released in the medium of the ECs when iron citrate was used as electron acceptor during the anaerobic growth. Yet, another peak centered at -0.1 V which corresponds to the redox potential of OMCs was found in the case of iron citrate (**Red line**; **Figure 2.3**). This highlight an adjustments of the specific EET pathways in response to these two different electron acceptors. Thus, there is an overlapping of the two EET mechanisms independently from the electron acceptor used during the growth curve.

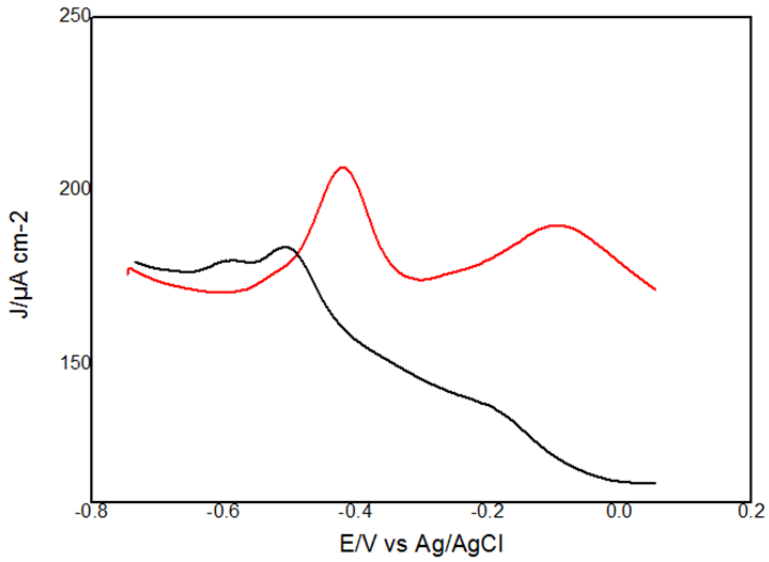


**Figure 2.3:** Differential pulse voltammetry comparison of *S.loihica PV-4* on graphite electrode P240 in presence of different electron acceptors during growth curve in DM

medium. **(Red line)** *S.loihica* growth with 40 mM iron citrate, (**Black line**) *S.loihica* growth with 20 mM fumarate. **N=3**

The first derivative of CVs of *S. loihica PV-4* shown that the peak centered at -0.1 V is actually also visible when fumarate was used as electron acceptor during the anaerobic growth in DM medium, but this peak was totally irreversible, as shown by the absence of the cathodic peak. This means that either the kinetic of electron transfer is so slow that it is impossible to maintain the Nernstian equilibrium, or there could be a fast following chemical reaction. Yet, the peak current (Ip) decreases when fumarate was used as electron acceptor prior to inoculation into ECs (**Figure 2.4**) for both riboflavin and OMCs.

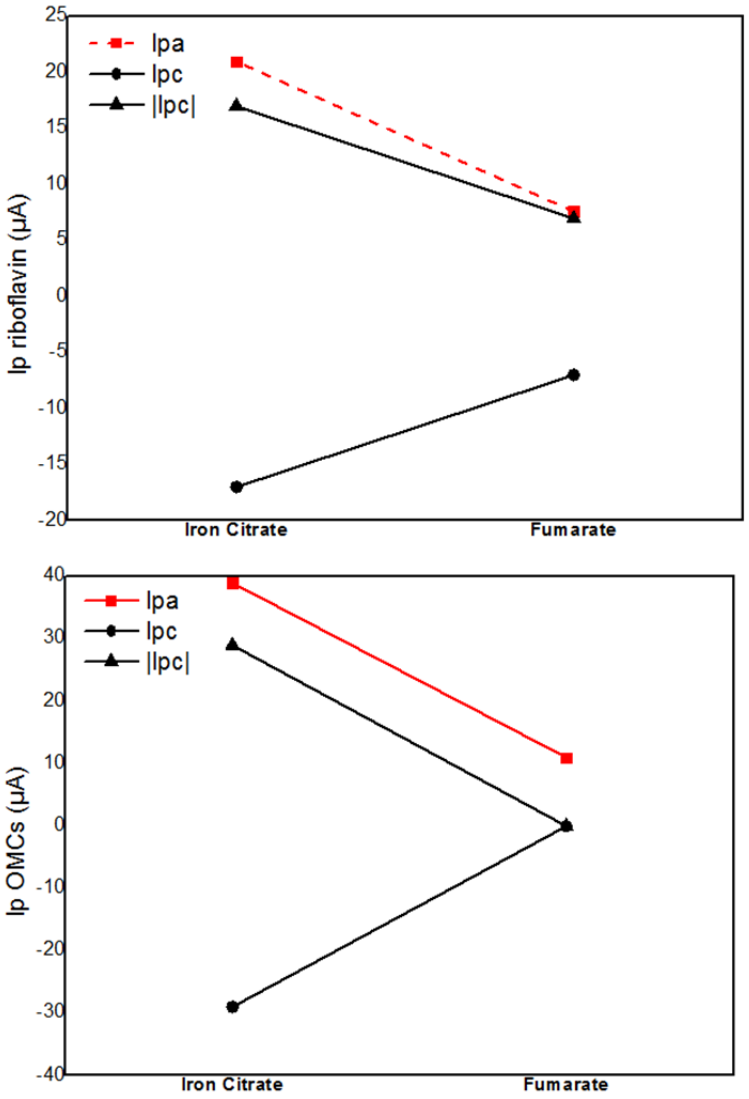

**Figure 2.4:** Anodic and cathodic current intensity of the peak centered at -0.44V and -0.1 V vs. time of *Shewanella loihica PV-4*. (**Top panel**) Ip related with the riboflavin (-0.44V), (**Bottom panel**) Ip related with OMCs (-0.1V).

While, when iron citrate was used as electron acceptor both peaks centered at -0.44V± 0.06 V and -0.1V resulted reversible (**Figure 2.5; Redline; Bottom panel**), suggesting a better promotion of electron transfer between cells and electrode.

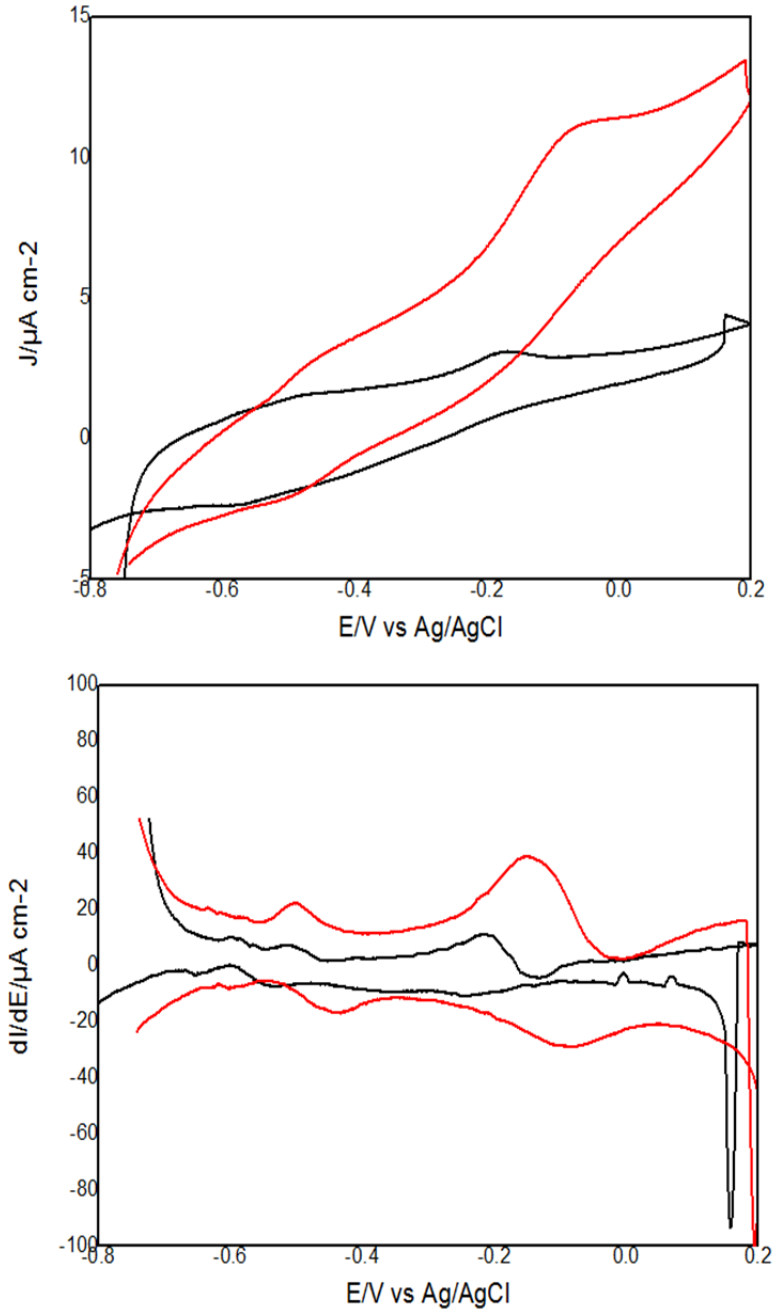


**Figure 2.5:** Cyclic voltammetry comparison of *S.loihica PV-4* graphite electrode P240 in presence of different electron acceptors during growth curve in DM medium. **(Red line)**

*S.loihica* growth with 40 mM iron citrate, (**Black line**) *S.loihica* growth with 20 mM fumarate. **(Top panel)** Cyclic voltamogram once current stabilized; **(Bottom panel)** First derivatives of corresponding CVs. **N=3**

### 2.3.3 Effect of lactate concentration on EET in *S.loihica PV-4*

A small lactate concentration (10 mM) resulted in lowest current production with 44.52± 6 $\mu Acm^{-2}$ (**Figure 2.6**) when compared with 20 mM lactate which resulted in higher current production with 106 ± 5 $\mu Acm^{-2}$ produced. Surprisingly, the current output was only 18.86 ± 0.5 $\mu Acm-^{2}$ and with a big lag phase when 40 mM of lactate was used as carbon source, possibly because of substrate inhibition. Lactate consumption was evaluated by HPLC once the current had stabilized in all the conditions studied. The residual lactate concentration in the spent medium is reported in Figure 2.6 upon the corresponding curves. Once current had stabilized, lactate was completely consumed in the case of 10 mM carbon source. In the other two cases 0.22 mM and 5.32 mM lactate were left when 20 and 40 mM lactate where respectively used as carbon source. These findings suggest that the differences in current densities are not related to a change in the metabolic rate with which *S. loihica PV-4* consumes a carbon source for extracellular electron transfer.

According to the equation 3 (Lovley *et al*., 1989, 1992):

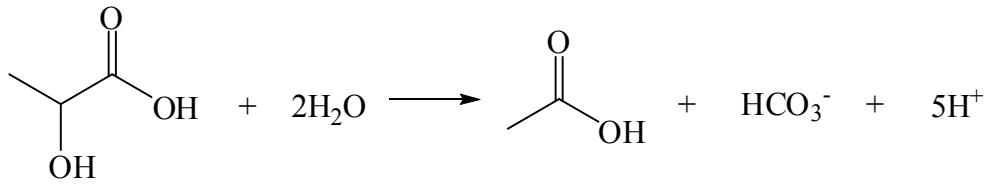


**(3)**

The coulombic yield based on partial lactate oxidation ($4e^{-}$ $mol^{-1}$ lactate) was much higher when 20mM lactate was used as carbon source (25.63 ± 3.11%) compared with the other concentrations. Similar lower values were found when 10 and 40 mM carbon source were used (4.43± 8.5 % and 6.35 ± 2.3 %).

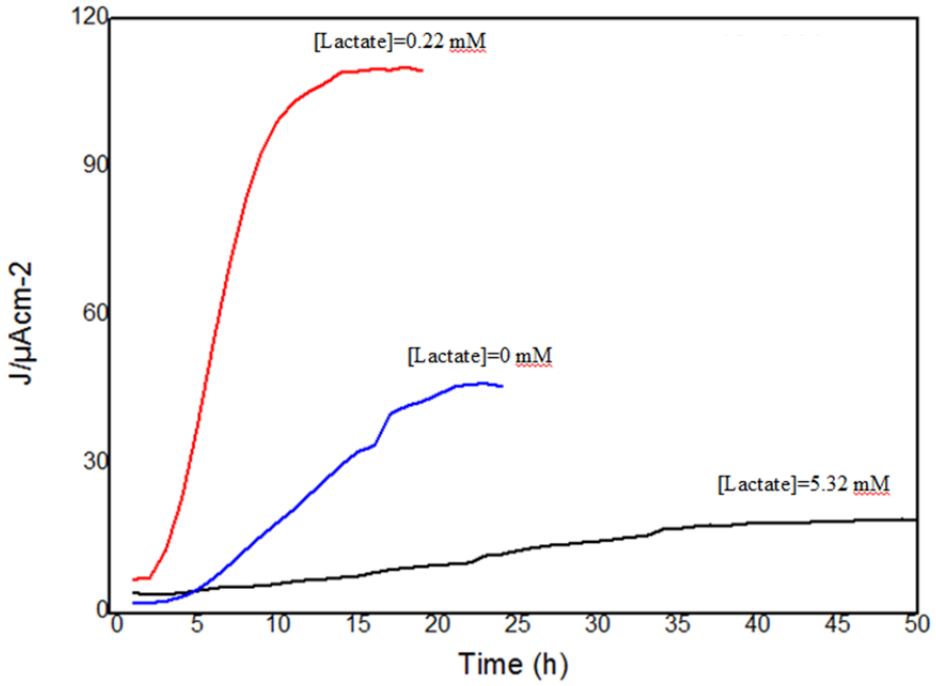


**Figure 2.6:** Chronoamperometry comparison of *S.loihica PV-4* on graphite electrode P240 in presence of different concentrations of carbon source. **(Red line)** 20 mM lactate, (**Blue line**) 10 mM lactate, (**Black line**) 40 mM lactate. N=3

By looking at the differential pulse voltammogram (**Figure 2.7**) a clear peak is visible at -0.44V, corresponding to the electron shuttle named flavin. The concentration of the riboflavin (i.e., the height of the DPV peak) correspond roughly to current density output (**Figure 2.6**), indicating that lactate concentration affects both cell growth in the biofilm (direct electron transfer) and planktonic cells (mediated electron transfer), as also confirmed in previous study by Wu *et al.*; (2014). Our results are compatible with those by Longfei and Verwoerd, (2014). Indeed, they have shown that further increase in lactate uptake rate (>11.05 mmol/gDW/h) can lead to a plateau of the flavin production, thus the conversion of the substrate into electricity.

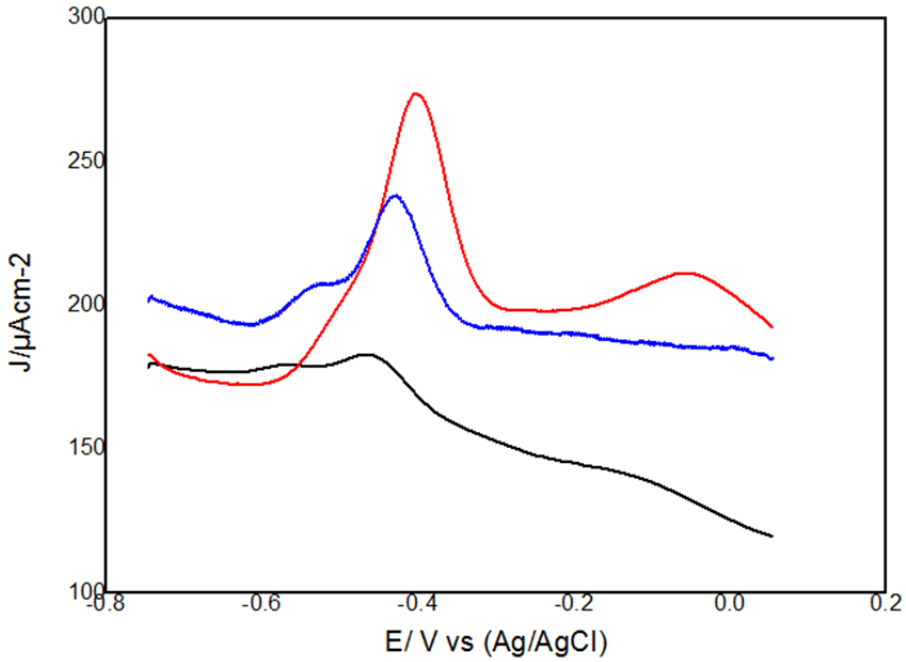


**Figure 2.7:** Differential pulse voltammetry comparison of *S.loihica PV-4* on graphite electrode P240 in presence of different concentrations of lactate as carbon source. **(Red line)** 20 mM lactate, (**Blue line**) 10 mM lactate, (**Black line**) 40 mM lactate. N=3

Cyclic voltammetry illustrates well-defined sigmoidal curve when 20 mM lactate were used. This suggests that when 20 mM lactate are used as carbon source, *S.loihica* forms a more stable and conducting biofilm-electrode than when 10 and 40 mM where used (**Figure 2.8; Top panel**) with an increasing of current flow from 10 to 20 mM lactate, as well as from 40 to 20 mM, which confirms the CAs results in Figure 2.2.First derivative of the corresponding CVs (**Figure 2.8; Bottom panel**) shows two redox centers **RC (i)** = -0.1 ± 0.04 V and **RC (ii)** = -0.44V ± 0.03 V. From previous study RC (i) is related to the OMCs at the biofilm/electrode interface (Jain *et al.*; 2012). Whereas, the RC (ii) is related to the soluble electron shuttle named riboflavin (Von Canstein *et al.*; 2008). These results indicate that an overlapping of the two EET mechanisms occurs under all the conditions studied.

The Ip (Anodic and cathodic current) of the two peaks are shown as a function of the lactate concentration in **Figure 2.9**. The heights of oxidation and reduction peaks increased from 10 mM to 20 mM of lactate but then decreased again when 40 mM lactate were used.

The value of |Ipa/Ipc| approaches to 1 for both **RC (i) and RC (ii)** with the increasing of lactate from 10 to 20 mM. This reflects and improvement of the reversibility of the reactions at the electrode surface when 20 mM lactate were used. Whereas, in the case of 40 mM lactate the value |Ipa/Ipc| increased.

Thus, 20 mM concentration of lactate was chosen for further studies of *Shewanella loihica PV-4* EET (**see section 2.3.3 and 2.3.4 and chapter 3**).

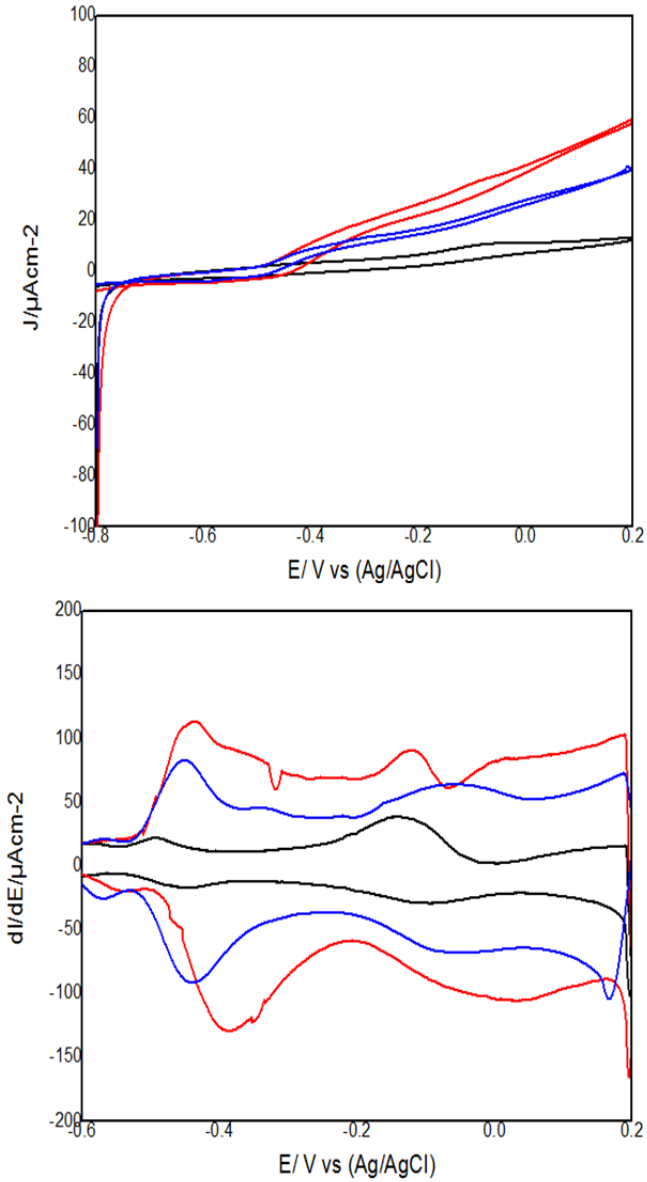


**Figure 2.8:** Cyclic voltammetry comparison of *S.loihica PV-4* on graphite electrode P240 (top panel) and their corresponding first derivatives (bottom panel) in presence of different concentration of carbon source. **(Red line)** 20 mM lactate, (**Blue line**) 10 mM lactate, (**Black line**) 40 mM lactate. N=3

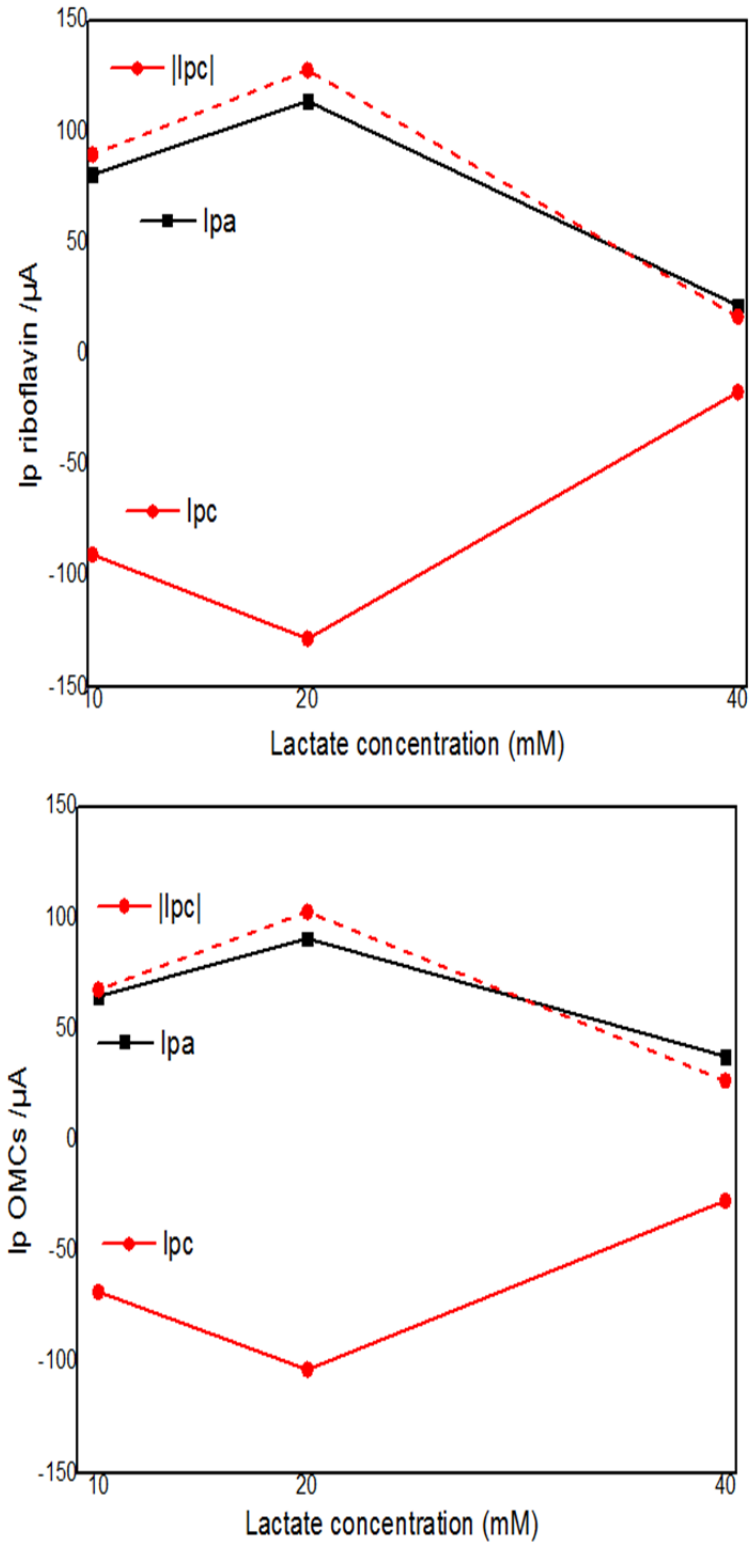


**Figure 2.9:** Anodic and cathodic current intensity of the peak centered at -0.44V and -0.1 V vs. lactate concentration used as carbon source in *S.loihica PV-4.* (**Top panel**) Ip related to the riboflavin (-0.44V), (**Bottom panel**) Ip related to OMCs (-0.1V).

### 2.3.4 Interplay between Direct Electron Transfer and Mediated Electron Transfer

CV of *S.loihica PV-4* cell suspension shows clear sigmoidal shaped curves (**Figure 2.10**) alike to those reported in previous studies (Coursolle *et al*.; 2010, Roy *et al*.; 2010) with the onset of the turnover at -350 mV to – 400 mV.

The corresponding CVs first derivative illustrates that MET (peak centered at -0.44 ± 0.04 V) plays a main role within the first 12 h, and just after also the DET (peak centered at 0.1 ± 0.03 V) starts to interplay a role in the EET (**Figure. 2.11 F-H**).

Another peak centered at -0.2 V is also clearly visible at 12 h after inoculation and it is close to the midpoint of quinone derivates (-0.27 V) thus this peak is also due to the MET (Newton *et al*.; 2009).

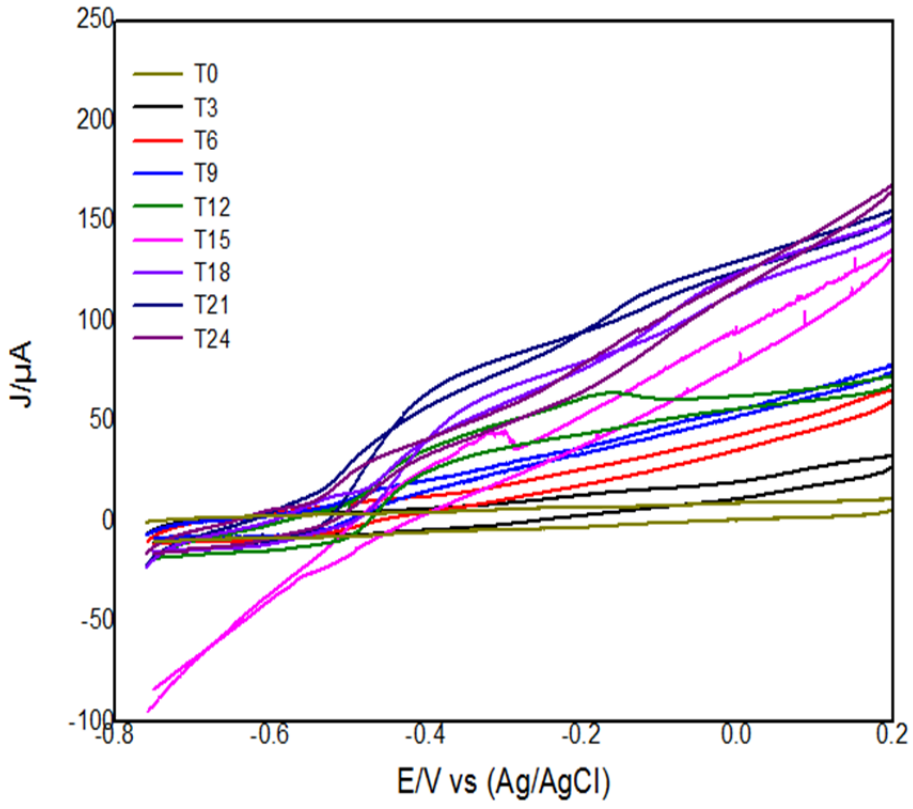


**Figure 2.10:** Cyclic voltammetries of *S.loihica PV-4* on graphite electrode P240 recorded every 3 h till current had stabilized (approx. 21 h) **N=2.**

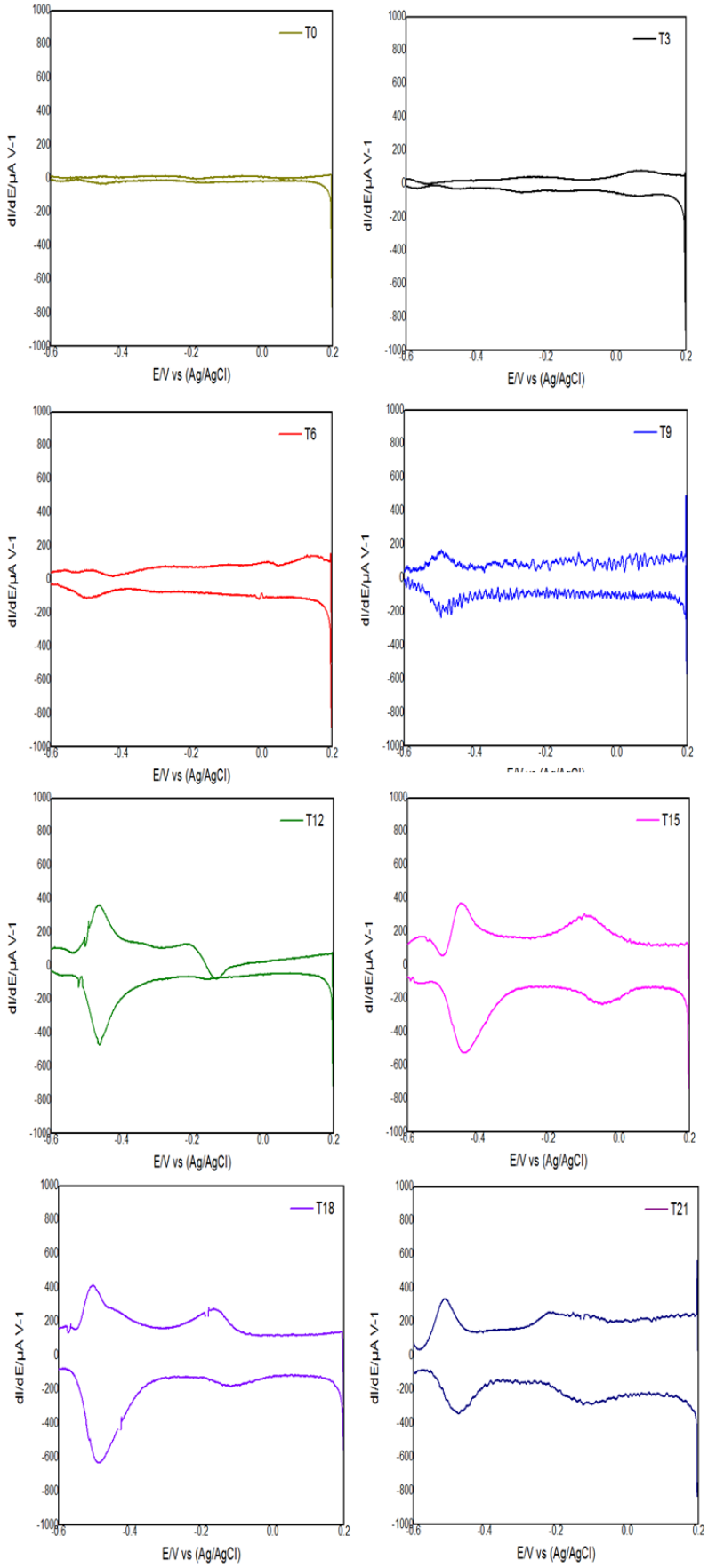


**Figure 2.11**: First derivatives of CVs shown in Figure 2.10.

Riboflavin peak intensity (Ip) increases up to 18 h to then remains quite stable once the current had stabilized at approximately 21 h (**Figure 2.12 top panel**), while OMCs related peak are visible from 15 h until the current intensity stabilized. This suggests that EET in *S.loihica* is mostly based on the MET and only later, DET starts to have a role in the EET.

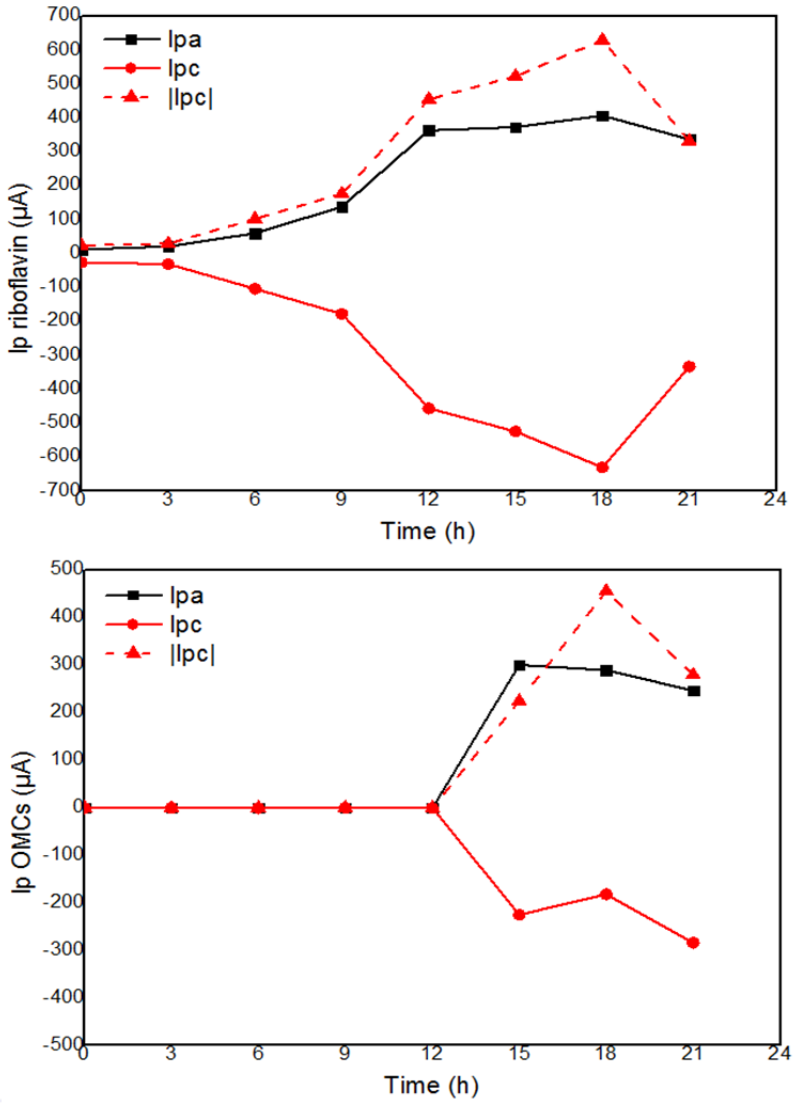


**Figure 2.12:** Anodic and cathodic current intensity of the peak centered at -0.44V and -0.1 V vs. time of *Shewanella loihica PV-4*. (**Top panel**) Ip related with the riboflavin (-0.44V), (**Bottom panel**) Ip related with OMCs (-0.1V).

This can be explained by an essential need for the formation of an extended respiratory chain, where OMCs have a role as transient electron storage while the concentration of carbon source is low and so probably limiting for an active secretion of electron shuttles *(Richter et al.*,2012). Mao and Verwoerd, (2014) demonstrated that the secretion of flavins can preclude the need for direct contact until when the self-synthesized flavins are not sufficient to convey all the available electrons inside the metabolism towards the electrode.

Protein analysis illustrates that planktonic cells start to be attached on the electrode after just 3 h. The cells, however do not form a uniform biofilm (**see SEM image, Figure 3.15A, chapter 3**), they keep getting detached. This indicates that the main role of EET is maintained through the release of riboflavin. This is also confirmed by spectrofluorometer analysis (**Figure 2.13**). In particular, the resulting excitation peak centered at 445 nm was used to calculate the riboflavin concentration; this is because in aqueous solution, the electronic spectrum of riboflavin consists of three bands centered at 265, 375, and 445 nm. While the 375 nm band is sensitive to solvent effects, and blue-shifts as solvent polarity decreases, the 445 nm band shows a smaller red-shift as solvent polarity decreases.

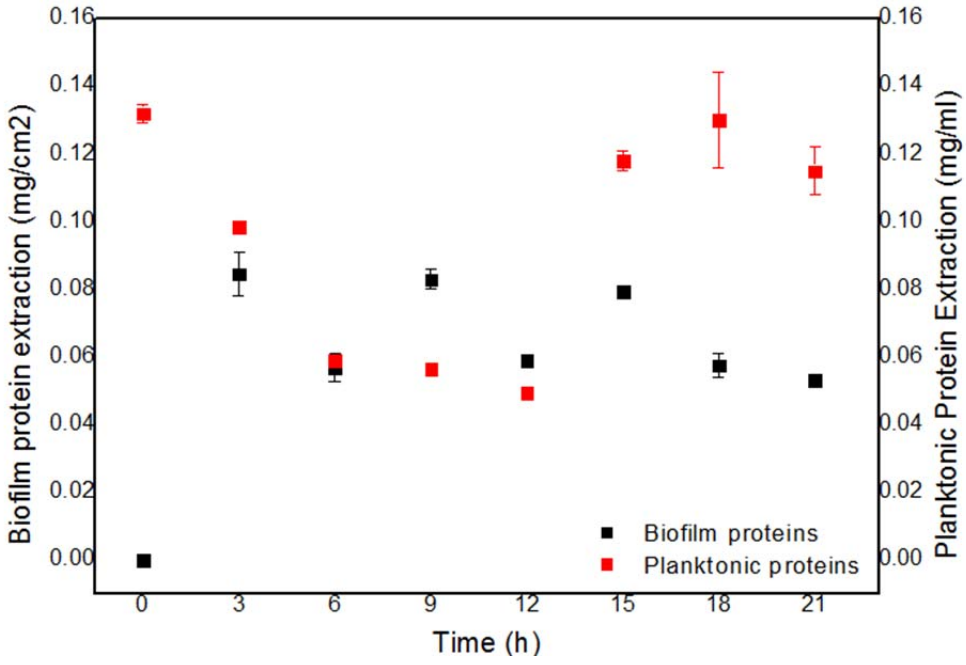


**2.13** Planktonic and biofilm protein extracts of *S.loihica PV*-4 vs. time

The riboflavin concentration increases also when DET starts to have a role in the EET (time 15-21 h). Yet, the quantity of electric charge nearly double at 21 h from 4 ± 0.5 C to 8.39 ±0. 4 C along with riboflavin concentration which increases from 1± 0.1 mM to 1.7± 0.2 mM (**Figure 2.14**).

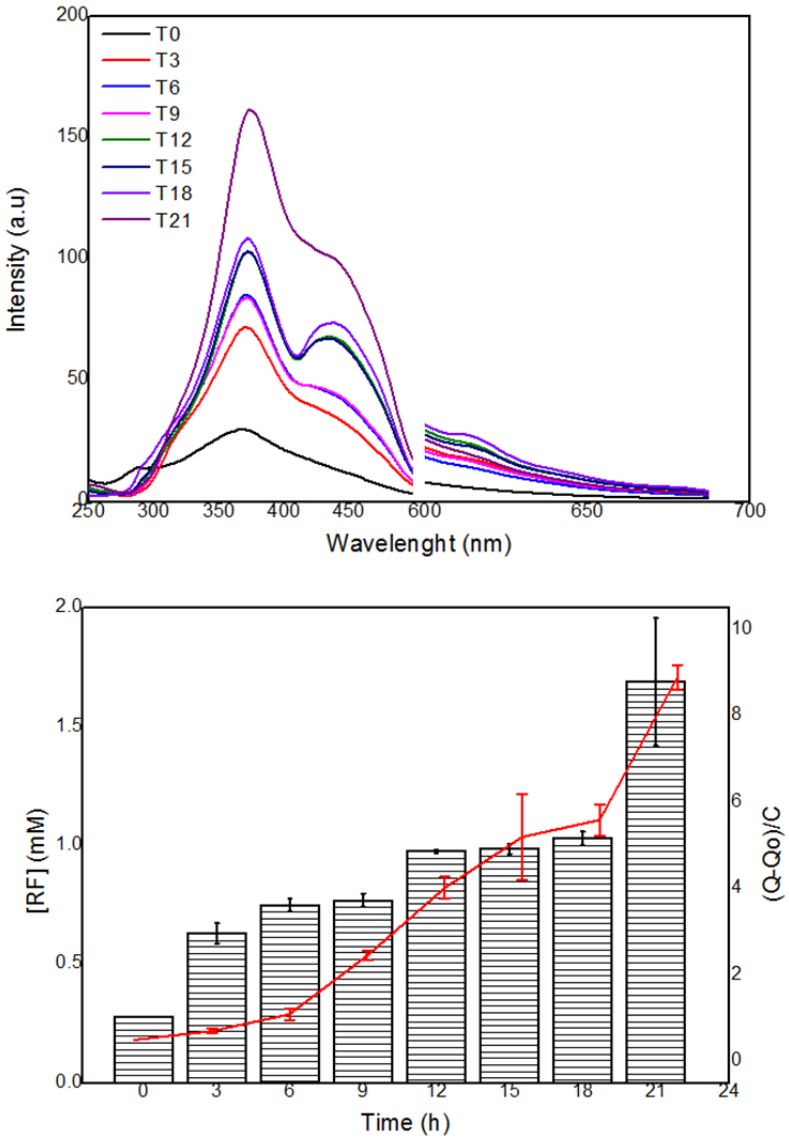


**Figure 2.14:** Fluorescence excitation and emission spectra (**A**) of the cell free supernatant collected from inoculation into ECs to current stabilization (approx. 21 h) from *S.loihica PV-4* biofilm associated with graphite electrode P240; (**B**) Riboflavin concentration vs. time (**histogram**) and electric charge flux from the cells to the electrode surface (**red line**).

## 2.4 Conclusions

It was demonstrated that both electron donor and acceptor play an important role in the electrochemical performances of *S.loihica PV*-4 thus maximizing its electroactivity.

In particular, amongst three different concentrations of lactate, the highest electroactivity (~26 %) was recorded using 20 mM of lactate than using 10 and 40 mM.

Yet, when three different electron acceptors ($O_2$, iron citrate and fumarate) were used during the bacteria growth prior inoculation into the ECs, *S.loihica PV-4* resulted differently electroactive when the electrochemical experiments were performed.

Indeed, when the bacteria were grown in presence of iron citrate, nearly 50% higher current was recorded when compared with the bacteria grown in presence of fumarate. This condition was also compared with the aerobic growth in order to support the hypothesis in which *S. loihica PV-4* grown in anaerobic condition would be more electro-active than its aerobically-grown counterparts.

However, the anaerobic inoculum did not show a higher current output than the aerobic counterpart, conversely it resulted to behave likewise. In fact, 110.49 $\mu Acm^{-2}$ and 106 ± 5 $\mu Acm^{-2}$ were respectively produce by the anaerobic inoculum (iron citrate as e- acceptor) and the aerobic one.

This result discourage the use of the anaerobic inoculum in effort to develop a novel inoculum-preparation protocol which maximizes *S. loihica*'s electroactivity. Yet, by taking into account that a much more laborious protocol is needed to prepare the anaerobic inoculum, this condition was discarded and only the aerobic condition was use for further study on *S.loihica PV-4* electroactivity.

Other experiments will be based on the need to clarify the interplay between mediated electron transfer and direct electron transfer and how one mechanism or the other or the cooperation of the two of them is affected by the surrounding environment (electrode material and surface).

In the next chapters, it will be discussed how the removal of riboflavin from the inoculum as well as the use of different electrode materials, roughness and coatings (air plasma and carbon nanotubes) will affect the EET mechanism in *S.loihica PV-4* in potentiostat controlled ECs.

# CHAPTER 3

# INVESTIGATION OF SYSTEM DESIGN PARAMETERS

(**Part 1**: Electrode surface abrasion and functionalization)

***Related publication***

**Monica Epifanio**, Saikumar Inguva, Michael Kitching, Jean-Paul Mosnier, Enrico Marsili (2015) Effects of atmospheric air plasma treatment of graphite and carbon felt electrodes on the anodic current from *Shewanella* attached cells; Bioelectrochemistry.

**Abstract**

The attachment of electrochemically active microorganisms (EAM) on an electrode is determined by both the chemistry and topography of the electrode surface. Pre-treatment of the electrode surface by atmospheric air plasma introduces hydrophilic functional groups, thereby increasing cell attachment and electroactivity in short-term experiments. In this study, we use graphite and carbon felt electrodes to grow the model EAM *Shewanella loihica PV-4* at oxidative potential (+0.2 V vs. Ag/AgCl). Cell attachment and electroactivity are measured through electrodynamic methods. Atmospheric air plasma pre-treatment increases cell attachment and current output at graphite electrodes by 25%, while it improves the electroactivity of the carbon felt electrodes by 450%. Air plasma pre-treatment decreased the coulombic efficiency on both carbon felt and graphite electrodes by 60% and 80%, respectively. Microbially produced flavins adsorb preferentially at the graphite electrode, and air plasma pre-treatment results in lower flavin adsorption at both graphite and carbon felt electrodes. Results show that air plasma pre-treatment is a feasible option to increase current output in bioelectrochemical systems.

## 3.1 Introduction

The goal of this study was to ascertain the contribution of the electrode materials and surface roughness in *S.loihica PV-4* biofilm current production. Another parameter, which was taken into account was the effects of atmospheric air plasma pre-treatment on the current output from attached *S. loihica PV-4* cells on different electrode materials. The electrode materials used were graphite, polished with various levels of roughness of sandpapers (P240> P400> P600) and carbon felt electrodes. It was demonstrated that plasma pre-treatment increases the maximum current output and adsorption of microbially produced flavins, which are the main driver for electricity production.

## 3.2 Materials and Methods

### 3.2.1 Bacterial strain

*S. loihica PV-4* (DSM 17748) was purchased from DSMZ (Germany). Stock cultures were prepared by transferring 1 mL of actively growing culture to a cryo-tube containing 0.5 mL of 50% DMSO and storing at −80 °C.

### 3.2.2 Microbiological methods

*S. loihica PV-4* was cultured in Luria-Bertani medium (LB) and incubated at 30 °C for 24 h on an aerobic rotary shaker at 150 rpm. 2 μM $MgSO_4$ and 0.1 μM $CaCl_2$ were added as growth stimulants for the early exponential phase. Three milliliters of the culture at optical density OD600 = 1.0 was then added to 30 mL of defined medium (DM) containing per liter: $NaHCO_3$ 2.5 g, $CaCl2{\cdot}H_2O$ 0.08 g, $NH_4C_l$ 1 g, $MgCl_2{\cdot}6H_2O$ 0.2 g, NaCl 10 g, HEPES buffer 7.2 g, yeast extract 0.5 g, trace mineral solution 10 mL, and vitamin solution 1 mL (Rob *et al.*, 2006). pH was adjusted to 7.6 through the addition of 0.1 M HCl, 20 mM of lactic acid was used as the carbon source and 5 g $L^{-1}$ filter-sterilized casaminoacids was used as a growth stimulant.

The cells were grown aerobically in defined medium at 30 °C for 24 h, under shaking condition at 150 rpm. In the **unwashed inoculum** experiments, 5 mL of the bacterial suspension were then directly injected in each electrochemical cell and added to 5mL of fresh defined medium with 40 mM lactate and no added riboflavin. In other '**washed inoculum'** experiments, 5 mL of the bacterial suspension was centrifuged for 10 min at 5000 rpm, the

bacterial pellet was resuspended in 10 mL of fresh defined medium with 20mM lactate and no added riboflavin, and then injected into the electrochemical cells. The washing procedure ensures removal of microbially-produced soluble redox mediators.

### 3.2.3 Electrode preparation

The carbon felt and graphite (isotropic graphite Grade 347 from Tokai Carbon Co. Japan) sheets were both cut into 2 × 1 × 0.2 cm electrodes, defining a geometric surface area of 5.2 $cm^2$. Current output values were normalized to the electrode surface area. The graphite electrodes were sanded with either P240 (grit diameter 58.5 μm), P400 (grit diameter 35 μm) or P600 (grit diameter 25.8 μm) P-graded sandpapers in order to obtain different surface roughness. The roughest graphite electrode surface was thus obtained by polishing with P240 sandpaper. All electrodes were cleaned overnight in 1 M HCl and then stored in deionized water. Some of the P240 graphite and carbon felt electrodes were also plasma pre-treated.

### 3.2.4 Plasma pre-treatment

The plasma apparatus used in this work has been described in detail previously (Connolly *et al*., 2013). Oscilloscope traces of the discharge current patterns show that the atmospheric air plasma is typical of a dielectric barrier discharge (DBD). Such DBD plasmas are out of equilibrium (nonthermal) plasmas characterized by electron temperatures of the order of 1 Ev while the gas remains at room temperature and by the abundant production of reactive oxygen species such as ozone and atomic oxygen (Connolly *et al*.,2013, Becker *et al*., 2005) . The carbon felt and graphite electrodes were placed inside a commercial 5 L zip-lock polyethylene bag and in-between the pair of high-voltage discharge electrodes separated by a 1 cm gap. The plastic package ensured containment of the active gaseous species during operation. The plastic bag was flushed with ambient air, then zip-lock sealed and the 15 kV high-voltage, 50 Hz source switched on for 120 s, producing a discharge power of ~0.1Wcm−2. These operational conditions were typical of those required for surface functionalization via DBD air-plasma treatment (Becker *et al*., 2005).

### 3.2.5 Electrochemical cell set-up

A 5 channel potentiostat (VMP, BioLogic, France) was connected to three-electrode cells described (**Figure 1**). These three-electrode potentiostat-controlled electrochemical cells (Bioscience, Ireland) were closed by a custom made Teflon lid. Electrode capillaries were inserted through ports in the custom made Teflon lid which was sealed with an O-ring gasket.

This lid fit onto a 20 mL conical electrochemical cell (Bioscience, Ireland), which had been previously washed in 8 M $HNO_3$ . After the addition of a small magnetic stir bar, and 10 mL of deionized water, the cell was autoclaved for 20 min. Following autoclaving, the salt bridge was filled with 0.1 M $Na_2SO_4$ in 1% agar. A saturated reference electrode (Fisher Scientific, Ireland) was placed at the top of this agar layer and covered in additional 1 M $Na_2SO_4$ to ensure electrical contact. The reactors were connected to a water bath kept at 32 °C to maintain cells at 30°C. To maintain the strict anaerobic conditions required by bacteria, all reactors were operated under a constant flow of sterile humidified $N_2$:$CO_2$ (80:20 [vol/vol]), which had been passed over a heated copper column to remove trace oxygen. Each reactor was located above an independent magnetic stirring unit.

Autoclaved bioreactors flushed free of oxygen, filled with sterile and anaerobic DM medium and incubated at 30°C were analysed before each experiment to verify anaerobicity and the absence of redox-active species. Electrochemical cells showing residual peaks in differential pulse voltammetry (DPV), or baseline noise were discarded as possibly having possible electrode cleanliness or connection noise issues. These autoclaved, verified bioreactors were then used for growth of cultures.

Spent growth medium was replaced with fresh growth medium at approximately 22 h. Cyclic voltammetry (CV), differential pulse voltammetry (DPV), and electrochemical impedance spectroscopy (EIS) were performed after inoculation (t = 0 h), before medium change (t = approx. 22 h), after the medium change (t = approx. 22–24 h), and at the end of the experiment (t= approx. 48 h).

### 3.2.6 Chronoamperometry and electrochemistry measurements

The electrical current produced by cells colonizing the working electrode was measured over a period of approximately 48 h on a Bio-Logic VMPR Multichannel Potentiostat. Measurements were performed via an electrochemical procedure known as chronoamperometry. Chroamperometry (CA) is the quantification of the net flow of electrons in or out of a working electrode while that electrode is established at a constant electric potential. During all CA experiments the working electrode was poised at a + 0.2 V vs. Ag/AgCl and electrical current was measured every 900 s. The chamber was stirred during chronoamperometry to reduce the limiting effects of lactate diffusion on electrical current production. Once current reached the plateau, CA was stopped; DPV was performed, followed by another 24 h of CA.

CV was begun from an Ei of –0.8 V vs. Ag/AgCl and ended at an E of 0.2 V vs. Ag/AgCl. The scan direction was then reversed and the potential was swept back to the original E value of -0.8 V vs Ag/AgCl. CV was performed at a scan rate of 1.0 mV $s^{-1}$. CV was always followed by DPV. DPV was also performed immediately after the inoculation of the electrochemical cell and after medium replacement. DPV was begun from an Ei of –0.8 V vs. Ag/AgCl and ended at an Ev of 0.2 V vs Ag/AgCl. DPV scan rate was 4 mV/s. DPV and CV were always performed without stirring to avoid influencing the results with the implementation of faster diffusion.

### 3.2.7 Atomic force microscopy (AFM)

AFM (Dimension 3100 controlled by a NanoScope IIIa controller, Digital Instruments, USA) was used to determine the surface morphology of P240, P400, and P600 graphite electrodes. Carbon felt electrodes could not be imaged with AFM, as the AFM tip remained entangled in the carbon felt thin fibre. Images were taken in tapping mode, using standard aluminum coated silicon AFM probe (Tap 300Al-G, Budget Sensors, Bulgaria) with a force constant of 40 N $m^{-1}$. The AFM images were acquired by scanning areas of dimensions 20 μm ×20 μm with a fixed resolution of 512 × 512 pixels. Although a precise evaluation of the resolution would require the knowledge of the AFM tip shape and size, we can estimate, from the knowledge of standard AFM performance and the present acquisition conditions, the lateral and vertical (z-axis) resolutions to be at least 50 nm and greater than 1 nm, respectively. The latter value, quite lower than typical AFM performance, is due to the inherent roughness of the bare graphite electrode (A.Jain *et al*., 2013), which tends to blunt the tip during scans. Where possible, AFM scans for the electrodes were repeated several times at different locations over the electrode surface. The surface rms roughness (Rq) of each electrode was evaluated from image pixel data analyses using the WSXM software (I. Horcas *et al*., 2007). The Rq value is specified in this work, instead of the average roughness (Ra), as Rq is more sensitive to large differences in the surface peaks and valleys, which allows for the effects of plasma treatment at the sub-μm level to be better ascertained.

3.2.8 Confocal microscopy

*S. loihica PV- 4* biofilms grown on diverse roughness graphite electrodes (P240, P400 and P600) either treated with plasma or not was collected approximately after 24h of the EC operation. The samples were removed from the EC in an anaerobic chamber (Coy Laboratory, USA), followed by staining for 30 min in 1 mg $mL^{-1}$ acridine orange. After rinsing with DM medium to eliminate excess of dye, the samples were fixed on a glass slide with a super glow. The electrodes were then covered on the top with a square glass slide cover. Two blank electrodes were used to balance the differences of height between the two cover glasses between the electrodes. The confocal images were captured with a laser scanning microscope (Zeiss LSM 510, USA), using argon laser 488 nm as excitation source. The objective was 20X, with numerical aperture 1.40. Fluorescence was recorded with a low pass filter at 505 nm.

**3.2.9 Chemical analysis**

Lactate concentration from electrochemical cells supernatant was measured via high performance liquid chromatography instrumentation (Shimadzu, Japan), using a Supelcolgel C-610 carbohydrate column with integrated guard column (Sigma-Aldrich, Ireland). The flow rate was 0.5mL min−1 and column temperature was 35 °C. The expected retention time for lactate in the columnwas 17.61 min, with 0.09% uncertainty. The coulombic efficiency of each growth culture was calculated according to **equation 1** (Logan *et al*., 2008):

$$\text{Coulombic efficiency} = \frac{M_s \int_0^{t_b} I dt}{Fb_{es} V_{Cell} \Delta c} 100 \qquad \textbf{(1)}$$

where Δc is the change in lactate concentration over the time tb, Ms is the molecular weight of lactate, I is the current output, F is the Faraday constant (96,485 C $(mol\ e^{-})^{-1}$), Vcell is the volume of the electrochemical cell, and bes are the moles of electrons exchanged during the partial oxidation of lactate to acetate. The integral of the current over tb was calculated through the EC-Lab electrochemical software.

### 3.2.10 Determination of adsorbed and soluble flavins in viable cultures

Riboflavin, a close analogue to microbially produced flavins, was calibrated by DPV and fluorescence spectroscopy (JASCO FP FP-8300, USA) in order to understand its later released concentration in the medium by *S. loihica PV-4* (detected by fluorescence spectroscopy) under turn-over condition in presence of different electrodes, and the its absorbed concentration (DPV) on the different electrode material (**see Appendix section**, **Figure A1-2**).

#### 3.2.10.1 Absorbed riboflavin on different electrode materials: Detection by Differential Pulse Voltammetry

Riboflavin (Fisher Science, Ireland) was added to defined medium in the concentration range from 0 to 5 μM and DPV was performed after each riboflavin addition. Riboflavin was calibrated on both sterile carbon felt and P240 graphite electrodes, with and without atmospheric plasma pre-treatment. The riboflavin peak height was centered at −0.45 ± 0.05 V. Calibration points were fitted to a straight-line equation. The fitting parameters from riboflavin calibration on sterile electrodes (see **Appendix 1; Fig.A1** ) were used to estimate the concentration of microbially produced flavins in growth cultures at various stages, named as **AI** = after inoculation; **BMC** = before medium change, 20-22 h; **AMC** = after medium change, 22-24 h; **END** = end of the experiment, ~48 h.

#### 3.2.10.2 Secreted riboflavin in presence of different electrode materials: Detection by Fluorescence Spectroscopy

Standard solutions of riboflavin (Fisher Science, Ireland) in concentration range from 0 to 5 μM were prepared in DM medium and analysis by spectrofluorometer (JASCO FP FP-8300, USA) was undertaken. The resulting peaks and their intensity were fitted to a straight-line equation and the corresponding linear equations were used to determine flavins in the supernatant of viable cultures at 22 and 48 h. In particular, the resulting excitation peak centered at 445 nm was used to calculate the riboflavin concentration; this is because in aqueous solution, the electronic spectrum of riboflavin consists of three bands centered at 265, 375, and 445 nm. While the 375 nm band is sensitive to solvent effects, and blue-shifts as solvent polarity decreases, the 445 nm band shows a smaller red-shift as solvent polarity decreases. In brief, the supernatant was centrifuged at 13,500 rpm for 10 min and then

residual cells were removed through filtration on 0.22 μm filters (Millipore, USA). The emission spectra (450-700 nm) at excitation wavelength of 372 nm and the excitation spectra (250-530 nm) at emission wavelength of 540 nm were recorded.

### 3.2.11 Electrochemical impedance spectroscopy (EIS)

EIS measurements were carried out at approximately 48 h, when the current output stabilized for P240 and carbon felt electrodes either treated or not with air plasma. The frequency range used was from 100 kHz to 50 mHz with an AC signal of 30 mV amplitude. EIS was begun from an Ei of –0.8 V vs. Ag/AgCl and ended at an Ev of 0.2 V vs Ag/AgCl, and it was always performed without stirring.

### 3.2.12 Contact angle measurement

The water contact angle (WCA) measurements were taken on carbon felt (CF) and graphite electrodes (P240-400-600-1000) before and after air plasma treatment (see section 3.2.4 )by a computer-controlled WCA commercial instrument (FTA200 USA) implementing the sessile drop technique. In all the WCA experiments, high-purity water was used and released at a flow rate of 1.5 μL/s from a needle tip 2 mm above the electrode surface.

### 3.2.13 Scanning Electron Microscopy (SEM)

Biofilms on electrodeswere fixed with 5% glutaraldehyde for 30min and then dehydrated step-wise with ethanol (30%, 50%, 70%, 90% and 100%) for 5 min each step. Following dehydration, electrodes were sputtered-coated with gold (60 s, 40 μA) and then imaged with a Hitachi-S3400 SEM (Hitachi, Japan) at 20 kV using a secondary electron detector. For graphite electrodes a sample site was imaged at ×1.0 k magnification and 10 sub-samples were subsequently taken at ×10.0 k magnification to observe a representative sample of the bacterial coverage. For carbon felt, which comprised a non-linear surface, the total area was divided into quadrants. One sample site, comprising one strand, was imaged at ×1.0 k magnification in each quadrant and three subsequent samples at ×10.0 k magnification were imaged. In these conditions, the SEM images represent electrode surface areas of dimensions (L ×W) 130 μm×96 μm. Features with typical length scales of at least several μm, e.g., single fiber of carbon felt, are thus clearly resolved in the SEM images.

## 3.3 Results

### 3.3.1 Chronoamperometry and electrochemistry measurements

#### 3.3.1.1 Effect of electrode roughness on current output in *S. loihica PV-4* attached cells

Previous studies with *G. sulfurreducens* have shown that the rougher surface obtained with sandpaper polishing treatment increased the current output in electrochemically active biofilms (Marsili *et al*., 2008). Here similar results were obtained with P240, P400, and P600 sanded graphite electrodes. The lag phase increased with the P-grade of the sandpaper used, e.g., 240 < 400 < 600, from 2 to 6 h and the maximum current density in the initial growth phase (approx. 15–20 h) decreased from 104 ± 9 to 67±2 μA $cm^{-2}$, respectively (**Figure 3.1**).

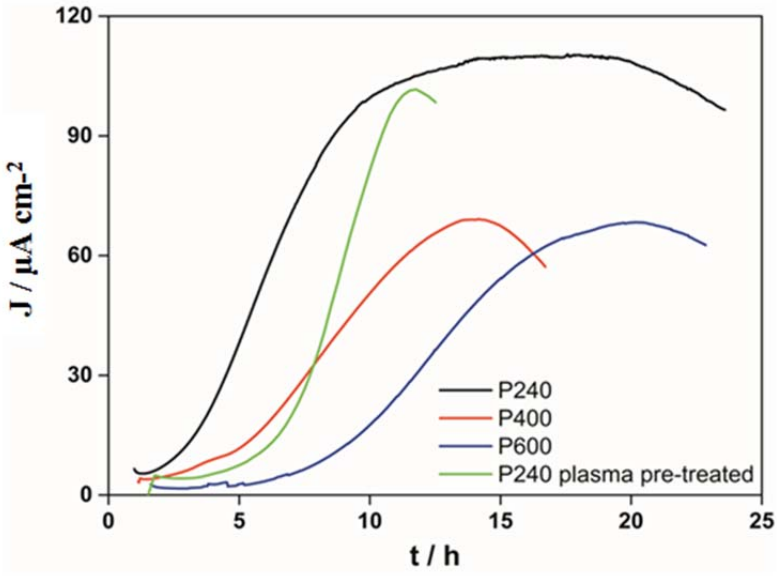


**Figure 3.1:** Initial current output for *S. loihica* growth cultures on graphite electrodes polished with P240 (**black**), P400 (**red**) and P600 (**blue**), and P240 air plasma pre-treated graphite (**green**). Unwashed inoculum. **N=4**

These results are consistent with slow attachment and growth of the biomass on smoother electrodes. This was also proved by smaller biomass coverage on the electrodes P400 and P600 compared with P240 (**Figure 3.2**). Indeed, the electrode P400 shows clumping of cells indicating that this surface still allows biofilm formation. On P600 there are more single cells attached than a biofilm formation, indicating a continuous detachment of cells, thus a not suitable surface for biofilm formation.

*S.loihica PV-4* biofilm appears more homogeneously distributed over the entire surface in the elecrodes polished with the sandpaper P240 and the population decreases as the decreasing of electrodes roughness (P240>P400>P600). In fact, it is known that both surface topography and chemistry determine current output enhancement in electrochemically active biofilms (Fan *et al*., 2011). The surface rms roughness of the polished graphite electrodes calculated from the AFM images (**Figure 3.3**) of the P240, P400 and P600 graphite electrodes were 0.74 ± 0.14, 06 ± 0.3, and 1.14± 0.43 μm, respectively. The relative uncertainty on the rms roughness for the P400 and P600 graphite is likely to be comparable to the P240 surface and thus at least 20%. Therefore, these differences in surface roughness are marked but not significant from the viewpoint of the sandpaper P-grade (see grit diameters quoted above). The surface roughness of P240 graphite electrodes increased by 75% to 1.301 μm after plasma pre-treatment, as expected and in accordance with previous works (Cvelbar *et al*., 2003; Cui *et al*., 2002). The AFM results show the surface roughness at the nm scale level while the SEM images show surface topography details at the μm scale level. Following plasma pre-treatment, the lag phase on P240 graphite electrodes increased from approximately 1 to 5 h and the current slope, roughly corresponding to cell attachment rate, increased by 45%, while the maximum current density (101±1.5 μAcm−2, n=3), in contrast did not change significantly with respect to the untreated P240 graphite electrodes. Interestingly, the current stabilized sooner for the plasma pre-treated electrode but decreased rapidly after the maximum (data not shown). This might be due to diffusional limitations at the interface cells/electrode caused by rapid cell attachment.

Experiments with washed inocula were then performed to determine the effect of soluble flavin concentration on the current output at different electrodes.

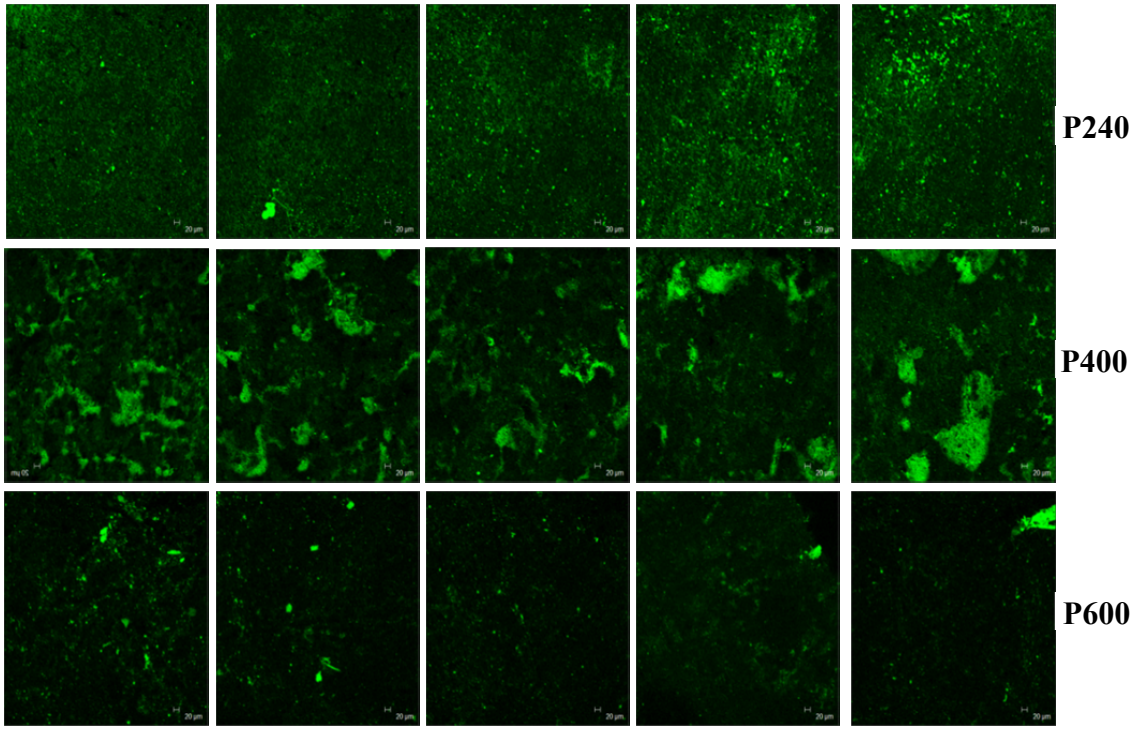


**Figure 3.2**: Confocal selections of graphite electrodes polished with three different sandpapers. (**Top panel**) P240; (**Middle panel**) P400; (**Bottom panel**) P600. Electrodes were collected from ECs run under electrogenic conditions with an aerobic inoculum. Lactate supplied was 20 mM. **Magnifications 20X.**

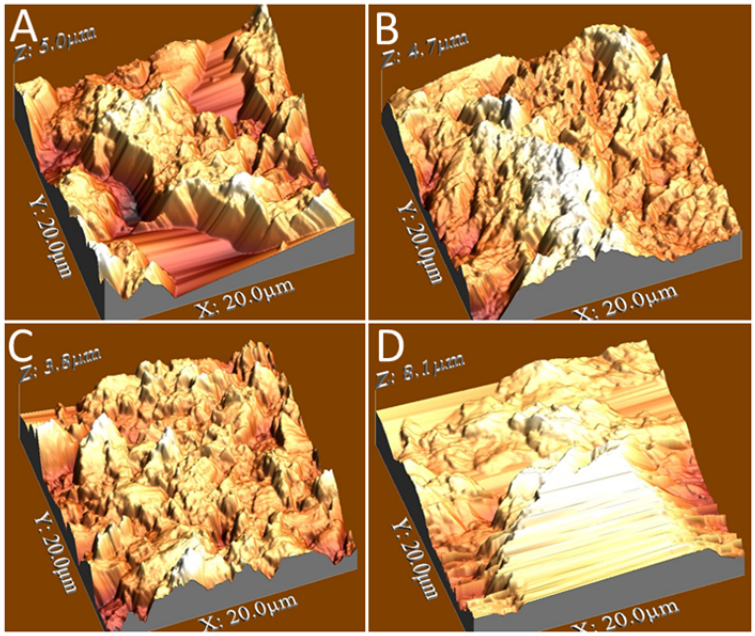


**Figure 3.3** AFM images of graphite electrodes. (A) P600, (B) P400, (C) P240 and (D) plasma pre-treated P240 sterile graphite electrodes.

### 3.3.1.2 Effect of washing step on current output

*S. loihica PV-4* cultures were grown on P240 graphite and carbon felt electrodes, with and without plasma pretreatment (**Figure 3.3**). Only the first phase of growth is reported, to show the difference between materials and inocula pretreatment, before biofilm formation and accumulation of microbially produced flavins. The unwashed inoculum produced a current mostly via soluble or adsorbed flavins (mediated electron transfer), while the initial current output observed in washed inocula was mostly due to direct electron transfer at the cell/electrode interface. When unwashed inoculum were used, the maximum current output for plasma pre-treated P240 graphite and carbon felt electrodes was similar and 20% lower than the untreated P240 graphite and carbon felt electrode, respectively (**Figure 3.3** and **Table 1**). These results for P240 graphite electrodes are not in conflict with reports from long-term biofilm experiments on electrode treated with oxygen plasma (V. Flexer *et al*., 2013), as the short-term effects were not investigated. The actual hydrophobicity/ hydrophilicity of the flavin mix produced by *S. loihica* cells has not been previously characterized; therefore, concentration of adsorbed flavins should be estimated to determine

whether the hydrophobic functional groups introduced by the plasma pre-treatment on the electrode either increase or have no effect on flavin adsorption on the electrode surface (**see Section 3.2.10**). Overall, the experiments with unwashed inoculum confirm that availability of microbially produced flavins in the supernatant is the main driver for current output. It Was found that for the washed inoculum, the current output was much lower than for unwashed inoculum, as most of the microbially produced flavins were removed before inoculation and direct electron transfer was predominant. However, the current output on carbon felt electrodes is not easily interpreted, as it depends also on the electrode pre-treatment. The highest current output corresponds to the washed inoculum on plasma pre-treated electrode, approximately 450% higher (243.7± 5.4 μA than the untreated carbon felt electrode. A previous long-term study with a biofilm grown on a plasma pre-treated electrode shows a small increase in the current output for carbon felt (Flexer *et al*., 2013) and an approximate 20% increase on $N_2$ plasma pre-treated carbon paper (He *et al*., 2012). Therefore, the higher biocompatibility of plasma pre-treated electrodes resulted in a 25% and 450% increase of the maximum current output for P240 graphite and carbon felt electrodes, respectively (**Figure 3.3** and **Table 1**).

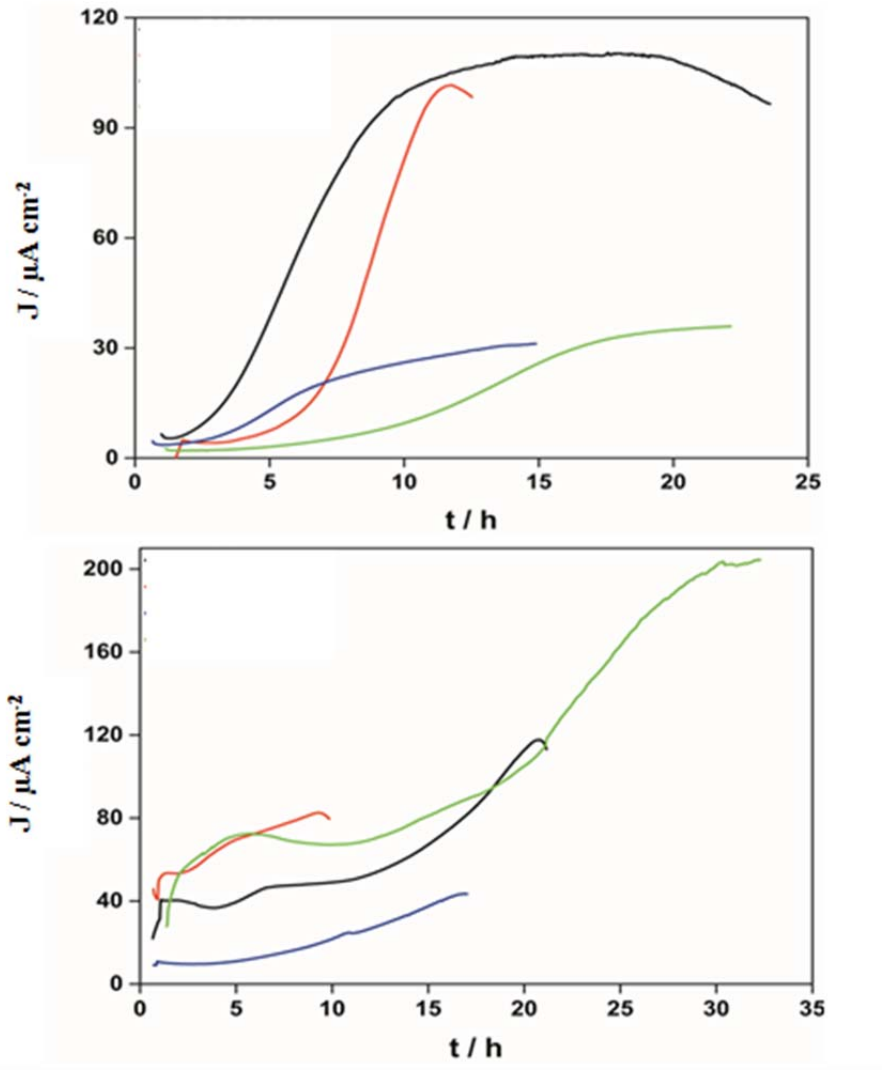


**Figure 3.4**: Current output in the initial attachment phase for various electrode materials. (**Top panel**) P240 graphite electrodes; (**Bottom panel**) carbon felt electrodes. *S. loihica PV-4* poised at 0.2 V vs Ag/AgCl. Unwashed inoculum, untreated electrode (**black**); unwashed inoculum, air plasma pre-treated electrode (**red**); washed inoculum, untreated electrode (**blue**); washed inoculum, air plasma pre-treated electrode (**green**). N=4

**Table 1**- Maximum current output for each electrode material (number of replicates= 4).

| Electrode material | Plasma pre-treatment | Washed/unwashed inoculum | Maximum current in the initial attachment phases/μA $cm^{-2}$ |
|---|---|---|---|
| P240 | YES | UNWASHED | 100.6 ± 1.5 |
| P240 | YES | WASHED | 36.5 ± 1.0 |
| P240 | NO | UNWASHED | 103.7 ± 9.0 |
| P240 | NO | WASHED | 29.6 ± 2.3 |
| CF | YES | UNWASHED | 82.9 ± 0.6 |
| CF | YES | WASHED | 243.7 ± 5.4 |
| CF | NO | UNWASHED | 124 ± 9 |
| CF | NO | WASHED | 53.3 ± 14 |

### 3.3.1.3 Cyclic Voltammetry

From this investigation CVs of *S. loihica PV-4* on all the electrodes show well defined catalytic curves, similar to those reported in many previous studies (D. Coursolle *et al.,* 2010; J.N. Roy *et al*., 2012) (**Figure 3.4 and 3.5**).

Comparing the results of the cyclic voltammetry of both the treated and untreated electrodes under both conditions (washed vs unwashed inoculum) shows the similarity between the oxidation peaks of the two materials (graphite and carbon felt).

However, when an unwashed inoculum was used a peak centered at 0.2 ± 0.05V was observed on the graphite electrode air plasma treated indicating a diffusion-limited ET process at that potential. This can be likely attributed to the formation of biofilm on the electrode. This biofilm acts to impede the electron shuttled from oxidizing at the electrode (**see section 3.2.11**; **EIS**), a phenomenon well observed in previous research (Newman *et al*., 2000).

Yet, the peak centered at 0.2 ± 0.05V suggests that the current achieved in **Figure 3.3 (Top panel, red and green)** is a result of cells achieving electron transfer mostly by direct contact

with the electrode, rather than any formation of soluble electron shuttles such as quinones or favins. While earlier work by von Canstein indicated an expected value of 2 mM for flavins produced by *S. oneidensis MR-1*, it may be concluded that when grown under similar conditions an air plasma electrode will demote the production of flavins below this number (**see section 3.2.10.1**, *Determination of adsorbed and soluble flavins in viable cultures)*.

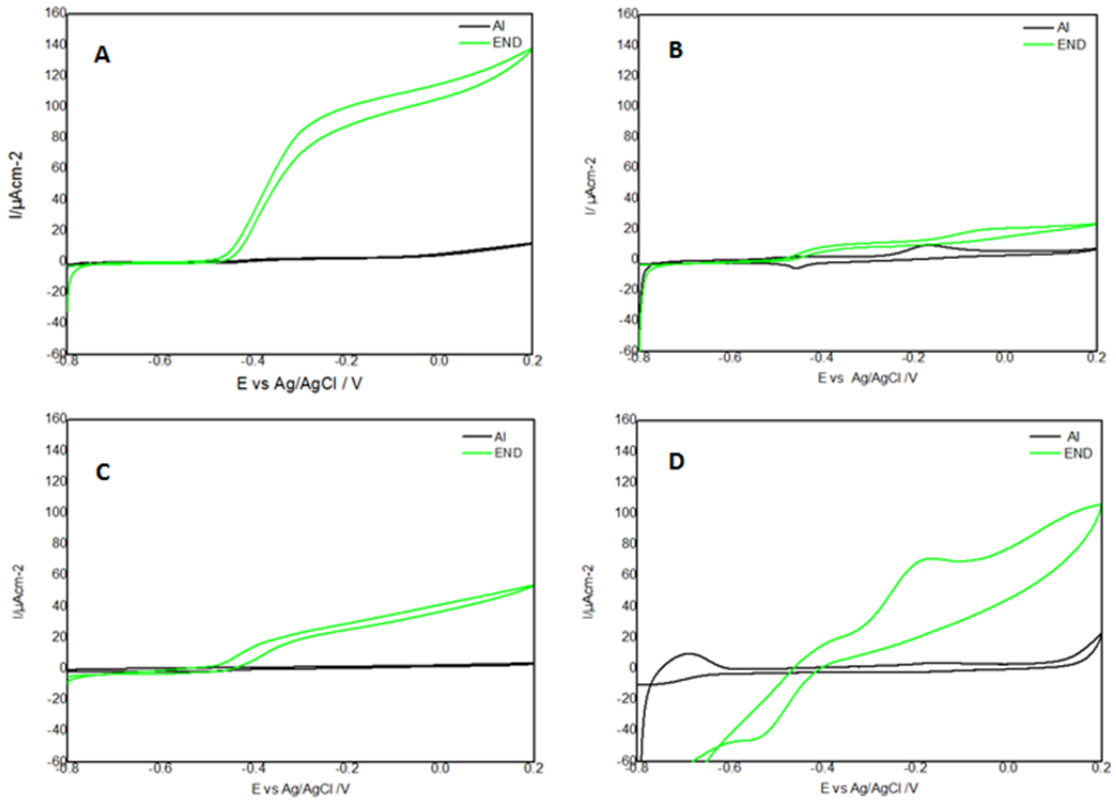


**Figure 3.4:** Cyclic voltammograms at scan rate= 1.0 mV/s of *S.loihica PV-4*. (**A**) Carbon felt; (**B**) Carbon Felt Plasma pre-treated; (**C**) P240 graphite; (**D**) P240 Plasma pre-treated. **AI** = after inoculation; **END** = end of the experiment, ~48 h. Unwashed inoculum. N=4

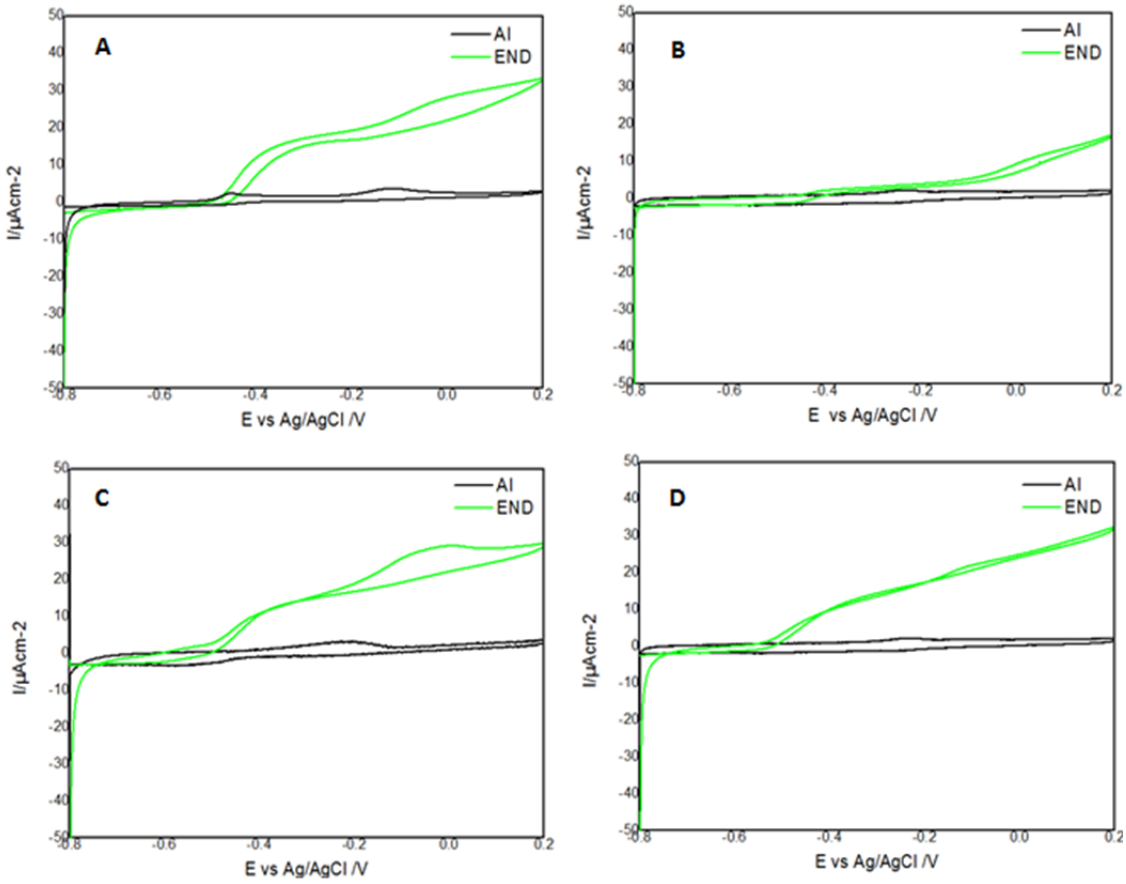


**Figure 3.5:** Cyclic voltammograms at scan rate= 1.0 mV/s of *S.loihica PV-4*. (**A**) Carbon felt; (**B**) Carbon Felt Plasma pre-treated; (**C**) P240 graphite; (**D**) P240 Plasma pre-treated. **AI** = after inoculation; **END** = end of the experiment, ~48 h. Washed inoculum. N=4

**Figure 3.6** depicts the first derivative of the CVs (i.e. of the data shown in **Figure 3.4 and 3.5**). Figure 3.6 shows three different redox centers **RC (i)** = -0.07 ± 0.01 V, **RC (ii)** = -0.2 ± 0.05 V, **RC (iii)** = -0.44V ± 0.06 V. In particular, the RC (ii) and RC (iii) are related to the mediated electron transfer. Indeed, their potential is close to the midpoint potential of quinone derivates which was shown to be -0.27 V (Newton *et al*., 2009) and riboflavin, which was demonstrated to be at -0.44 V (Marsili *et al*., 2008). The remaining redox center placed at 0.07 V is related to direct electron transfer. In fact, the potential of the outer membrane protein "OmcA" has been reported to be -0.054 V in *Shewanella loihica PV-4* by Bretschger, *et al*., (2010).

In particular, when the washed inoculum was used both RC (i) and (iii) were found, indicating two simultaneous electron transfer processes (**Figure 3.7**).Whereas, in the case of unwashed inoculum just one kind of electron transfer was observed (**Figure 3.6**), indicated by

the presence of RC (iii) in all kind of electrodes, and of RC (ii) only in the case of the electrodes that had been pre-treated with air plasma (**Figure 3.6**, **blue and red line**).

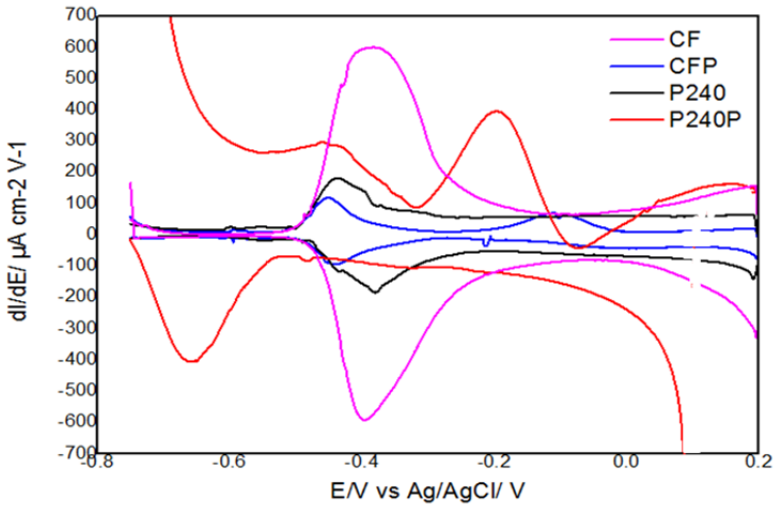


**Figure 3.6**: First derivative of corresponding CVs of unwashed *S.loihica PV-4* inoculum obtained at end of the experiment, ~48 h. **CF**= carbon felt, **CFP**= carbon felt air plasma pre-treated, **P240**=graphite electrode polished with sandpaper P240, **P240P**= graphite electrode polished with sandpaper and air plasma pre-treated. N=4

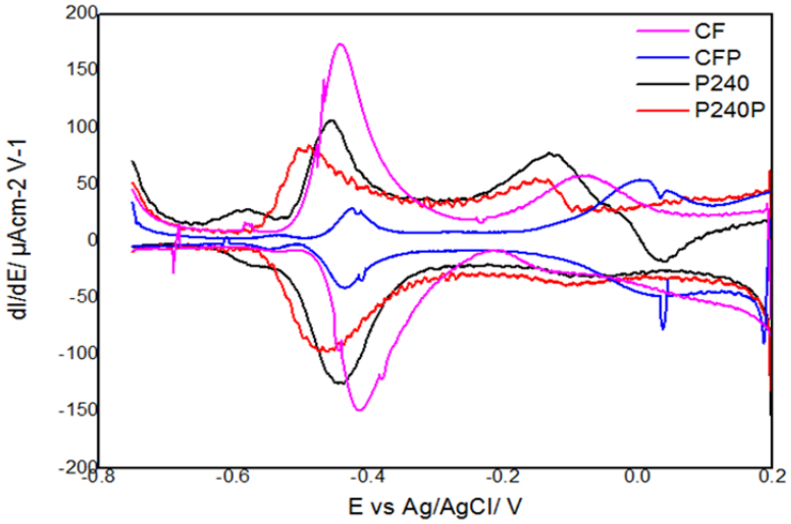


**Figure 3.7**: First derivative of corresponding CVs of washed *S.loihica PV-4* inoculum obtained at end of the experiment, ~48 h. **CF**= carbon felt, **CFP**= carbon felt air plasma pre-treated, **P240**=graphite electrode polished with sandpaper P240, **P240P**= graphite electrode polished with sandpaper and air plasma pre-treated. N=4

### 3.3.2 Chemical analysis

#### 3.3.2.1 Coulombic efficiency

The coulombic efficiency of all the conditions mentioned above was measured after approximately 22 h, before replacement of the spent growth medium, when residual lactate concentration was < 5 mM. Coulombic efficiency of unwashed graphite electrodes increased from 28 to 60% as the PPI of the polishing sandpaper increased from 240 to 600 (**Table 2**). Carbon felt electrodes have lower coulombic efficiency than P240 graphite electrodes and the plasma pre-treatment decreased the coulombic efficiency on both carbon felt and P240 graphite electrodes. The coulombic efficiency of electrodes inoculated with washed cells was much lower than in those with unwashed inocula, confirming the key role of microbially produced flavins in current production.

**Table 2-** Coulombic efficiency in *S. loihica PV-4* cultures poised at 0.2 V vs. Ag/AgCl. **CF**= carbon felt, **P240**= graphite electrode polished with sandpaper P240, **P400**= graphite electrode polished with sandpaper P400, **P600**= graphite electrode polished with sandpaper P600. N=3

| Electrode material | Plasma pre treatment | Washed/unwashed inoculum | Coulombic efficiency/ % |
|---|---|---|---|
| P240 | NO | UNWASHED | 27.6 ± 1.4 |
| P400 | NO | UNWASHED | 39.9 ± 0.7 |
| P600 | NO | UNWASHED | 59.8 ± 0.7 |
| P240 | YES | UNWASHED | 5.8 ± 0.4 |
| CF | NO | UNWASHED | 22.1 ± 0.4 |
| CF | YES | UNWASHED | 9 ± 0.7 |
| P240 | NO | WASHED | 5.0 ± 0.3 |
| P240 | YES | WASHED | 3.8 ± 0.7 |
| CF | NO | WASHED | 9.8 ± 4.0 |
| CF | YES | WASHED | 6.0 ± 0.5 |

### 3.3.3 Determination of adsorbed and soluble flavins in viable cultures:

#### 3.3.3.1 Absorbed riboflavin on different electrode materials: Detection by Differential Pulse Voltammetry

A previous study with mixed microbial consortia (Zaldivar *et al*., 2010) suggested that plasma pre-treatment of electrodes enhanced initial cell adhesion, thus leading to a faster biofilm development. Shewanella cells, however, secrete their own redox mediator (i.e., flavins) that facilitates EET either in the solution (Baron *et al*., 2009) or (once adsorbed) at the biofilm/electrode interface (Garcia *et al*., 1999). Therefore, flavin adsorption at plasma pre-treated electrodes should be studied without viable cells in order to de-couple the two EET mechanisms. Short-term bioelectrochemical experiments were performed with riboflavin on sterile electrodes to determine the effect of electrode material and plasma pre-treatment on flavin adsorption. Riboflavin was calibrated on both P240 graphite and carbon felt electrodes using DPV, with and without plasma pre-treatment. The riboflavin peak in the DPV of carbon felt electrode was three to four times higher than that recorded on P240 graphite, due to the large surface of the carbon felt electrode (**Figure 3**.7).

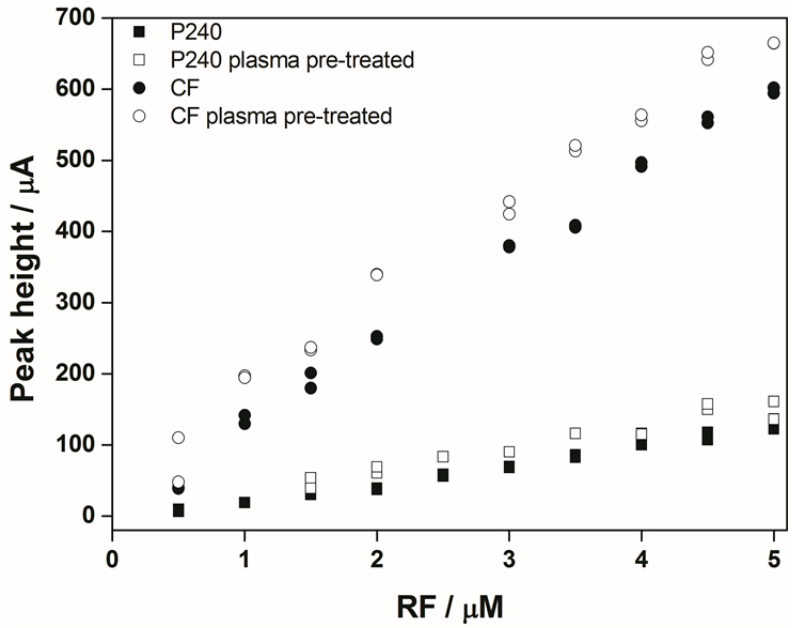


**Figure 3.7**: DPV calibration for riboflavin on sterile electrodes. (○) P240 graphite; (●) air plasma pre-treated P240 graphite; (□) carbon felt; (■) air plasma pre-treated carbon felt electrode. Carbon felt electrodes show a three to four times higher riboflavin signal than P240 graphite electrodes. Plasma pre-treatment slightly increased the riboflavin signal, particularly on carbon felt electrodes. N=4

The specific surfaces of carbon felt and P240 graphite electrodes are ~22 and ~13 $m^{-1}$, respectively (Garcia *et al*., 1999). Therefore, riboflavin adsorption occurs only on a small part of the carbon felt electrode surface. The electrochemical potential for riboflavin adsorption is similar to that observed for flavin mononucleotide and flavin adenine dinucleotide on titanium electrodes in HEPES buffer at pH 7 (Garjonyte *et al*,,2003).

The concentration of flavins absorbed on the different electrode surfaces was estimated as described above (**section 3.2.10, materials and methods**) and the related calibration plots are shown in the Appendix section **(Figure A1).**

The concentration of riboflavin was estimated at four stages: after inoculation, before medium change, after medium change, and at the end of the experiment. This was done for both washed and unwashed inoculum.

**Figure 3.8 and 3.9** show well defined DPV peaks in both graphite and carbon felt electrodes, at all the various stage of analysis. These peaks are centered at about -415±15 mV and they

correspond to riboflavin. It is notable that when the spent growth medium was removed, the concentration of flavins decreased, as a large proportion of the flavins were not absorbed on the electrode surface and hence they were removed with the medium. However, some of the flavins remained adsorbed to the electrode, as indicated by the residual peak following removal of the spent medium (**Figure 3.8 A-D and 3.9 A-C; AMC**). This is highly remarkable when the electrodes were plasma pre-treated.

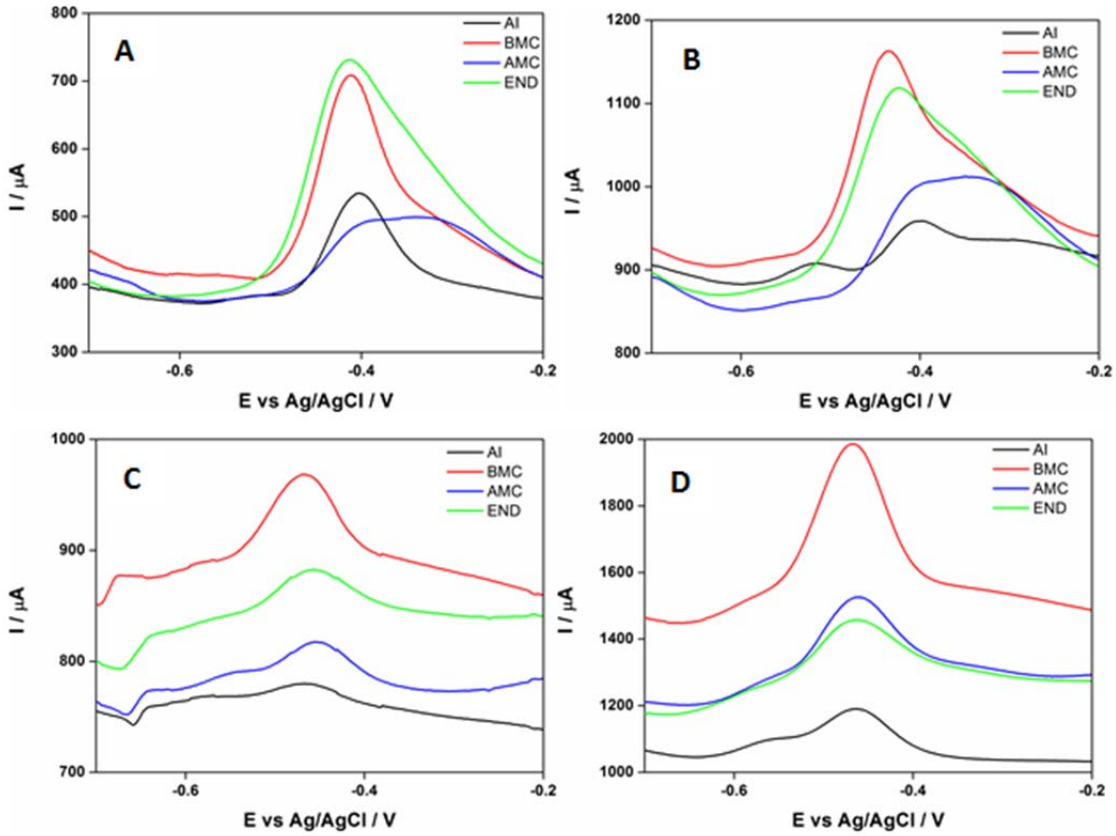


**Figure 3.8:** DPV of **unwashed** inoculum at various stages for all electrode materials tested, showing the flavins peak at -415±15 mV vs. Ag/AgCl. (**A**) Carbon felt; (**B**) Carbon Felt Plasma pre-treated; (**C**) P240 graphite; (**D**) P240 Plasma pre-treated. **AI** = after inoculation; **BMC** = before medium change, 20-22 h; **AMC** = after medium change, 22-24 h; **END** = end of the experiment, ~48 h. N=4

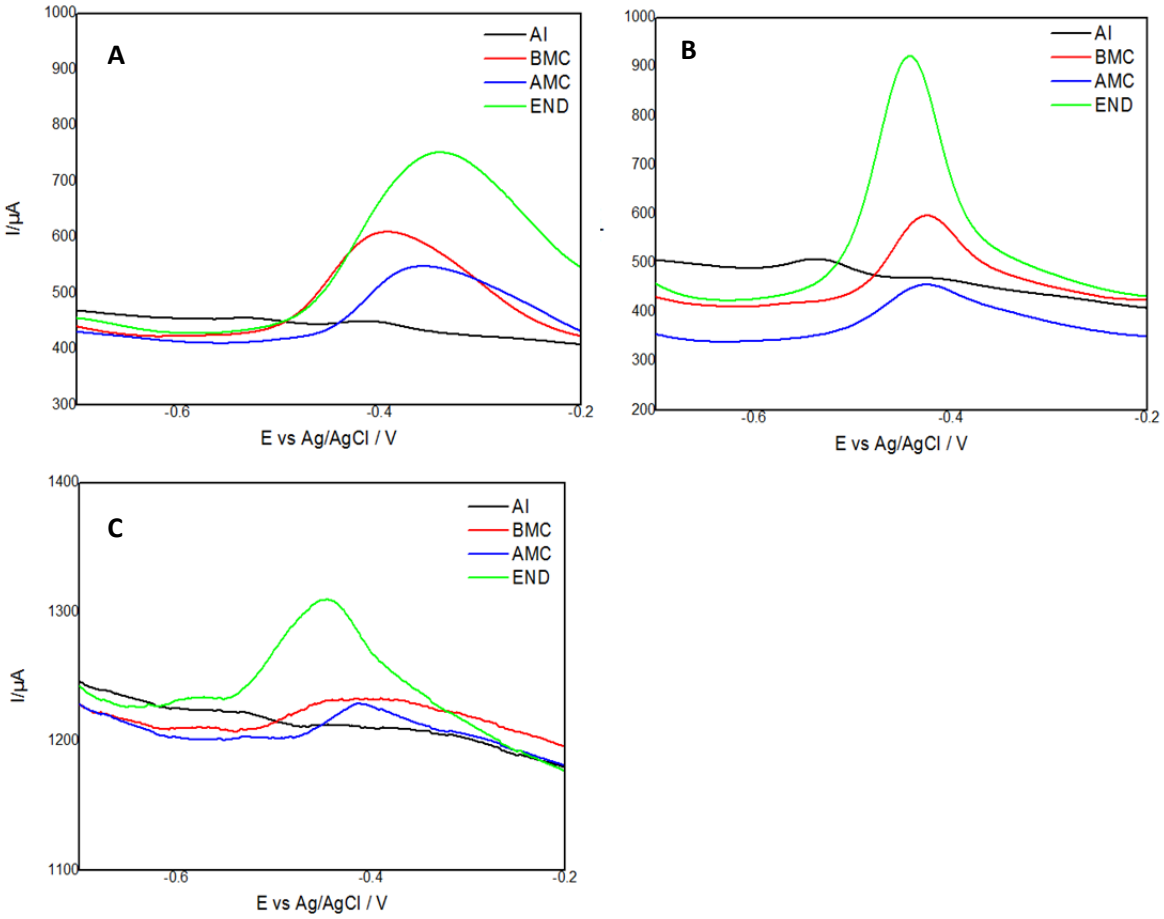


**Figure 3.9:** DPV of **washed** inoculum at various stages, showing the flavins peak at -415±15 mV vs. Ag/AgCl. (**A**) Carbon felt; (**B**) Carbon Felt Plasma pre-treated; (**C**) P240 Plasma pre-treated. **AI** = after inoculation; **BMC** = before medium change, 20-22 h; **AMC** = after medium change, 22-24 h; **END** = end of the experiment, ~48 h. N=4

### 3.3.3.2 Secreted riboflavin in presence of different electrode materials: Detection by fluorescence spectroscopy

To estimate the distribution of flavins between the solution and the electrode, the flavin concentration was measured in the supernatant using a spectrofluorometer, before medium change and at the end of each experiment (**Figure 3.10 and 3.11**). The peak height was calibrated to that of riboflavin. (**Section 3.2.7.1; Appendix- Figure A2**).

The ratio of the flavin concentration determined by DPV over the same concentration determined using a spectrofluorometer varied significantly with the electrode material (**Table 3**). The P240 graphite electrodes had the highest ratio, indicating a strong accumulation of flavins when unwashed inocula were used. On the other hand, the ratio for carbon felt was approximately 1 for all other electrodes, indicating that microbially-produced flavins did not adsorb on carbon felt. Furthermore, the air plasma pre-treatment resulted in a lower flavin adsorption on P240 graphite electrodes.

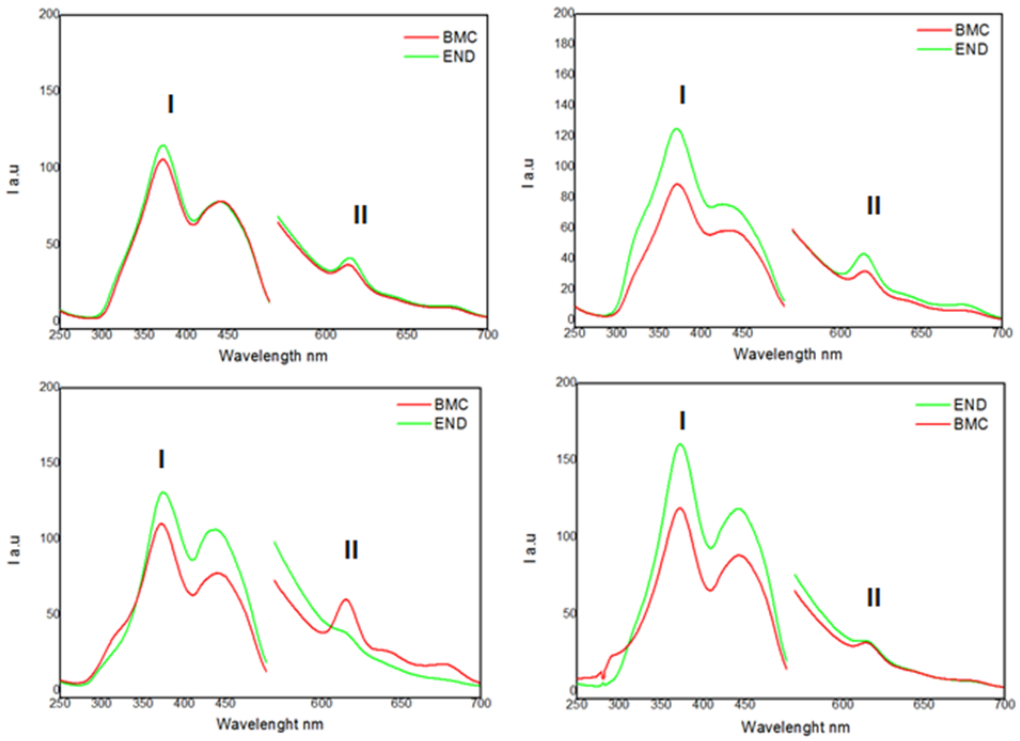


**Figure 3.10**: Fluorescence excitation and emission spectra of the cell free supernatant from *S. loihica PV-4* biofilms associated with (**A**) Carbon felt; (**B**) Carbon Felt Plasma pre-treated; (**C**) P240 graphite; (**D**) P240 Plasma pre-treated. **BMC** = before medium change, 20-22 h; **END** = end of the experiment, ~48 h. (**i**) Excitation spectrum, (**ii**) Emission spectrum. **Unwashed inoculum.** N=4.

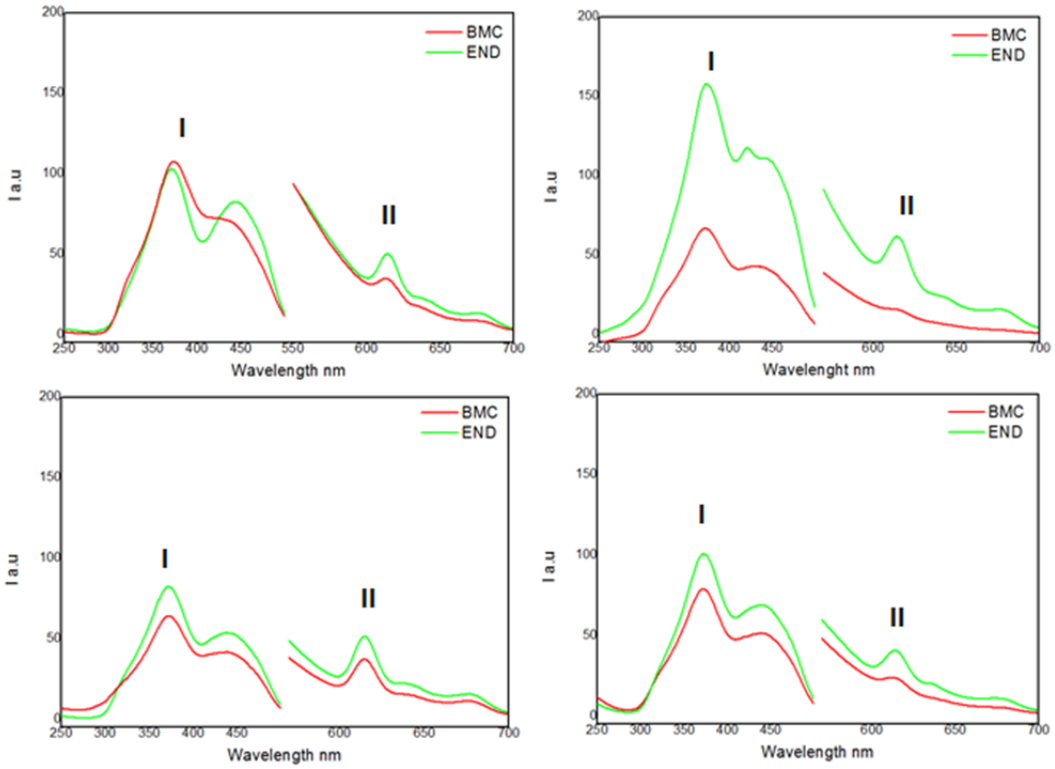


**Figure 3.11**: Fluorescence excitation and emission spectra of the cell free supernatant from *S. loihica PV-4* biofilms associated with (**A**) Carbon felt; (**B**) Carbon Felt Plasma pre-treated; (**C**) P240 graphite; (**D**) P240 Plasma pre-treated. **BMC** = before medium change, 20-22 h; **END** = end of the experiment, ~48 h. (**i**) Excitation spectrum, (**ii**) Emission spectrum. **Washed inoculum.** N=4.

**Table 3**- Ratio of flavin concentration determined by DPV over flavin concentration determined by spectrofluorometer for different electrode material and inoculum pretreatment (number of replicates= 4).

| Electrode material | Plasma Pre-treatment | Inoculum condition | Ratio $[flavin]_{DPV}$ / $[Flavin]_{sf}$ |
|---|---|---|---|
| **P240** | YES | UNWASHED | 3.28 ± 0.40 |
| **P240** | YES | WASHED | 1.09 ± 0.74 |
| **P240** | NO | UNWASHED | 7.91 ± 0.08 |
| **CF** | YES | UNWASHED | 1.02 ± 0.29 |
| **CF** | YES | WASHED | 0.76 ± 0.29 |
| **CF** | NO | UNWASHED | 1.14 ± 0.52 |
| **CF** | NO | WASHED | 1.09 ± 0.15 |

### 3.3.4 EIS

The potentiostatic EIS (**Figure 3.12**) shows the typical profile of *Shewanella* growth cultures (Wang *et al*.,2014). There was no difference in the impedance measured on P240 graphite electrodes at various stages of growth (data not shown). This is due to the low current output of *S. loihica PV-4*, approximately 20 times smaller than the current output of *Geobacter sp*. under anodic biofilm conditions (Jung *et al*., 2012). A two time-constant parallel model was applied to the EIS data at each potential (Jung *et al*., 2012). In this model, the time constant at low frequency corresponded to the charge transfer resistance at the cell/electrode interface and was measured at the various stages of cell attachment: immediately after inoculation; before spent medium replacement (approx. 22 h); after medium replacement (approx. 24 h); and after current stabilization (approx. 48 h). The charge transfer resistance followed the pattern previously observed for *Shewanella* on carbon felt electrodes, where charge transfer resistance decreased following cell growth, increased after removal of planktonic cells and spent medium, then decreased again as both suspended and attached cells grew (Wang *et al*., 2014). The charge transfer resistance at approximately 48 h showed that the use of washed cells as inoculum increase the charge transfer resistance, particularly on plasma pre-treated electrodes (**Figure 3.12**). This was consistent with flavins being the main driver for anodic current production and confirms that plasma pre-treatment improves the electroactivity of the cell/electrode interface.

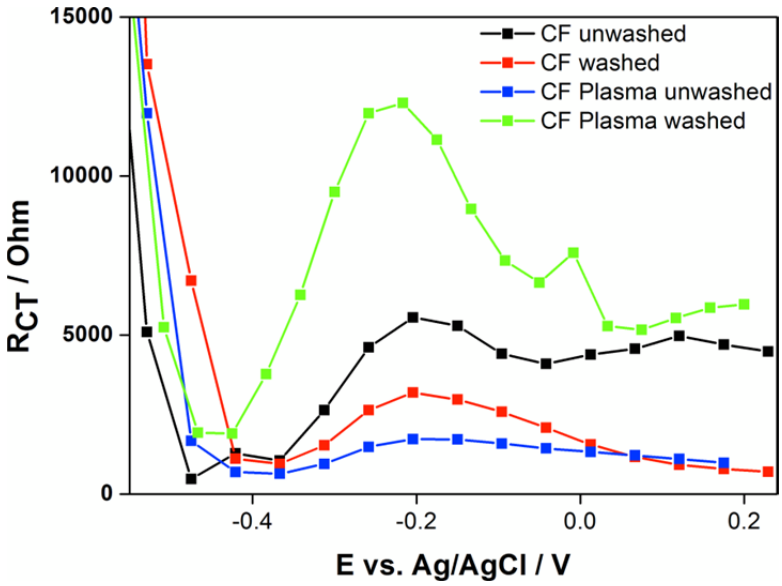


**Figure 3.12**: $R_{CT}$ for CF electrodes. The EIS spectrum was recorded at approx. 48 h, when the current output stabilized. The $R_{CT}$ at all anodic potential (E > -0.4 V vs. Ag/AgCl) was lowest for plasma pre-treated electrodes inoculated with unwashed cells, likely due to the large concentration of soluble flavins and the high cell attachment on the hydrophilic surface.

### 3.3.5 Contact angle measurement

It has been proved that the surface wettability of the electrodes affects the external electron transfer process in *Shewanella loihica PV-4* at a fixed external potential. Indeed, Kasmi *et al*., (1998) noticed that pure c-type cytochromes gave a $10^3$ fold higher electron transfer on COOH/OH-modified Au electrodes than on COOH-modified ones. This was explained through a higher hydrophobicity of the COOH/OH-modified Au electrodes. However, Ding et, (2015) have shown the opposite behavior by comparing SH-ITO (water contact angle= 62.4º; hydrophilic surface) and $CH_3$-ITO (water contact angle= 102.9º; hydrophobic surface). In fact, the former (the more hydrophilic) improved the EET of five times compared with the most hydrophobic with *S.loihica PV*-4 cultures.

This result, points out that the situation is complex and the EET in *S. loihica PV-4* has still to be clarified.

For this reason water contact angle measurements were taken on all the electrodes used above plus on graphite electrodes P400, P600 and P1000 which were also treated with air plasma.

Indeed, with this measure it is possible to establish whether a surface shows hydrophobic or hydrophilic behavior. Generally, if the water contact angle is smaller than 90°, the solid surface is considered hydrophilic and if the water contact angle is larger than 90°, the solid surface is considered hydrophobic (Arkles at al., 2006).

**Figure 3.13** illustrates that the hydrophobicity of the electrodes increases in a different proportions for the different electrodes.

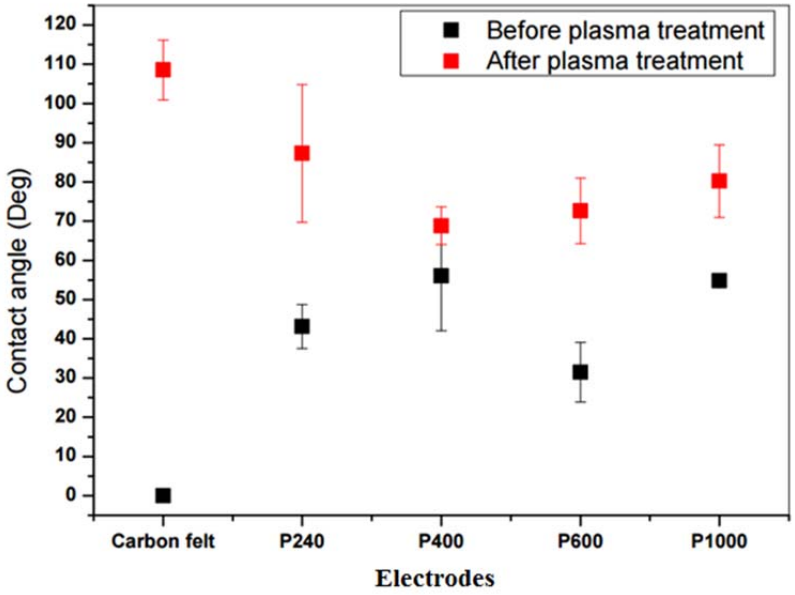


**Figure 3.13** Contact angle measurements of a water droplet on graphite and carbon felt electrodes, before and after air plasma treatment (120 s).

Specifically, the highest hydrophobicity was shown after air plasma treatment in the cases of P240 electrodes (increases of nearly 50 %) and on carbon felt (increases of approximately 110 %). Indeed, before the plasma treatment, the complete absorption of the water drop was observed on this surface (**Figure 3.14**) indicating the high hydrophilic surface of the carbon felt before the plasma treatment.

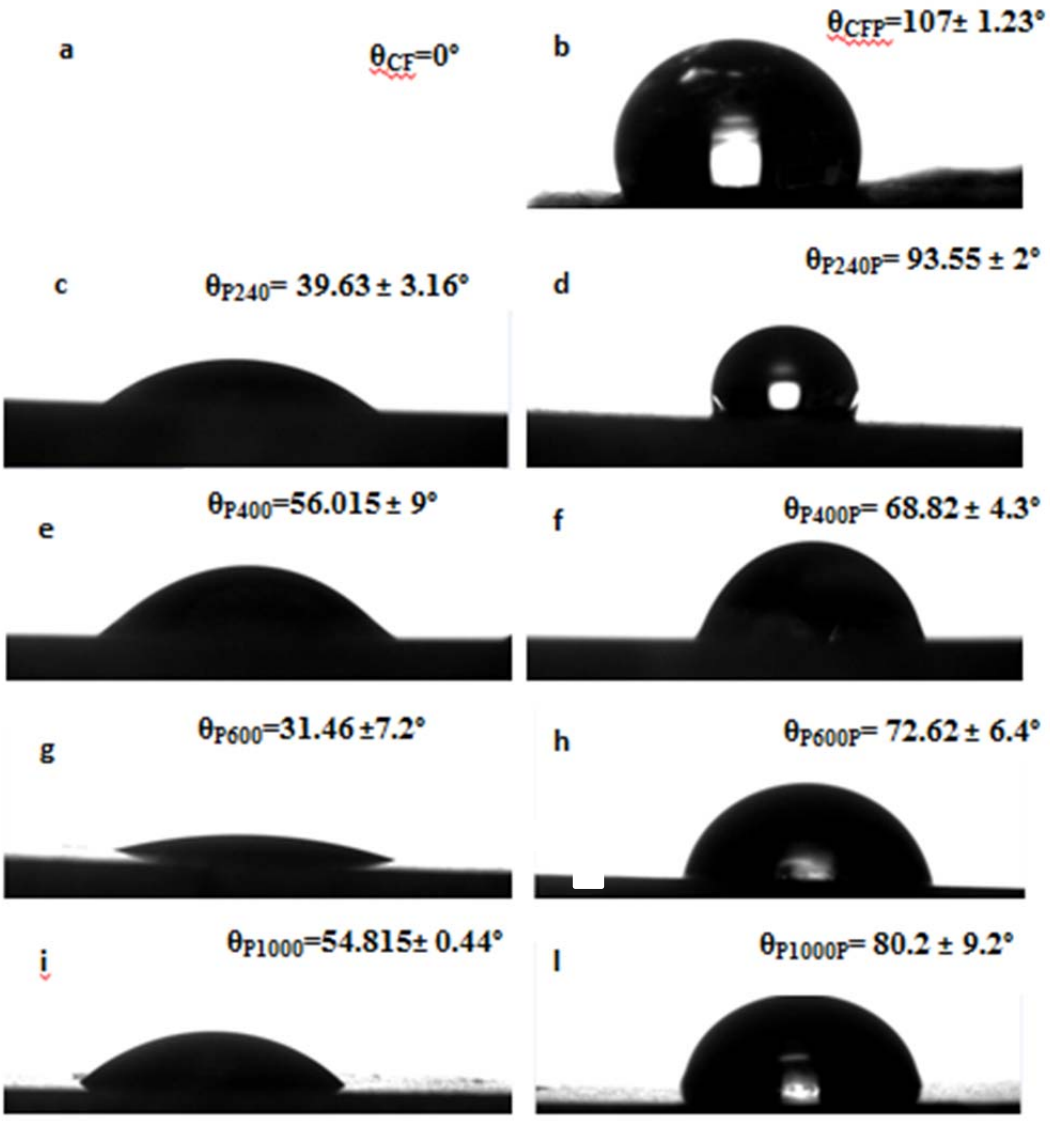


**Figure 3.14:** Images of contact angle measurements of a water droplet on graphite and carbon felt electrodes, before and after air plasma treatment (120’’). (**a**) CF (droplet was completed absorbed), (**b**) CFP (**c**) P240, (**d**) P240P (**e**) P400, (f) P400P, (g) P600, (h) P600P, (i) P1000, (l) P1000P (**Left panel**) Untreated electrodes; (**Right panel**) Air plasma treated electrodes.

### 3.3.6 SEM analysis

SEM images (**Figure 3.14 A-C**) of sterile P600, P400 and P240 graphite electrodes shown that surface feature size increased as the sandpaper P-grade decreased. The different initial textures of the graphite and carbon felt electrodes lead to different surface modifications upon plasma treatment. There was minimal visible change on the surface of the P240 graphite electrode after plasma treatment (**Figure 3.14D**). This is agrees with the AFM analyses, as plasma treatment significantly increases the surface rms roughness at the sub-µm level, which is beyond the resolution of the SEM images. On the contrary, the surface of plasma pretreated carbon felt samples (**Figure 3.14F**) appeared locally damaged, when compared with the untreated surface (**Figure 3.14E**).

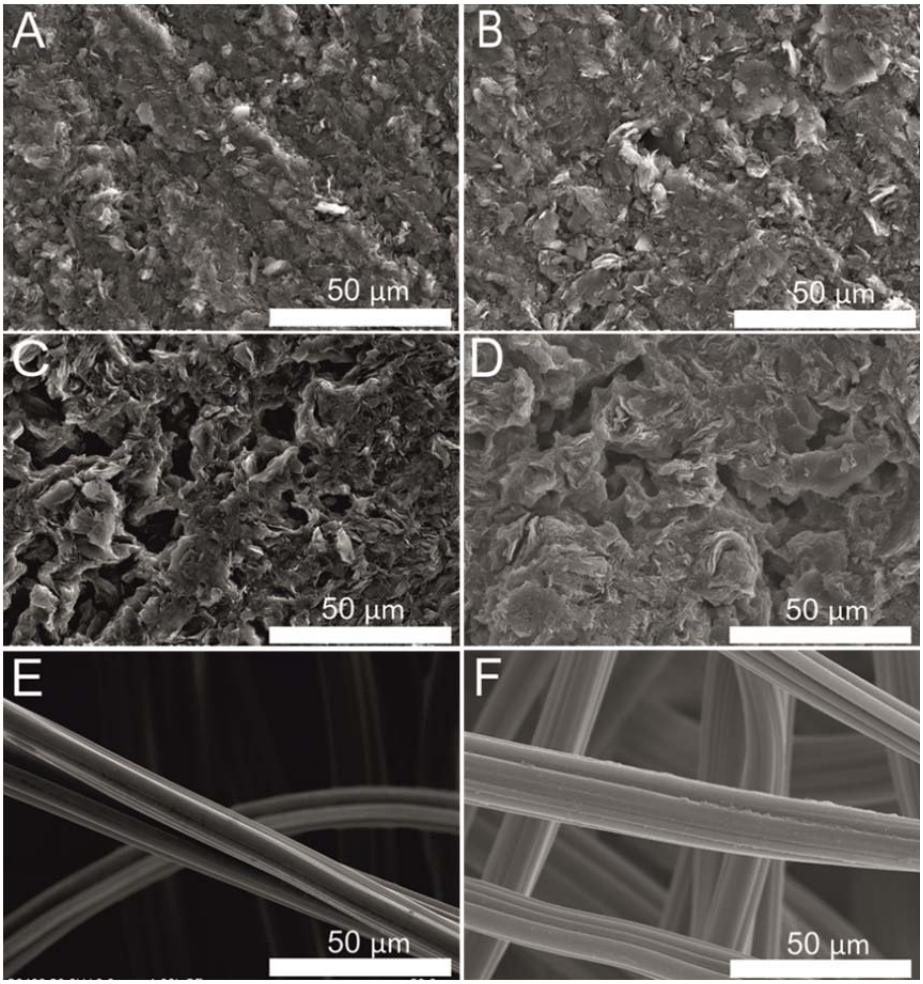


**Figure 3.14**: SEM images of polished graphite and CF electrodes, with and without plasma pre-treatment. (**A**) P600, untreated; (**B**) P400, untreated; (**C**) P240, untreated (**D**) P240, plasma pre-treated; (**E**) CF, untreated; (**F**) CF, plasma pre-treated.

This is likely to be due to the very open, skeleton-like, fibrous texture of carbon felt that presents a much higher surface area after the 120 s exposure to the plasma reactive oxygen species. At the end of the experiments, SEM images of P240 graphite electrodes (**Figure 3.15**) showed much higher coverage for unwashed inocula, which was consistent with the CA data (**Figure 3.3 black line**); the difference between untreated and plasma pre-treated electrodes is much less evident, and might be due to the change in surface conductivity and hydrophobicity following plasma pre-treatment (K.H. Becker *et al*.,2005).

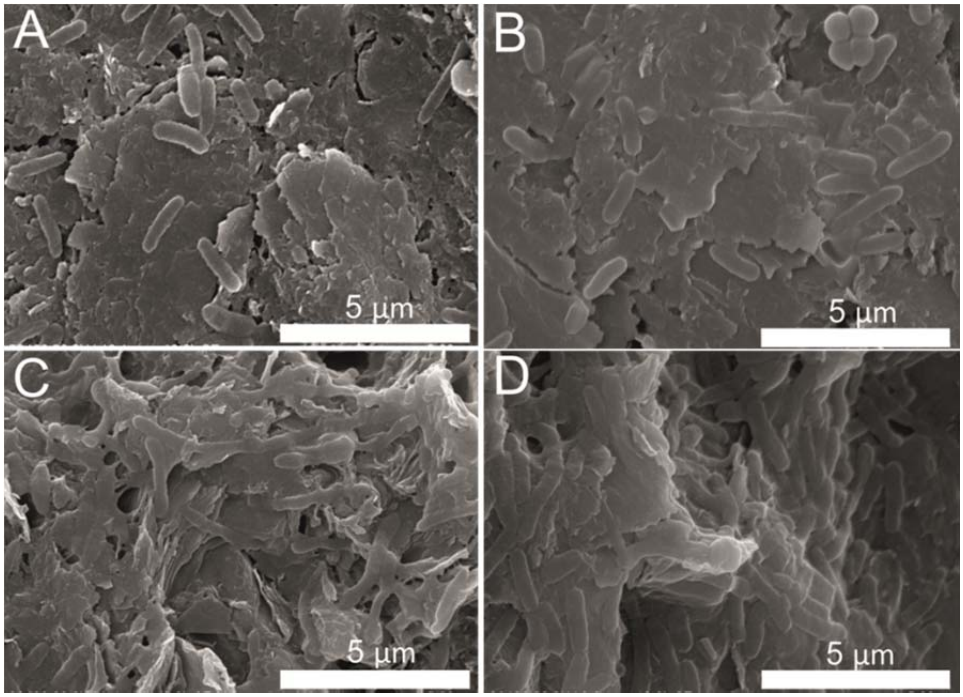


**Figure 3.15:** SEM images of *S. loihica PV-4*. P240 electrodes were imaged when current output stabilized, after approx. 48 h of growth at E = 200 mV vs. Ag/AgCl. (**A**) untreated, washed inoculum, (**B**) plasma pre-treated, washed inoculum, (**C**) untreated, unwashed inoculum, (**D**) plasma pre-treated, unwashed inoculum.

As for carbon felt electrodes, unwashed plasma pre-treated samples (**Figure 3.16D**) showed higher cell and biofilmmatrix concentration, which might cause diffusional limitation and explain lower current output with respect to the untreated electrode. All the other samples (**Figure 3.16A-C**) showed a thin layer of attached cells, with lower electrode coverage than the biofilm grown on carbon felt electrode with unwashed inoculum.

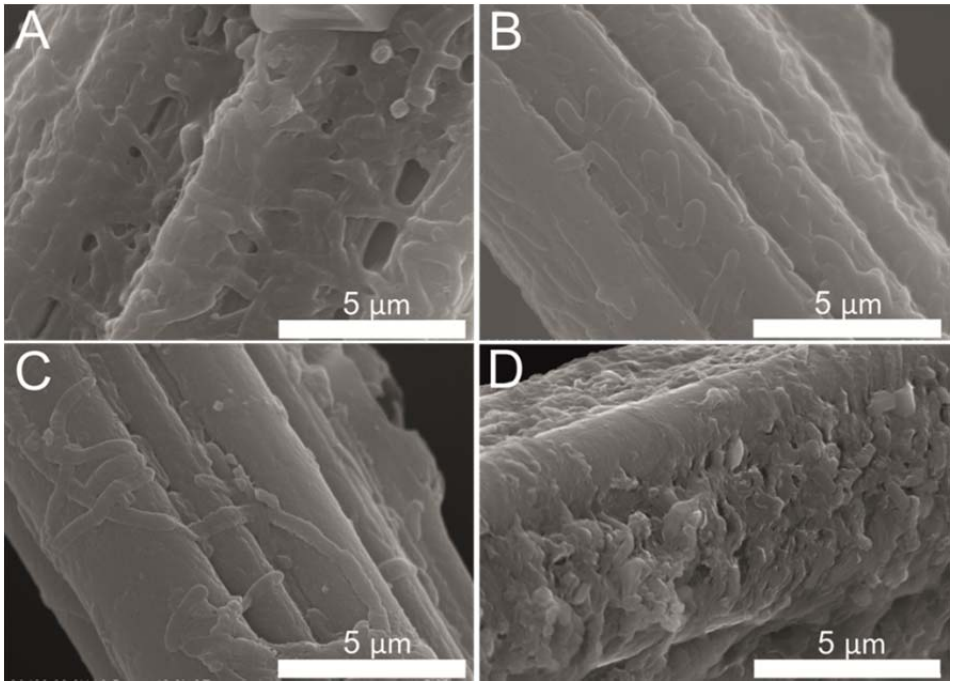


**Figure 3.16:** SEM images of *S. loihica PV-4*. CF electrodes were imaged when current output stabilized, after approx. 48 h of growth at E = 200 mV vs. Ag/AgCl. (**A**) Untreated, washed inoculum, (**B**) plasma pre-treated, washed inoculum, (**C**) untreated, unwashed inoculum, (**D**) plasma pre-treated, unwashed inoculum.

### 3.4 Conclusions

The aim of this study was to improve the current output in short-term experiments in potentiostat-controlled ECs with *S.loihica PV-4.*

The goal was achieved in certain cases. Indeed, plasma pre-treatment greatly improved the current output on carbon felt electrodes, but only where microbially produced soluble flavins were removed before inoculation (washed inocula). In the case of graphite not big different were recorded comparing the treated and the untreated electrode.

Furthermore, plasma pre-treatment increases the hydrophobicity of all the electrodes tested and in particular on P240 and CF thus increasing the cell attachment rate on all the electrodes tested. However, it decreased the coulombic efficiency in all the electrode tested.

This suggests that plasma pre-treatment is a feasible option to increase power output in bioelectrochemical systems in the absence of microbially produced redox mediators.

However, the effects of plasma pre-treatment are not all beneficial and the interplay between direct and mediated electron transfer must be considered when designing optimal electrode pre-treatment.

# CHAPTER 4

## INVESTIGATION OF SYSTEM DESIGN PARAMETERS

(**Part 2**: Electrode surface coating)

***Related publication***

Zhang Xiaoming, **Epifanio Monica,** Marsili Enrico (2013) Electrochemical characteristics of *Shewanella loihica* on carbon nanotubes-modified graphite surfaces. Electrochimica Acta 102, 252-258.

**Abstract**

High specific surface and electrocatalytic activity of the electrode surface favour extracellular electron transfer from electrochemically active biofilms to polarized electrodes. In order to increase the extracellular electron transfer rate in *S. loihica PV-4*, electrophoretic deposition was used to coat graphite electrodes with various layers of carbon nanotubes (CNTs). Cyclic voltammetry (CV) determined that 8 layers of CNTs ($CNT_{8)}$ were the optimal coating for the electroactive biofilm (EAB) experiments therefore $CNT_8$ was chosen as substrate to grow *S. loihica* PV-4 electroactive biofilm. The extracellular electron transfer rate was measured by Chronoamperometry (CA) and compared with unmodified electrodes. Current density on $CNT_8$-modified electrodes was 1.7 times higher than that observed on unmodified electrodes after 48 h post-inoculation. Rapid microbial cells attachment on $CNT_8$-coated electrodes, as determined from scanning electron microscopy, explained the rapid increase of the current. However, the electrocatalytic activity of the $CNT_8$-coated electrodes decreased as the biofilm grew thicker, likely because of poor electrical conductivity of the biofilm. These results confirmed that CNT-coated electrodes improves the electron transfer rate in thin biofilms (<5 μm), but they are not feasible for power production in long-term MFC experiments, where the biofilm thickness is much higher.

## 4.1 Introduction

Extracellular electron transfer (EET) from bacteria to electrode is the rate-limiting step for power production in anodic bioelectrochemical systems (BESs) (Rosenbaum *et al*., 2006). Chemistry and topography of the electrode determines both the EAB formation and the external electron transfer (EET) rate at the biofilm/anode interface. To support biofilm growth and enable facile EET, the ideal anode should have low electrical resistance, high surface area and biocompatibility, and chemical stability at circumneutral pH and ambient temperature. Higher catalytic activity results from a higher surface area and also from the homogenous dispersion of catalytic nanoparticles onto the surface of the electrode, as well as its functionalization with different chemical groups such as COOH, amine, etc (Santoro *et al,* 2015.)

Carbonaceous materials are the most widely used materials for BES anodes because of their relatively low cost, chemical inertness and good biocompatibility. Compared with other carbon electrodes, graphite-based electrode materials, such as graphite fibre brush (Logan *et al*., 2007), graphite plate (Pham *et al*., 2009) and graphite felt have (Jang *et al*., 2006) higher mechanical strength and are suitable for large-scale BESs. Surface treatments of graphite electrodes, increase their electroactivity and favour biofilm growth, are needed to improve the power output (Peng *et al*., 2010).

Recently, carbon nanotube-based (CNT) electrode materials have become extremely attractive for application in BESs, due to their high surface area and electric conductivity (Walcarius *et al*., 2013) as well as their mechanical strength and chemical stability. Furthermore, CNTs are biocompatible, allowing for bacteria immobilization and biofilm growth (Gutierrez *et al*., 2007).

CNTs are an allotrope of carbon. They are tube-shaped materials, having a diameter measuring on the nanometre scale. They are found in many structures, differing in length and thickness. They were discovered in 1991 by a Japanese physicist named Sumio Iijima. The graphite layer that makes up the nanotube looks like a rolled-up tube with a continuous unbroken hexagonal mesh of carbon (**Figure 4.1**). Such a tube can be considered as a fundamental structural unit, known as single-walled carbon nanotube (SWNT). Using that fundamental structural unit, a multi-walled carbon nanotube (MWNT) can be formed through a concentric nest of SWNTs, with a distance between the layers or walls equal to 0.34 nm.
Carbon Nanotubes typically have diameters ranging from <1 nm up to 50 nm. Their lengths are typically several microns, but recent advances have made the nanotubes much longer, and measured in centimetres.

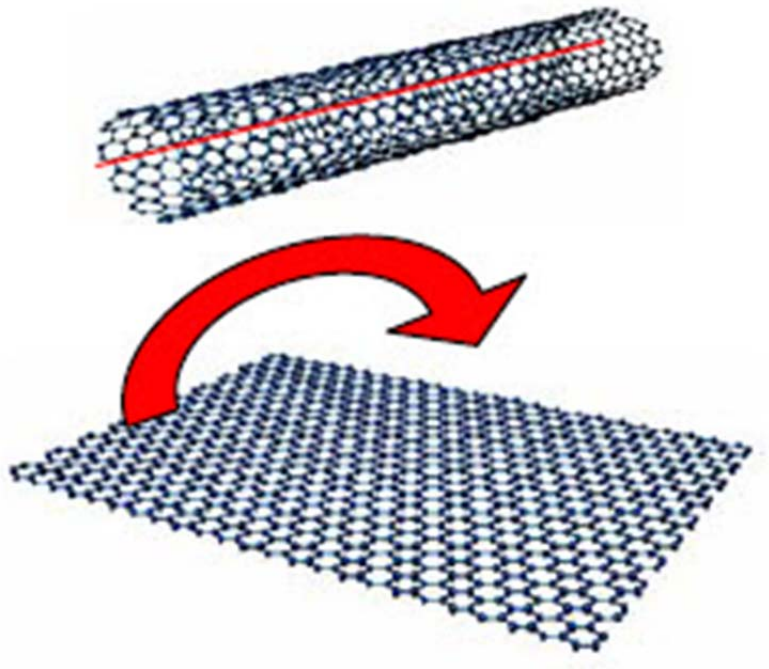

**Figure 4.1:** Plane graphene sheet **(Bottom panel)** and graphene sheet rolled up forming the so called structure carbon nanotube **(Top panel).**

In the last decade, several studies have been carried out on CNTs-modied electrodes due to their relevant properties for biocatalytic applications. Tsai *et al*., (2009) shown that carbon nanofibers modified graphite fibers (CNFs/GF) generated a peak current density 54% higher than the unmodified GF electrodes. Also, CNTs have been reported to display conductivities as high as $10^6$ S·m$^{-1}$ and $10^5$ S·m$^{-1}$ for single-walled carbon nanotubes (SWCNTs) and multi-

walled carbon nanotubes (MWCNTs), respectively, and high tensile strength up to 60 GPa (Thess, *et al*., 1996). Nambiar *et al*., (2009), showed that multi-walled carbon nanotubes enhanced 252.6% anodic performance of an *Enterobacter cloacae*-based fuel cell when compared to unmodified anodes. CNTs coating gave good performance when also used on glassy carbon electrodes (GCE), improving by 82 times the current density in *Shewanella oneidensis* biofilms, when compared to the unmodified electrodes (Peng *et al*. 2010). Different studies also report that CNTs-electrode coating can plug directly into individual redox enzymes for better EET at the enzyme/electrode interface (Guiseppi-Elie *et al*., 2002 Zhao *et al*., 2012). In fact, Guiseppi-Elie et al., 2002 demonstrated that SWCNTs-coating on glassy carbon electrodes lead to the achievement of direct electron transfer (DET) with the redox active centres of adsorbed oxidoreductase enzymes on the electrode surface. Zhao *et al*., 2012 observed the same behavior on MWCNTs -modified electrodes, which promoted the direct electron transfer (DET) of cytochrome c (Cyt c) by changing their secondary structure promoting the exposition of the active site, thus, the orientation of the heme groups was optimized and resulted in a more open microenvironment for electron transfer (Zhao *et al.,* 2012).

Therefore, CNTs-coating seems to be a suitable electrode modification for enhancing current output in BESs and convenient platform for fundamental understanding of biological redox reactions. However, the production of stable and controlled CNT-modified anodes in BES is not straightforward. The main challenges are: (**a**) to manipulate CNTs, individually or collectively, to produce a particular arrangement for a given application; (**b**) to disperse CNTs homogeneously in solvent or in a composite matrix (Van der Biest *et al*., 1999).

Electrophoretic deposition (EPD) offers a solution for these challenges to some extent. Compared with other methods it exhibits several advantages, such as high deposition rate, excellent uniformity and controlled thickness (Bon *et al*., 2010).

In this study, stable CNT coatings for electrochemically active biofilms applications were produced. Different layers of CNTs with negatively charged functional groups were used to coat commercial graphite electrodes by EPD. The modified electrodes were tested with the model EAB-forming microorganism *S. loihica PV-4.* Results of this work contribute to the understanding of the interaction between carbon nanostructures and viable biofilms.

## 4.2 Materials and methods

### 4.2.1 Activation of CNTs

Typically, 1 g of commercial nanotubes (NANOCYLTM NC3100, Belgium) was refluxed in 60 mL of 23% (v/v) HNO3 at 90 ◦C for 6 h. A nanotube mat was obtained after filtration using a 0.45 mm hydrophilic PTFE membrane and washed with deionized water until no acid was detected, followed by drying in oven. After the acid-treatment, the dried multiwalled nanotubes were dispersed in N-methyl-2-pyrrolidone (NMP) with 0.1% $MgCl_2 \cdot 2H_2O$ by sonication and stored for use.

### 4.2.2 Electrophoresis deposition (EPD)

Prior modification with CNTs, graphite sheets were cut into 1 × 2 × 0.3 cm electrodes and then polished with sandpaper (400 PPI). Residual graphite dust was removed by sonication for 2 min in distilled water. The CNTs coating was performed using a power supply (Consort EV200 unit, UK) that was capable of operating under conditions of constant voltage (up to 300 V).

The electrophoretic cell consisted of a glass beaker that contained a lid with electrodes attached, which ensured the parallelism of both electrode surfaces and maintained them at a constant distance (1 cm) so as to ensure an homogeneous deposition process (**Figure 4.2**).

Current density was kept at 4 mA $cm^{-2}$, and the time for deposition was 10 min. The final concentration of the CNT solution was 0.55 mg $mL^{-1}$, which has been reported as optimal for high quality electrophoretic deposition (*Ren et al.*, 2008). The charged carbon nanotubes were attracted towards the cathode (due to the adsorption of $Mg^{2+}$), thus forming the coating. All experiments were conducted at ambient temperature and samples were carefully and slowly pulled out of the suspension after EPD. Afterwards, the samples were dried for at least 24 h at room temperature in normal air and in horizontal position to achieve coatings as homogeneous and smooth as possible. Repeating the EPD process enables coating with various thicknesses of CNTs. No stripping off of the CNTs coating was found throughout the experiment for these prepared electrodes.

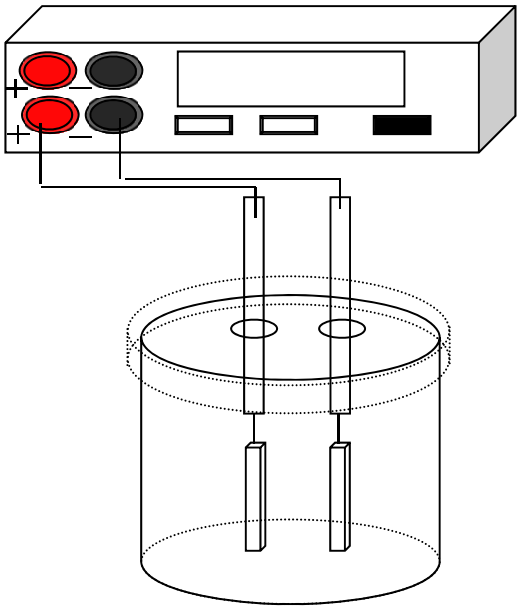

**Figure 4.2**: Sketch picture of electrophoretic deposition process

### 4.2.3. Bacterial culture

*S. loihica PV-4* was grown aerobically for 8 h at 30 ◦C in Luria-Bertani medium (LB) containing per litre: bacto trypton (Fisher, Ireland) 10 g, yeast extract 5 g, NaCl 10 g. Following initial growth to early stationary phase, at optical density (OD) 1.6, cultures were transferred and incubated under strict anaerobic conditions for 24 h at 30 ˚C without shaking in modified defined media (DM) containing per litre: $NaHCO_3$ 2.5 g, $CaCl_2 \cdot 2H_2O$ 0.08 g, $NH_4Cl$ 1.0 g, $MgCl_2 \cdot 6H_2O$ 0.2 g, NaCl 10 g, HEPES 7.2 g, trace mineral solution 10 mL (**see composition Appendix section; table A2**), and vitamin solution 1 mL (**see Appendix composition section; table A3**). Lactate (10 mM) and fumarate (10 mM) were added as electron donor and electron acceptor, respectively. Filter-sterilized casamino acids 0.5% (v/v) were added as a growth stimulant. After 16 h, cultures were centrifuged at 24450.6 g for 5 min to remove most of the extracellular matrix, and the resultant pellet was washed three times with MDM medium without electron acceptor, in order to remove soluble mediators and electron acceptor prior to inoculation into the electrochemical cells (ECs). All the above steps were taken into an anaerobic chamber in order to ensure the anaerobic condition.

### 4.2.4. Biofilm growth on electrodes

Water-jacketed ECs of 10 mL working volume with three electrodes configuration were used as previously described (Jain *et al*., 2012) . The cell suspension was diluted to OD 600nm = 1.4 and 5 mL of this suspension was added to the electrochemical cell containing 5 mL of MDM medium without fumarate and with 20 mM of NaCl. The cell suspension was purged for 10 min with $O_2$-free $N_2$ gas, obtained by passing $N_2$ through a heated copper column. The ECs were maintained at 30 ◦C throughout the experiment. The working electrode was poised at +0.2 V vs. standard calomel electrode (SCE) to facilitate attachment of cells to electrodes. After approximately 16 h, the medium was replaced with fresh MDM medium and the current was recorded for other 32 h. A complete experiment lasts approximately 48 h.

### 4.2.5. Electrochemical characterization

Cyclic voltammetry (CV) and differential pulse voltammetry (DPV) were used to characterize the CNTs-coated and uncoated graphite electrodes before and after the incubation with the electroactive model microorganism *S. loihica PV-4.* The parameters for the techniques were chosen as it follows: CV: scan rate, 1 mV/s; Ei = -0.8 V; Ef = 0.2 V; DPV: Ei = -0.8 V and Ef = 0.2 V; pulse height, 50 mV; pulse width, 300 ms; step height, 2 mV; step time, 500 ms; scan rate, 4 mV/s; accumulation time, 5s. s. CV and DPV were performed when current had stabilized.

### 4.2.6. Scanning electron microscopy

The electrode with attached cells was removed from the electrochemical reactor and rinsed with fresh MDM to remove loose bacteria. Then the specimen was fixed in the MDM with 5% v/v glutaraldehyde for 30 min, and dehydrated in alcohol (30, 50, 70, 90 and 100%, 15 min each step). All samples were coated with evaporated Au before being viewed using a S3400 (Hitachi) microscope at an operating voltage of 5 kV.

## 4.3 Results

### 4.3.1 CNTs coating by EPD method

Negligible CNTs deposition was observed when the coating process was carried in N-methyl-2-pyrrolidone without 0.1% v/v $MgCl_2 \cdot 2H_2O$. After $MgCl_2$ addition, CNTs migrated to the electrode and formed a CNT layer (Corni *et al*., 2008). Higher voltage or longer EPD time results in a thicker coating. However, high voltage also leads to CNT aggregation and to the evolution of $H_2$ and $O_2$ at the electrode, decreasing CNT adsorption. Therefore, high quality coatings were prepared by repeating the EPD process at 20 V/cm or at 4 $mA/cm^2$, and 10 min at each time (**see SEM images**; **Figure 4.5C**).

### 4.3.2. Electrochemical characterization of CNTs modified electrodes

Figure 4.3 shows the CV of CNT-coated electrodes without any bacteria, but just in presence of 1 M KCl containing 1.25 mM $K_3[Fe(CN)_6]$. It is clear that the height of oxidation and reduction peaks increased proportionally with the number of CNT deposition steps as these increased from 2 to 8 (Figure 1B). This is due both to the higher surface area of the modified electrode and to the high electrocatalytic activity of CNTs. Further, the peak separation Ep decreased slightly from 49 to 48 mV with the number of coating layers. These results indicate that the amount of coated CNTs for each layer is approximately constant. However, when the amount of CNTs exceeded 8 layers, the peak current decreased and the peak separation Ep increased to 52 mV, indicating that the redox reaction $Fe(CN)_6^{3-/4-}$ became less reversible. These results may be ascribed to slower mass transfer in thicker CNT films. A previous study (Guo *et al*., 2010) found that CNTs could block electron transfer when the amount of CNTs on electrode surface exceeded $30 g/cm^2$. Along with the growth of CNTs multi-films (from 2 to 8 deposition steps), the value of Ep for CNT modified electrodes remained approximately constant. However, the offset to negative of both anodic and cathodic peaks clearly showed that the CNT coating enhances the electron-transfer rate. The value |Ipa/Ipc| approaches to 1 with increasing CNTs amount from two to eight deposition steps. This means that the reversibility of electrode reaction improves with increasing CNT coating thickness. However, |Ipa/Ipc| decreases when the layers of coated CNTs exceeded 10. Therefore, $CNT_8$ was chosen as the optimal coating for the experiments with electroactive biofilms.

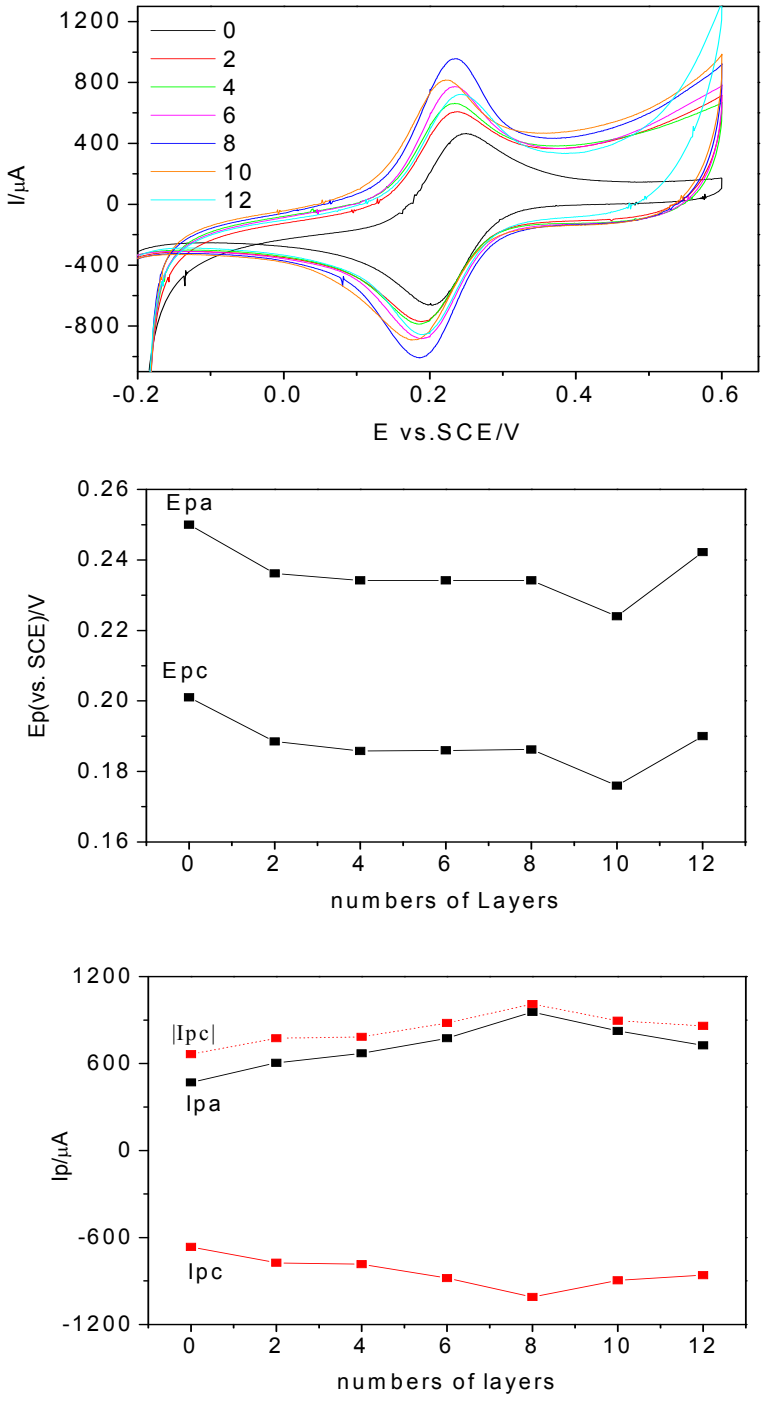


**Figure 4.3:** CVs (A), Ip (B), and Ep (C) vs. CNTn (n = 0, 2, 4, 6, 8, 10, 12 deposition steps) for CNT coating on graphite electrode. Scan rate was 10 mV s−1. n = 0 means plain graphite.

### 4.3.3 Electricity generation of biofilm on anodes

Figure 4.4 shows the chronoamperometry of *S.loihica PV-4* grown on either plain graphite electrode or CNTs-graphite coated electrode. It is clear that before the first medium change (approx.16 h) current density increases rapidly up to 88.7 ± 10 and 58.8 ± 5 μA/cm$^2$ at $CNT_8$ and unmodified electrodes respectively. Nearly 1.5 longer lag phase is visible on the plain electrode when compared with the CNTs-coated one. This shows that the electroactive biofilm "wired" more easily onto the CNT-modified electrode (Miguel *et al.,* 2004). Yet, this confirms that bacterial adhesion, the most important step in biofilm formation and growth, could be enhanced and accelerated by CNTs on the electrode (Peng *et al*., 2010). Following replacement of spent medium with fresh growth medium, current density at CNT-modified electrodes decreased of approximately 23%, while current density at plain electrodes was quite stable. This result may be attributed to a lower absorption of soluble electron shuttles on the CNTs coated electrode and to their easy removal from the medium (Epifanio *et al*., 2015). The slope of the current density vs. time decreases on both electrodes, but it remained higher at the CNT-modified electrode, showing that CNT coating favors both initial attachment and biofilm proliferation and growth. These results are consistent with other reports (Meng *et al*., 2009), which showed how cell growth, proliferation and absorption of the protein in serum on a CNT sheet were higher than on a uncoated graphite sheet.

Due to the fast proliferation on CNT-modified electrode, a maximum current density of 120 μA cm$^{-2}$ is obtained at around 40 h post-injection, which is much higher than that (74μA cm$^{-2}$) reported earlier for *S. loihica PV-4* on graphite electrode within the first two days (Jain *et al*., 2012). This is one of the best results reported so far, and is about 10 times larger than previous work (Erable *et al*., 2009). In addition, current dropped shortly after reaching a maximum. This might be due to the depletion of electron donor. On the contrary, on plain electrode, the current keeps increasing after 40 h. This is probably due to the lower electron donor consumption as less biofilm is found attached on the plain electrode (see SEM images **Figure 4.5**).

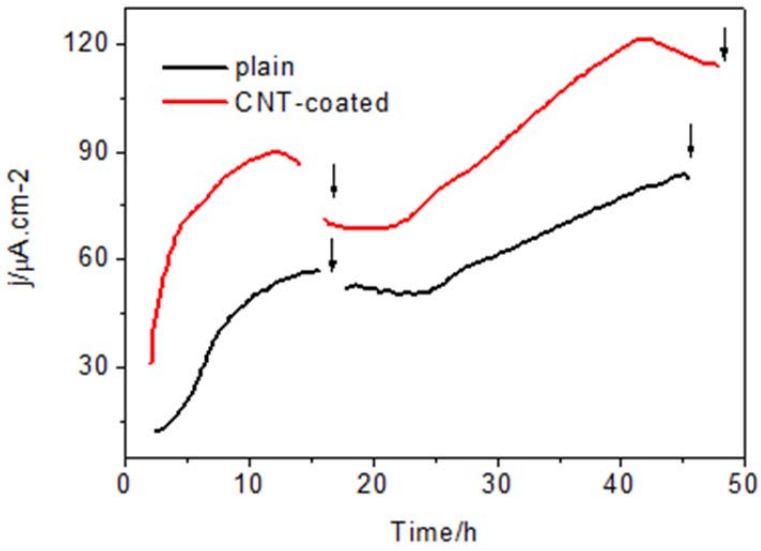


**Figure 4.4**: Chronoamperometry of *Shewanella loihica PV-4* biofilm grown on plain graphite and $CNT_8$-coated graphite electrode. The anodes were poised at +0.24 V vs. SCE. Medium was replaced by fresh DM at the time points indicated with arrows.

### 4.3.4 Scanning electron microscopy

A morphologic study of biofilm on plain and CNT-coated graphite surface obtained by scanning electron microscopy (SEM) is shown in Figure 4.5. The dark areas in Figure 4.5 A are CNT-coated regions. The CNTs films were not uniform at micrometre scale. This can be explained by the non-uniform distribution of the charges on the heterogeneous graphite surface, which increases the electrode surface and modifies the local chemistry (Lazic *et al*., 2010). Figure 4.5 B shows formation of monolayer or sub-monolayer biofilms on CNT-coated parts, while almost no cells were observed on exposed graphite parts. Under the same conditions, sparse bacterial cells were observed on plain graphite electrode, as shown in Figure 4.5 C. However, SEM images further confirmed the preferred attachment of *S. loihica PV-4* on the CNTs coating.

The improved biofilm formation (**Figure 4.5**) can be explained by the surface structure of multi-walled CNTs, indeed, the network structure from CNT-coating discernible in the SEM images) may enable the outer membrane cytochromes (OMCs) to make multiple polar contacts with the electrode and assist electro-oxidation of *Shewanella*'s OMCs, thus enhancing the heterogeneous EET rate (Peng *et al*., 2010).

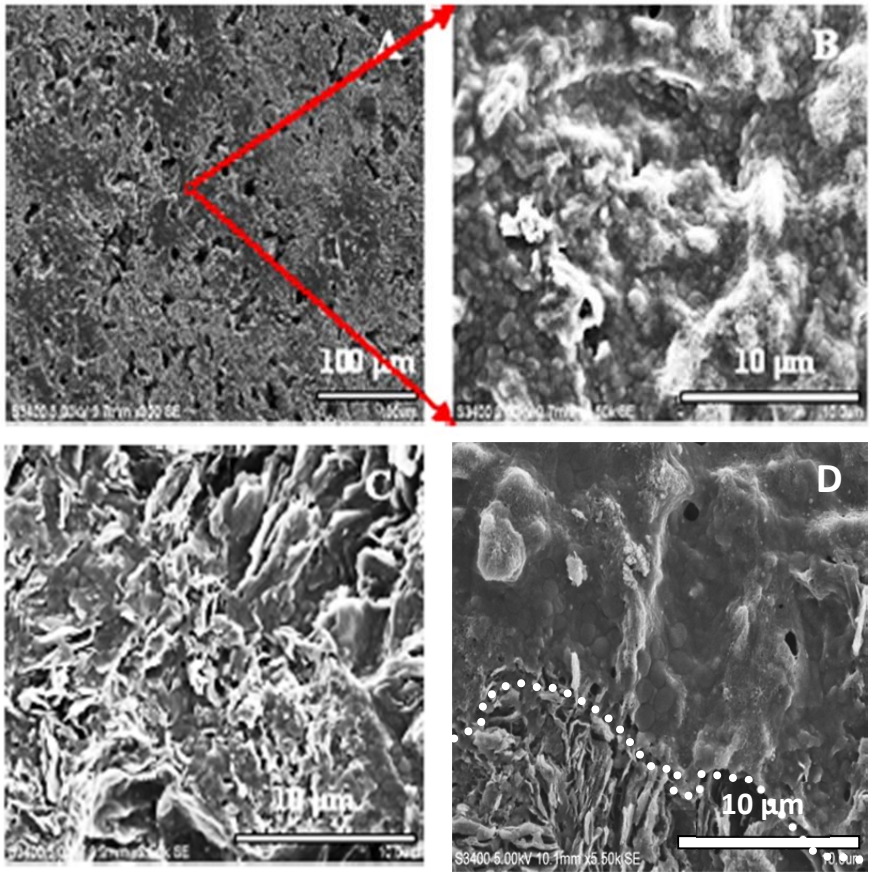


**Figure 4.5**: *Shewanella loihica PV-4* biofilm distributions on CNTs-coated (**A** and **B**), plain (**C**) plain graphite electrode. (D) Bacteria preferred to grow on CNTs-modified area (**upon white dotted line**) rather than on plain graphite area (**below white dotted line**). Panels B - D are at 10 X higher magnification than panel A.

### 4.3.5 Electrochemical characterization of *Shewanella loihica PV-4* biofilm on CNTs coated and uncoated graphite electrode

The cyclic voltammogram of *S. loihica PV-4* biofilm recorded after medium change shows several overlapping catalytic waves (**Figure 4.5, Top panel**). Different redox centers were detected with the first derivative analysis. As shown in Figure 4.5 (**Bottom panel**), the redox centers (RC) on plain graphite are as follows: RC (I) = −0.15 V, RC (II) = −0.38 V, RC (III) = −0.50 V and RC (IV) = −0.60 V. The corresponding redox species on CNT-modified graphite are RC (I) = −0.10 V, RC (II) = −0.38 V, RC (III) = −0.50 V and RC (IV) = −0.60 V respectively. From previous studies, it is possible to assign RC (I) as OMCs at the interface biofilm/electrode (Jain *et al*., 2012). However, the formal potential of OMCs is strongly dependent upon their microenvironment, as OMCs are found in a broad potential between −,

RC (III) = −0.5V (Carmona *et al*., 2011). RC (II) and RC (IV) likely indicate mediated ET, as their potentials are located in the range of soluble electron shuttles of *Shewanella* in other studies(Van der Biest *et al*., 1999; Schröder *et al*., 2007). These data confirmed an interplay of two simultaneous EET mechanisms in *S. loihica PV-4* either in plain or CNTs coated electrodes.

The different redox potentials for the cytochromes-related EET between the two electrodes can be attributed to the different biofilms formed at unmodified and CNT-coated electrodes. Yet, the negative shift (from -0.10 V to -0.15 V) of the OMC-related potential at the modified electrode indicates that CNT modify the microenvironment at the biofilm/electrode interface, thus facilitating EET between electron surface and membrane proteins.

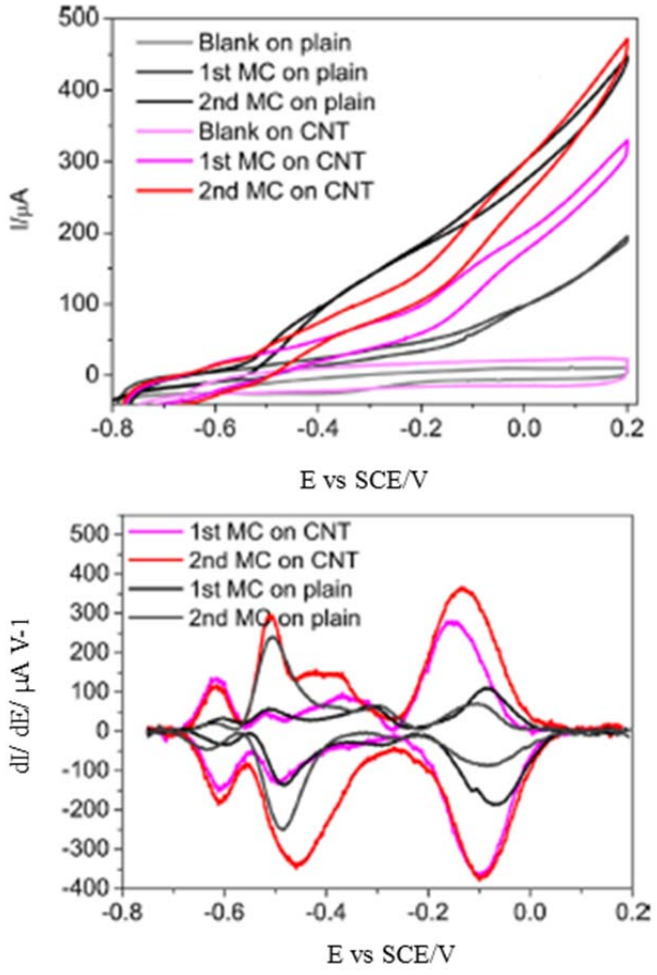


**Figure 4.6:** Cyclic voltammetry (Top panel) and related first-derivative (Bottom panel) of *S.loihica PV-4* biofilm on plain graphite and $CNT_8$-coated graphite electrode. MC=medium change.

**Table-1** Comparison between the DPV related peak positions in the plain and CNT-coated electrode.

| Plain | CNT |
|---|---|
| **DET - 0.10 V** | **- 0.15 V** |
| **MET -0.38 V** | **- 0.38 V** |
| **MET -0.6 V** | **- 0.6 V** |

Also, the differential pulse voltammetry shows also a much higher current response on CNT-modified electrode compared with the plain one, which corresponds to a higher faradaic current on the modified electrode (**Figure 4.7**).

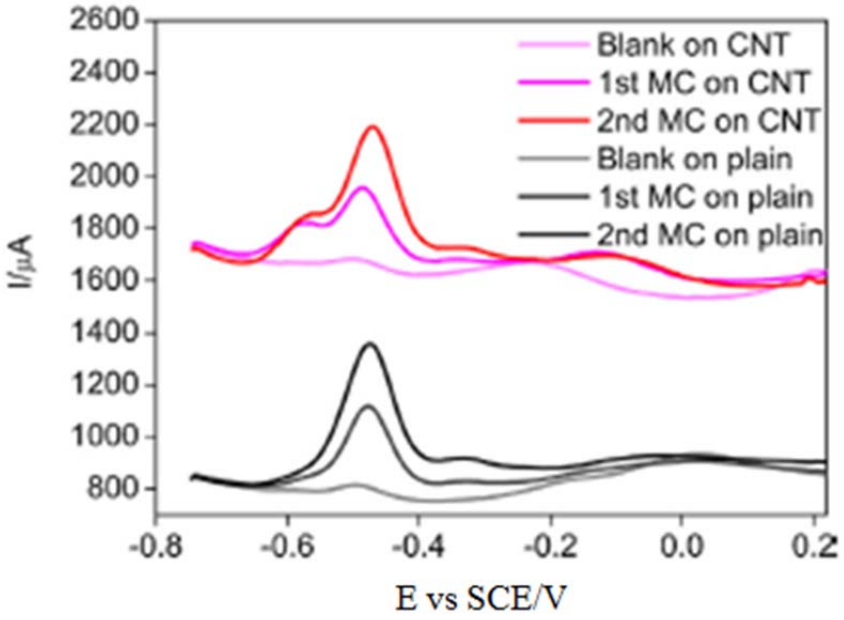


**Figure 4.7:** Differential pulse voltammetry of *S. loihica PV-4* biofilm on plain graphite and $CNT_8$-coated graphite electrode. MC=medium change

## 4.4 Conclusion

In order to maximize *S.loihica PV-4* external electron transfer, commercially available CNTs were deposited on graphite electrode by an electrophoretic deposition (EPD) process.

The EPD process resulted in the rapid formation of a uniform coating of defined thickness, which is ideal for growth of electroactive biofilm (EAB). The optimal thickness was defined as a compromise between the high electrode surface and mass transfer limitations.

*S. loihica PV-4* grown on $CNT_8$ graphite electrodes developed faster and showed a higher EET rate. Higher electron transfer rate at CNT-modified electrodes is likely due to the geometry of CNT layers, which facilitates both direct and mediated electron transfer. Indeed, molecules, such as the outer membrane proteins strongly prefer specific orientations inside CNTs, and these orientations are related to the CNT's helical structures (Mao *et al*., 2002).

Yet, CNT–graphite has better electro-kinetic properties than graphite to support thin biofilm-driven reduction reactions.

# CHAPTER 5

# CONCLUSION AND FUTURE WORK

## 5.1 Conclusion

The present study aimed to maximize electricity generation in the EAM *S. loihica PV-4* grown in potentiostat-controlled three electrodes electrochemical cells.

The parameters investigated included biological aspects, such as the growth conditions (different concentrations of lactate as carbon source and presence or absence of oxygen, with fumarate and iron citrate used as electron donor instead of the oxygen). Also investigated were system design parameters, such as electrode surfaces (graphite electrodes with different roughness) and chemistry (atmospheric air plasma treatment and carbon nanotubes coating).

Regarding the optimization of culture conditions, results suggest that the concentration of lactate has an important role in the electrochemical performances of bioelectrochemical systems (BESs) and the optimal lactate concentration was found to be 20 mM, giving higher current output (82% more than with 40 mM lactate were used) by a greater production of electron shuttles (riboflavin). Anaerobic growth in DM medium with iron citrate as electron acceptor prior inoculation into ECs gave 57% more current intensity driven mostly by electron shuttles than when fumarate was used during the anaerobic growth. There were not significant differences in term of current output between *S. loihica* grown under aerobic and anaerobic condition prior inoculation into ECs. Therefore, 20 mM of lactate where used as electron donor during the further electrochemical experiment as well as aerobic growth prior inoculation into the ECs.

Regarding the design parameters, the possibility of producing a *S. loihica PV-4* biofilm with a higher extracellular electron transfer rate was investigated via (i) polished graphite electrodes with different roughness of sandpaper and (ii) by treating different electrode materials such as graphite and carbon felt with atmospheric air plasma, as well as (iii) carbon nanotubes coating on graphite electrodes.

It had been hypothesized that electrodes with a higher surface area would result in greater current generation, due to the availability of more space for bacterial attachment, and so for electroactive biofilm formation.

Results showed that rougher surfaces gave higher current output (P240 < P400 < P600), as well as a shorter lag phase. Thus, the graphite electrode polished with sandpaper P240 was used for further studies.

Atmospheric air plasma pre-treatment of graphite polished with sandpaper P240 showed a longer lag phase, which increased from approximately 1 to 5 h and the current slope, roughly corresponding to cell attachment rate, increased by 45%. Yet, the current stabilized sooner for the plasma pre-treated electrode than for the untreated electrodes. In addition, flavins adsorbed more on the untreated graphite electrode, which showed higher hydrophilicity than the air plasma counterpart.

Therefore, experiments with washed inocula (removal of flavins from the medium) were performed to determine the effect of soluble flavin concentration on the current output at different electrodes.

Overall, the experiments with unwashed inoculum confirm that availability of microbially produced flavins in the supernatant is the main driver for current output. For washed inoculum, the current output was much lower than for unwashed inoculum, as most of the microbially produced flavins were removed before inoculation and direct electron transfer was predominant.

Another electrode material was used to the role of flavins in the EET.Carbon felt is a very porous material; thus, it preferably absorbs flavin more easily than graphite electrodes, and so should yield to a higher current output.

Results show that in both graphite and carbon felt electrodes and inoculum condition, air plasma pre-treatment made both surfaces more hydrophobic, resulting in lower flavin adsorption.

However, the highest current output corresponds to the washed inoculum on plasma pre-treated electrode, approximately 450% higher (243.7± 5.4 μA) than the untreated carbon felt electrode.
These results show that air plasma pre-treatment is a feasible option to increase current output in bio-electrochemical systems.

Concerning the carbon nanotubes coating, results show that the higher catalytic activity was given by depositing 8 layers of CNTs on graphite electrodes. When 10 or 12 layers were used, the peak current decreased and the peak separation Ep increased, suggesting slower mass transfer in thicker CNT films. When *S. loihica* was grown on graphite electrodes coated

with 8 layers of CNTs, a higher current density was produced with 88.7 ± 10 and 58.8 ± 5 $\mu A/cm^2$ on the coated and uncoated electrodes, respectively. Yet, nearly 1.5 times longer lag phase was visible on plain electrode when compared with the CNTs-coated one. In addition, higher biofilm coverage was found when the electrodes were coated with 8 layers of CNTs.

The work undertaken in this research project demonstrates that the performance of electroactive bacteria such as *S. loihica* can be enhanced by optimizing culture conditions and working electrode characteristics.

### 5.2 Future work

Considering that this project has shown that a large portion of EET goes through MET, it is important to determine how this balance changes when flavins are washed out by medium replacement, in both aerobic and anaerobic inocula.

To accomplish this goal, an electrochemical continuous flow cell already built in our laboratory could be used (**Appendix; Figure A3**). Fluorescence spectroscopy and high-performance liquid chromatography could be used to make a quantitative and qualitative analysis of the riboflavin present in the washed media.

Yet, direct quantification of *S. loihica PV-4* biofilm thickness and population formed on the electrode surface can be performed by confocal microscopy and/or biochemical assays (protein extraction and quantification) together with electrochemistry. This will better elucidate the ratio of DET that affects the current production output in *S. loihica PV-4.*

## APPENDIX

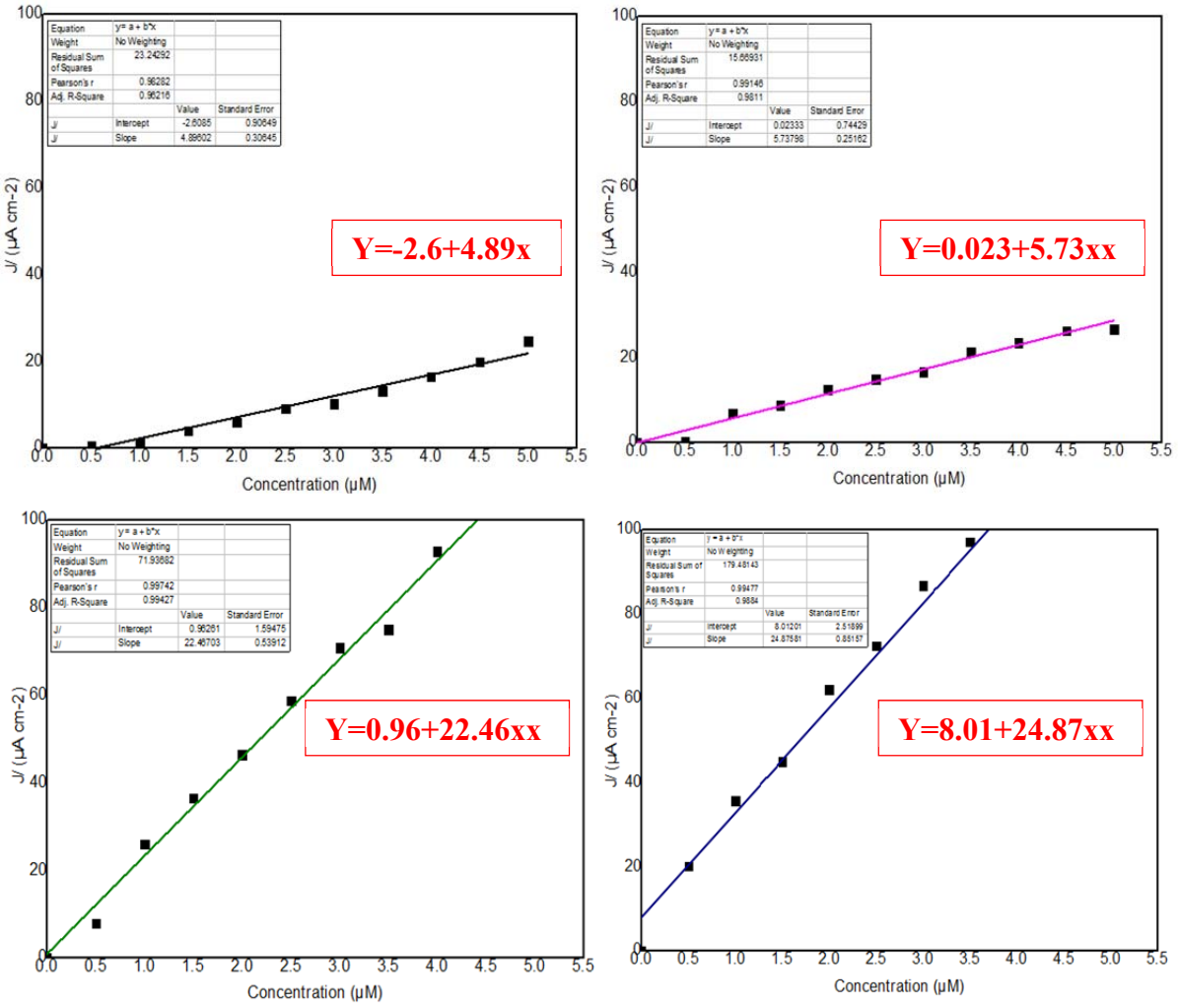


**Figure A1:** Calibration curve of DPVs of riboflavin peak (centered at -0.45 V) intensity vs. its concentration. Graphite electrode polished with sandpaper P240 either untreated (**Black line**) or treated by air plasma (**Purple line**), and carbon felt either untreated (**Green line**) or treated by air plasma (**Dark blue**).

**Table A1-** Mean and standard deviation of the riboflavin peak intensity versus its concentration, recorded from P240 either treated or not with air plasma (**A**), and CF either treated or not with air plasma (**B**).

**A**

| | P240 | | | | P240 plasma | | | |
|---|---|---|---|---|---|---|---|---|
| [RF]µM | $J_1$ (µAcm$^{-2}$) | $J_2$ (µAcm$^{-2}$) | Mean(µAcm$^{-2}$) | std (J) | $J_1$ (µAcm$^{-2}$) | $J_2$ (µAcm$^{-2}$) | Mean (µAcm$^{-2}$) | std (J) |
| **0** | 0 | 0 | 0 | 0 | 0 | 0 | 0 | 0 |
| **0.5** | 0.56 | 0.5 | 0.53 | 0.04 | 0.35 | 0.43 | 0.39 | 0.053 |
| **1** | 1.43 | 1.36 | 1.40 | 0.04 | 7.40 | 6.61 | 7.00 | 0.55 |
| **1.5** | 3.75 | 4.26 | 4.01 | 0.35 | 9.49 | 8.15 | 8.82 | 0.94 |
| **2** | 6.20 | 5.90 | 6.05 | 0.21 | 12.0 | 12.99 | 12.50 | 0.70 |
| **2.5** | 8.76 | 9.61 | 9.18 | 0.60 | 15.44 | 14.33 | 14.89 | 0.78 |
| **3** | 10.86 | 9.83 | 10.34 | 0.72 | 17.06 | 16.12 | 16.59 | 0.66 |
| **3.5** | 13.54 | 12.99 | 13.26 | 0.39 | 22.03 | 20.75 | 21.39 | 0.90 |
| **4** | 14.90 | 18.12 | 16.51 | 2.27 | 23.43 | 23.50 | 23.47 | 0.05 |
| **4.5** | 19.62 | 20.18 | 19.90 | 0.40 | 25.71 | 26.81 | 26.26 | 0.77 |
| **5** | 25 | 24.45 | 24.72 | 0.38 | 27.20 | 26.18 | 26.69 | 0.72 |

**B**

| | CF | | | | CF plasma | | | |
|---|---|---|---|---|---|---|---|---|
| | $J_1$ (µAcm$^{-2}$) | $J_2$ (µAcm$^{-2}$) | Mean(µAcm$^{-2}$) | std (J) | $J_1$ (µAcm$^{-2}$) | $J_2$ (µAcm$^{-2}$) | Mean (µAcm$^{-2}$) | std (J) |
| [RF]µM | | | | | | | | |
| **0** | 0 | 0 | 0 | 0 | 0 | 0 | 0 | 0 |
| **0.5** | 8.26 | 7.75 | 8.00 | 0.36 | 20.35 | 20.07 | 20.21 | 0.20 |
| **1** | 27.28 | 24.86 | 26.07 | 1.70 | 34.03 | 37.41 | 35.72 | 2.38 |
| **1.5** | 38.33 | 34.69 | 36.51 | 2.57 | 45.50 | 44.47 | 44.99 | 0.73 |
| **2** | 46.75 | 46.07 | 46.41 | 0.48 | 60.69 | 63.56 | 62.13 | 2.027 |
| **2.5** | 58.45 | 59.15 | 58.80 | 0.49 | 73.32 | 71.58 | 72.45 | 1.22 |
| **3** | 71.52 | 70.18 | 70.85 | 0.94 | 86.28 | 87.33 | 86.81 | 0.74 |
| **3.5** | 71.98 | 78.13 | 75.05 | 4.34 | 97.39 | 96.92 | 97.16 | 0.33 |
| **4** | 94.54 | 91.33 | 92.94 | 2.26 | 105.56 | 111.07 | 108.32 | 3.89 |
| **4.5** | 102.45 | 103.90 | 103.17 | 1.02 | 118.54 | 121.03 | 119.79 | 1.76 |
| **5** | 111.79 | 109.35 | 110.57 | 1.72 | 120.56 | 128.66 | 124.61 | 5.72 |

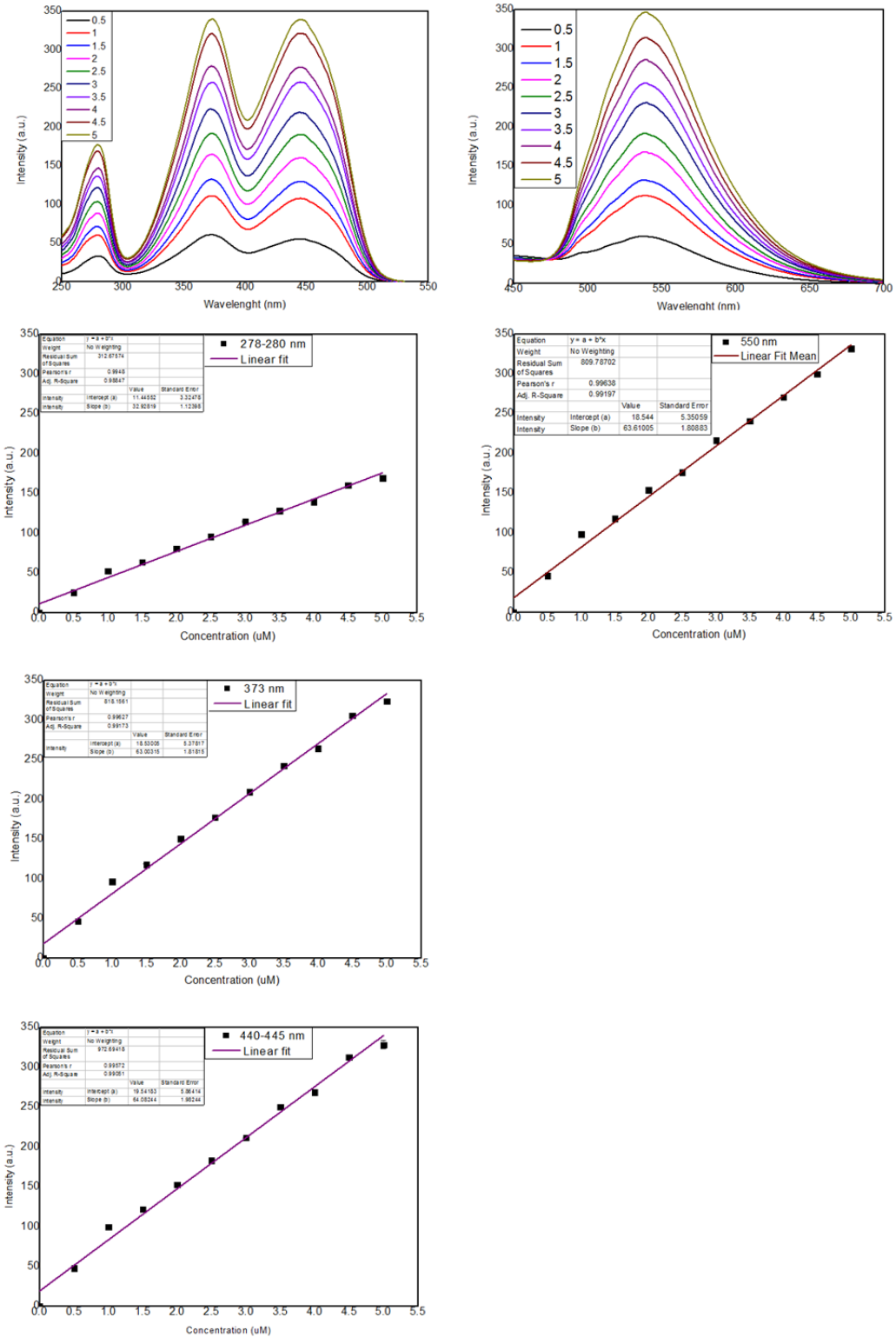


**Figure A2**: Emission (**A**) and excitation spectra (**B**) of commercial riboflavin. Intensity of riboflavin peaks centered at 278-280 nm, 373 nm and 440-445 nm as per the emission spectrum and 550 nm as per excitation spectrum vs its concentration (0.5-5 µM) with their respective linear fitting and equations.

**Table A2 – Composition of trace mineral solution used in the DM medium**

| Constituents | Concentration (g/L) |
|---|---|
| $FeCl_3.4H_2O$ | 0.2 |
| $MgCl.6H_2O$ | 0.1 |
| Sodium tungstate | 0.02 |
| $MnCl_2.4H_2O$ | 0.1 |
| $CoCl_2.4H_2O$ | 0.1 |
| $CaCl_2.4H_2O$ | 1 |
| $ZnCL_2$ | 0.05 |
| $CuCl_2.2H2O$ | 0.002 |
| $H_3BO_3$ | 0.005 |
| Sodium Molybdate | 0.01 |
| NaCl | 1 |
| $Na_2SeO_4$ | 0.017 |

**Table A3 – Composition of vitamins solution used in the DM medium**

| Composition | Concentration g/L |
|---|---|
| Biotin | 0.002 |
| Folic acid | 0.002 |
| Pyridoxine HCl | 0.01 |
| Thiamine | 0.005 |
| Nicotinic acid | 0.005 |
| Pantothenic acid | 0.005 |
| B-12 | 0.0001 |
| P-aminobenzoic acid | 0.005 |
| Thioctic acid | 0.005 |

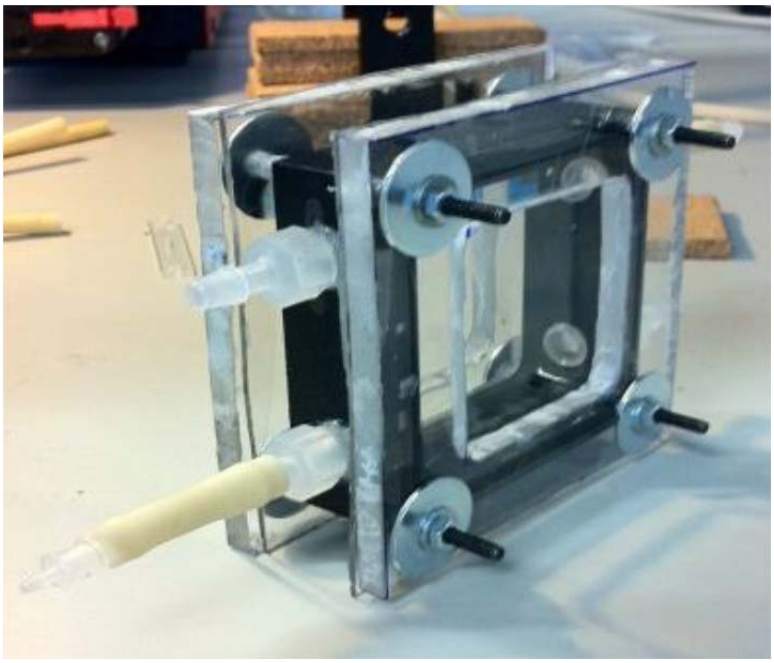

**Figure A3**: Electrochemical flow chamber

## REFERENCES

A. El Kasmi, J. M. Wallace, E. F. Bowden, S. M. Binet, R. J. Linderman, J. Am. Chem. Soc. 1998, 120, 225 – 226.

A. Jain, J. O'Connolly, R. Woolley, S. Krishnamurthy, E. Marsili, Extracellular electron transfer mechanism in Shewanella loihica PV-4 biofilms formed at indium tin oxide and graphite electrodes, Int. J. Electrochem. Sci. 8 (2013) 1778–1793.

A. Jain, X. Zhang, G. Pastorella, J.O. Connolly, N. Barry, R. Woolley, S. Krishnamurthy, E. Marsili, Electron transfer mechanism in Shewanella loihica PV-4 biofilms formed at graphite electrode, Bioelectrochemistry 87 (2012) 28

A. Miguel, N. Wagner, J. Rojas-chapana, C. Morsczeck, M. Thie, M. Giersig, Fabrication
A. Walcarius, S. D. Minteer, J. Wang, Y. Lin and A. Merkoci, J. Mater. Chem. B, 2013, 1, 4878–4908.

A.A. Carmona-Martinez, F. Harnisch, L.A. Fitzgerald, J.C. Biffinger, B.R. Ringeisen, U. Schröder, Cyclic voltammetric analysis of the electron transfer of Shewanella oneidensis MR-1 and nanofilament and cytochrome knock-out mutants, Bioelectrochemistry 81 (2011) 74.

Arkles, B. (2006). and Silanes. *Gelest Inc.*, (October), 10.

Beliaev, A. S., Saffarini, D. A., McLaughlin, J. L., & Hunnicutt, D. (2001). MtrC, an outer membrane decahaem c cytochrome required for metal reduction in Shewanella putrefaciens MR-1. *Molecular Microbiology*, *39*(3), 722–730. doi:10.1046/j.1365-2958.2001.02257.x

B. Erable, N. Duteanu, S.M.S. Kumar, Y. Feng, M.M. Ghangrekar, K. Scott, Nitric acid activation of graphite granules to increase the performance of the non-catalyzed oxygen reduction reaction (ORR) for MFC applications, Electrochemistry Communications 11 (2009) 1547.

B.E. Logan, Microbial Fuel Cells, Wiley & Sons, New York, 2008.

B.E. Logan, S. Cheng, V. Watson, G. Estadt, Graphite fiber brush anodes for increased power production in air-cathode microbial fuel cells, Environmental Science and Technology 41 (2007) 3341.

B.V. Wang, M. Yuan Li Tan, K. Sivakumar, B. Cao, Q. Zhang, G.C. Bazan, S.C.J. Loo, E. Marsili,Water-soluble conjugated oligoelectrolytes cannot establish direct extracellular electron transfer across bacterial membrane of Shewanella oneidensis, Electrochem. Commun. 41 (2014) 55–58

Block, J. C., Haudidier, K., Paquin, J. L., Miazga, J., & Levi, Y. (1993). Biofilm accumulation in drinking water distribution systems. *Biofouling*, *6*(4), 333–343. doi:10.1080/08927019309386235

Borole, A. P., Reguera, G., Ringeisen, B., Wang, Z.-W., Feng, Y., & Kim, B. H. (2011). Electroactive biofilms: Current status and future research needs. *Energy & Environmental Science*, *4*, 4813. doi:10.1039/c1ee02511b

Boukhalfa, H., Icopini, G. a, Reilly, S. D., Neu, P., & Neu, M. P. (2007). Plutonium ( IV ) Reduction by the Metal-Reducing Bacteria Geobacter metallireducens GS15 and Shewanella Plutonium ( IV ) Reduction by the Metal-Reducing Bacteria Geobacter metallireducens GS15 and Shewanella oneidensis MR1 , *73*(Iv), 5897–5903. doi:10.1128/AEM.00747-07

Breuer, M., Rosso, K. M., Blumberger, J., & Butt, J. N. (2015). Multi-haem cytochromes in Shewanella oneidensis MR-1 : structures , functions and opportunities, (Im).

Brown, A. P., & Anson, F. C. (1977). Cyclic and differential pulse voltammetric behavior of reactants confined to the electrode surface. *Analytical Chemistry*, *49*(11), 1589–1595. doi:10.1021/ac50019a033

Brutinel, E. D., & Gralnick, J. a. (2012). Shuttling happens: Soluble flavin mediators of extracellular electron transfer in Shewanella. *Applied Microbiology and Biotechnology*, *93*(1), 41–48. doi:10.1007/s00253-011-3653-0

C. Biffinger, R. Ray, B. J. Little, L. A. Fitzgerald, M. Ribbens, S. E. Finkel and B. R. Ringeisen, Biotechnol. Bioeng., 2009, 103, 524–531

D. Coursolle, D.B. Baron, D.R. Bond, J.A. Gralnick, The Mtr respiratory pathway is essential for reducing flavins and electrodes in Shewanella oneidensis, J. Bacteriol. 192 (2010) 467–474.

D.B. Baron, E. LaBelle, D. Coursolle, J.A. Gralnick, D.R. Bond, Electrochemical measurement of electron transfer kinetics by Shewanella oneidensis MR-1, J. Biol. Chem. 284 (2009) 28865–28873.

Derby, H. a, & Hammer, B. W. (1931). Bacteriology of butter. IV. bacteriological studies on surface taint butter. *Iowa Agric Exp Stn Res Bull*, (145), 387–416.

Dichristina, T. J., Moore, C. M., Carolyn, a, & Haller, C. a. (2002). Dissimilatory Fe ( III ) and Mn ( IV ) Reduction by Shewanella putrefaciens Requires ferE , a Homolog of the pulE ( gspE ) Type II Protein Secretion Gene Dissimilatory Fe ( III ) and Mn ( IV ) Reduction by Shewanella putrefaciens Requires ferE , a Homolog. *Journal of Bacteriology*, *184*(1), 142–151. doi:10.1128/JB.184.1.142

D.C. Meng, J. Ioannou, A.R. Boccaccini, Bioglass-based scaffolds with carbon nanotube coating for bone tissue engineering, Journal of Materials Science Materials in Medicine 20 (2009) 2139.

D.V. Bax, A. Kondyurin, A. Waterhouse, D.R. McKenzie, A.S Weiss, M.M.M. Bilek, Dianne K Newman and Roberto Kolter. A role for excreted quinones in extracellular electron transfer. Nature, 405(6782):94{97, 2000.

E. Marsili, D.B. Baron, I.D. Shikhare, D. Coursolle, J.A. Gralnick, D.R. Bond, Proc. Natl. Acad. Sci. USA, 105 (2008) 3968-3973

E. Marsili, J. Sun and D. R. Bond, Electroanalysis, 2010, 22, 865–874.

E. Marsili, J.B. Rollefson, D.B. Baron, R.M. Hozalski, D.R. Bond, Microbial biofilm voltammetry: direct electrochemical characterization of catalytic electrode-attached biofilms, Appl. Environ. Microbiol. 74 (2008) 7329–7337.

EIMekawy A, Hegab HM, Dominguez-Benetton X, Pant D: Internal resistance of microfluidic microbial fuel cell: Challenges and potential opportunities. Bioresour Technol 2013, 142:672–682.

Farahi, a., Lahrich, S., Achak, M., El Gaini, L., Bakasse, M., & El Mhammedi, M. a. (2014). Parameters affecting the determination of paraquat at silver rotating electrodes using differential pulse voltammetry. Analytical Chemistry Research, 1, 16–21. doi:10.1016/j.ancr.2014.05.001

Fredrickson, J. K., Romine, M. F., Beliaev, A. S., Auchtung, J. M., Driscoll, M. E., Gardner, T. S.,Tiedje, J. M. (2008). Towards environmental systems biology of Shewanella. *Nature Reviews Microbiology*, *6*(8), 592–603. doi:10.1038/nrmicro1947

Gorby, Y. a, Yanina, S., McLean, J. S., Rosso, K. M., Moyles, D., Dohnalkova, A., … Fredrickson, J. K. (2006). Electrically conductive bacterial nanowires produced by Shewanella oneidensis strain MR-1 and other microorganisms. Proceedings of the National Academy of Sciences of the United States of America, 103(30), 11358–11363. doi:10.1073/pnas.0604517103

G.J. Newton, S. Mori, R. Nakamura, K. Hashimoto, K. Watanabe, Appl. Environ. Microbiol., 75 (2009) 7674-7681.

H. Pham, N. Boon, M. Marzorati, W. Verstraete, Enhanced removal of 1,2- dichloroethane by anodophilic microbial consortia, Water Research 43 (2009) 2936.

H. Von Canstein, J. Ogawa, S. Shimizu, J.R. Lloyd, Secretion of flavins by Shewanella species and their role in extracellular electron transfer, Applied and Environment Microbiology 74 (2008) 615.

Heidelberg, J. F., Paulsen, I. T., Nelson, K. E., Gaidos, E. J., Nelson, W. C., Read, T. D., … Fraser, C. M. (2002). Genome sequence of the dissimilatory metal ion-reducing bacterium Shewanella oneidensis. *Nature Biotechnology*, *20*(November), 1118–1123. doi:10.1038/nbt749

I. Horcas, R. Fernandez, J.M. Gomez-Rodriguez, J. Colchero, J. Gomez-Herrero, A.M. Baro,WSXM: a software for scanning probemicroscopy and a tool for nanotechnology, Rev. Sci. Instrum. 78 (2007) 013705.

J. Biffinger, M. Ribbens, B. Ringeisen, J. Pietron, S. Finkel and K. Nealson, Biotechnol. Bioeng., 2009, 102, 436–444

J. C. Biffinger, J. Pietron, R. Ray, B. Little and B. R. Ringeisen, Biosens. Bioelectron., 2007, 22, 1672–1679.

J. C. Biffinger, R. Ray, B. J. Little, L. A. Fitzgerald, M. Ribbens, S. E. Finkel and B. R. Ringeisen, Biotechnol. Bioeng., 2009, 103, 524–531.

J. Gonzalez-Garcia, P. Bonete, E. Exposito, V. Montiel, A. Aldaz, R. Torregrosa-Macia, Characterization of a carbon felt electrode: structural and physical properties, J. Mater. Chem. 9 (1999) 419–426

J. O. Kamgang, M. Naitali, J.-M. Herry, M.-N. Bellon-Fontaine, J.-L. Brisset and R. Briandet Increase in the hydrophilicity and Lewis acid-base properties of solid surfaces achieved by Electric gliding discharge in humid air: Effects on bacterial adherence, Plasma Sci. Technol., 11(2009), 187–193.

J.N. Roy, H.R. Luckarift, C. Lau, A. Falase, K.E. Garcia, L.K. Ista, P. Chellamuthu, R.P. Ramasamy, V. Gadhamshetty, G. Wanger, Y.A. Gorby, K.H. Nealson, O. Bretschger, G.R. Johnson, P. Atanassov, A study of the flavin response by Shewanella cultures in carbon-limited environments, RSC Adv. 2 (2012) 10020–10027.

J.O. Kamgang, M. Naitali, J.M. Herry, M.N. Bellon-Fontaine, J.L. Brisset, R. Briandet, K. Jang, I.S. Chang, H. Moon, K.H. Kang, B.H. Kim, Nitrilotriacetic acid degradation under microbial fuel cell environment, Biotechnology and Bioengineering 95 (2006) 772.

Jiang, D.Q., Li, B.K., 2009. Novel electrode materials to enhance the bacterial adhesion and increase the power generation in microbial fuel cells (MFCs). Water Sci. Technol. 59, 557-563.

Juárez, O., & Barquera, B. (2012). Insights into the mechanism of electron transfer and sodium translocation of the Na+-pumping NADH:quinone oxidoreductase. *Biochimica et* Biophysica Acta - Bioenergetics, 1817(10), 1823–1832. doi:10.1016/j.bbabio.2012.03.017

K.H. Becker, U Kogelschatz, KH Schoenbach and RJ Barker Editors, Institute of Physics Series in Plasma Physics, IOP PublishingLtd (2005), Chapter 9, pp 597- 621.

K.H. Becker, U. Kogelschatz, K.H. Schoenbach, R.J. Barker (Eds.), Non-Equilibrium Air Plasmas at Atmospheric Pressure, Institute of Physics Series in Plasma Physics, IOP Publishing Ltd 2005, pp. 597–621 (Chapter 9).

Kim, H.J., Hyun, M.S., Chang, I.S., Kim, B.H., 1999. Journal of Microbiology and Biotechnology 9 (3), 365–367.

Landoulsi J., et al. (2008). Enzymatic Approach of Microbial Influenced Corrosion, a Review Based on Stainless Steel in Natural Seawater. *Environment Science Technologies, 42, 42*(7), 2233–2242,.

Leung, K. M., Wanger, G., El-Naggar, M. Y., Gorby, Y., Southam, G., Lau, W. M., & Yang, J. (2013). Shewanella oneidensis MR-1 bacterial nanowires exhibit p-type, tunable electronic behavior. *Nano Letters*, *13*(6), 2407–2411. doi:10.1021/nl400237p

L. Peng, S.J. You, J.Y. Wang, Carbon nanotubes as electrode modifier promoting direct electron transfer from Shewanella oneidensis, Biosensors and Bioelectronics 25 (2010) 1248

Lies, D. P., Hernandez, M. E., Kappler, A., Mielke, R. E., Gralnick, J. A., & Newman, D. K. (2005). Shewanella oneidensis MR-1 uses overlapping pathways for iron reduction at a distance and by direct contact under conditions relevant for biofilms. Applied and Environmental Microbiology, 71(8), 4414-4426

Logan, B. E., & Regan, J. M. (2006). Electricity-producing bacterial communities in microbial fuel cells. *Trends in Microbiology*, *14*(12), 512–518. doi:10.1016/j.tim.2006.10.003

Lovley, D. R., and E. J. P. Phillips. 1988. Novel mode of microbial energy metabolism: organic carbon oxidation coupled to dissimilatory reduction of iron or manganese. Appl. Environ. Microbiol. 54:1472-1480.

Lovley, D. (2000). Dissimilatory Fe ( III ) - and Mn ( IV ) -Reducing Prokaryotes Microorganisms, (Iii), 1–28.

Lovley, D. R. (2008). The microbe electric: conversion of organic matter to electricity. *Current Opinion in Biotechnology*, *19*(6), 564–71. doi:10.1016/j.copbio.2008.10.005

M. C. Gutierrez, Z. Y. Garcia-Carvajal, M. J. Hortiguela, L. Yuste, F. Rojo, M. L. Ferrer and F. del Monte, J. Mater. Chem., 2007, 17, 2992–2995. Jiang, D. Q.; Li, B. K. Water Sci. Technol. 2009, 59, 557.

M. Rosenbaum, U. Schröder, F. Scholz, Investigation of the electrocatalytic oxidation of formate and ethanol at platinum black under microbial fuel cellconditions, Journal of Solid State Electrochemistry 10 (2006) 872.

Mao, L., & Verwoerd, W. S. (2014). Theoretical exploration of optimal metabolic flux distributions for extracellular electron transfer by Shewanella oneidensis MR-1. *Biotechnology for Biofuels*, *7*(1), 118. doi:10.1186/s13068-014-0118-6

Myers, C. R., & Myers, J. M. (1992). Localization of Cytochromes to the Outer-Membrane of Anaerobically Grown Shewanella-Putrefaciens Mr-1. *Journal of Bacteriology*, *174*(11), 3429–3438. Retrieved from <Go to ISI>://WOS:A1992HX27800002

Myers, C. R., & Myers, J. M. (2003). Cell surface exposure of the outer membrane cytochromes of Shewanella oneidensis MR-1. *Letters in Applied Microbiology*, *37*(3), 254–258. doi:10.1046/j.1472-765X.2003.01389.x

Myers, C. R., & Myers, J. M. (2004). The outer membrane cytochromes of Shewanella oneidensis MR-1 are lipoproteins. *Letters in Applied Microbiology*, *39*(5), 466–470. doi:10.1111/j.1472-765X.2004.01611.x

Myers, C. R., & Nealson, K. H. (1988). Bacterial manganese reduction and growth with manganese oxide as the sole electron acceptor. *Science (New York, N.Y.)*, *240*(4857), 1319–1321. doi:10.1126/science.240.4857.1319

N.Y. Cui, N.M.D. Brown, Modification of the surface properties of a polypropylene (PP) film using an air dielectric barrier discharge plasma, Appl. Surf. Sci. 189 (2002) 31–38.

Newton, G. J., Mori, S., Nakamura, R., Hashimoto, K., & Watanabe, K. (2009). Analyses of current-generating mechanisms of Shewanella loihica PV-4 and Shewanella oneidensis MR-1 in microbial fuel cells. *Applied and Environmental Microbiology*, *75*(24), 7674–81. doi:10.1128/AEM.01142-09

O. Bretschger, A.C.M. Cheung, F. Mansfeld, K.H. Nealson, Electroanal., 22 (2010) 883- 894.

O.O. Van der Biest, L.J. Vandeperre, Electrophoretic deposition of materials, Annual Review of Materials Science 29 (1999) 327.

P. Lazic, B.N.J. Persson, Surface-roughness-induced electric-field enhancement and triboluminescence, Europhysics Letters 91 (2010) 46003.

Parot, S., Vandecandelaere, I., Cournet, A., Délia, M.-L., Vandamme, P., Bergé, M., … Bergel, A. (2011). Catalysis of the electrochemical reduction of oxygen by bacteria isolated from electro-active biofilms formed in seawater. *Bioresource Technology*, *102*(1), 304–11. doi:10.1016/j.biortech.2010.06.157

Parsek, M. R., & Singh, P. K. (2003). Bacterial biofilms: an emerging link to disease pathogenesis. *Annual Review of Microbiology*, *57*, 677–701. doi:10.1146/annurev.micro.57.030502.090720

Picioreanu C, Head IM, Katuri KP, van Loosdrecht MCM, Scott K (2007) A computational model for biofilm-based microbial fuel cells.

Pirbadian, S., Barchinger, S. E., Leung, K. M., Byun, H. S., Jangir, Y., Bouhenni, R. a., … El-Naggar, M. Y. (2014). Shewanella oneidensis MR-1 nanowires are outer membrane and periplasmic extensions of the extracellular electron transport components. *Proceedings of the National Academy of Sciences*, *111*(35), 1–6. doi:10.1073/pnas.1410551111

Polizzi, N. F., Skourtis, S. S., & Beratan, D. N. (2012). Physical constraints on charge transport through bacterial nanowires. *Faraday Discussions*, *155*, 43. doi:10.1039/c1fd00098e

R. Garjonyte, A. Malinauskas, L. Gorton, Investigation of electrochemical properties of FMN and FAD adsorbed on titanium electrode, Bioelectrochemistry 61 (2003) 39–49

R.J. Zaldivar, J. Nokes, G.L. Steckel, H.I. Kim, B.A. Morgan, The effect of atmospheric plasma treatment on the chemistry, morphology and resultant bonding behavior of a pan-based carbon fiber-reinforced epoxy composite, J. Compos. Mater. 44 (2010) 137–156

Reguera, G., Nevin, K. P., Nicoll, J. S., Covalla, S. F., Woodard, T. L., & Lovley, D. R. (2006). Biofilm and nanowire production leads to increased current in Geobacter sulfurreducens fuel cells. *Applied and Environmental Microbiology*, *72*(11), 7345–7348. doi:10.1128/AEM.01444-06

Richardson, D. J. (2000). Bacterial respiration: a flexible process for a changing environment. *Microbiology (Reading, England)*, *146*, 551–571. doi:so

Richter, K., Schicklberger, M., & Gescher, J. (2012). Dissimilatory reduction of extracellular electron acceptors in anaerobic respiration. *Applied and Environmental Microbiology*, *78*(4), 913–921. doi:10.1128/AEM.06803-11

Riding, R. (2000). Microbial carbonates: the geological record of calcified bacterial-algal mats and biofilms. *Sedimentology*, *47*, 179–214. doi:10.1046/j.1365-3091.2000.00003.x

Roden, E. E., & Zachara, J. M. (1996). Microbial Reduction of Crystalline Iron ( III ) Oxides : Influence of Oxide Surface Area and Potential for Cell Growth Microbial Reduction of Crystalline Iron ( III ) Oxides : Influence of Oxide Surface Area and Potential for Cell Growth, *30*(5), 1618–1628. doi:10.1021/es9506216

S. B. Bon, L. Valentini, J. M. Kenny, L. Peponi, R. Verdejo and M. A. Lopez-Manchado, Phys. Status Solidi A, 2010, 207, 2461.

S. Jung, Impedance analysis of Geobacter sulfurreducens PCA, Shewanella oneidensis MR-1, and their co-culture in bioelectrochemical systems, Int. J. Electrochem. Sci. 7 (2012) 11091–11100.

S. Nambiar, C. A. Togo and J. L. Limson Application of multi-walled carbon nanotubes to enhance anodic performance of an Enterobacter cloacae-based fuel cell y Vol. 8 (24), (2009) pp. 6927-6932

S. Srikanth, E. Marsili, M. C. Flickinger and D. R. Bond, Biotechnol. Bioeng., 2008, 99, 1065–1073

S.R. Higgins, D. Foerster, A. Cheung, C. Lau, O. Bretschger, S.D. Minteer, K. Nealson, P. Atanassov, M.J. Cooney, Fabrication of macroporous chitosan scaffolds doped with carbon nanotubes and their characterization in microbial fuel cell operation, Enzyme and Microbial Technology 48 (2011) 458

S.V. Liu, J. Zhou, C. Zhang, D.R. Cole, P. Gajdarziska-Josifovska, T.J. Phelps, Thermophilic Surface plasma modification and tropoelastin coating of a polyurethane co-polymer for enhancedcell attachment and reduced thrombogenicity, Biomaterials, 35 (2014) 6797–6809.

Satomi, M., Oikawa, H., & Yano, Y. (2003). Shewanella marinintestina sp. nov., Shewanella schlegeliana sp. nov. and Shewanella sairae sp. nov., novel eicosapentaenic-acid-producing marine bacteria isolated from sea-animal intestines. *International Journal of Systematic and Evolutionary Microbiology*, *53*(2), 491–499. doi:10.1099/ijs.0.02392-0

Schwalb, C., Chapman, S. K., & Reid, G. a. (2002). The membrane-bound tetrahaem c-type cytochrome CymA interacts directly with the soluble fumarate reductase in Shewanella. *Biochemical Society Transactions*, *30*, 658–662. doi:10.1042/BST0300658

Shi, L., Deng, S., Marshall, M. J., Wang, Z., Kennedy, D. W., Dohnalkova, A. C., … Fredrickson, J. K. (2008). Direct involvement of type II secretion system in extracellular translocation of Shewanella oneidensis outer membrane cytochromes MtrC and OmcA. *Journal of Bacteriology*, *190*(15), 5512–5516. doi:10.1128/JB.00514-08

Shi, L., Rosso, K. M., Clarke, T. A., Richardson, D. J., Zachara, J. M., & Fredrickson, J. K. (2012). Molecular Underpinnings of Fe(III) Oxide Reduction by Shewanella Oneidensis MR-1. *Frontiers in Microbiology*, *3*, 50. doi:10.3389/fmicb.2012.00050

T. K. Hong, D. W. Lee, H. J. Choi, H. S. Shin and B. S. Kim, ACS Nano, 2010, 4, 3861

Thess, A.; Lee, R.; Nikolaev, P.; Dai, H.; Petit, P.; Robert, J.; Xu, C.; Lee, Y.H.; Kim, S.G.; Rinzler, A.G.; et al. Crystalline ropes of metallic carbon nanotubes. Science 1996, 273, 483–487

Tian, M., Kanavillil, N., Davey, L., Leung, K. T., Schraft, H., & Chen, A. (2007). Direct growth of biofilms on an electrode surface and its application in electrochemical biosensoring. *Journal of Electroanalytical Chemistry*, *611*(1-2), 133–139. doi:10.1016/j.jelechem.2007.08.009

Tsai, H. Y.; Wu, C. C.; Lee, C. Y.; Shih, E. P. J. Power Sources 2009,194, 199

U. Cvelbar, S. Pejovnik, M. Mozetiè, A. Zalar, Increased surface roughness by oxygen plasma treatment of graphite/polymer composite Appl, Surf. Sci. 210 (2003) 255–261.

U. Schröder, Anodic electron transfer mechanisms in microbial fuel cells and their energy efficiency, Physical Chemistry Chemical Physics 9 (2007) 2619.

Velasquez-Orta, S. B., Head, I. M., Curtis, T. P., Scott, K., Lloyd, J. R., & Von Canstein, H. (2010). The effect of flavin electron shuttles in microbial fuel cells current production. *Applied Microbiology and Biotechnology*, *85*(5), 1373–1381. doi:10.1007/s00253-009-2172-8

Venkateswaran, K., Moser, D. P., Dollhopf, M. E., Lies, D. P., Saffarini, D. a, MacGregor, B. J., … Nealson, K. H. (1999). Polyphasic taxonomy of the genus Shewanella and description of Shewanella oneidensis sp. nov. *International Journal of Systematic Bacteriology*, *49 Pt 2*(1 999), 705–724. doi:10.1099/00207713-49-2-705

Water Res 41(13):2921–2940; Torres CI, Kato Marcus A, Rittmann BE (2007) Kinetics of consumption of fermentation products by anode-respiring bacteria. Appl Microbiol Biotechnol 77(3):689–697

X. Xie, M. Pasta, L. Hu, Y. Yang, J. McDonough, J. Cha, C.S. Criddle, Y. Cui, Nanostructured textiles as high-performance aqueous cathodes for microbial fuel cells, Energy & Environmental Science 4 (2011) 1293

Y. Fan, S. Xu, R. Schaller, J. Jiao, F. Chaplen, H. Liu, Nanoparticle decorated anodes for enhanced current generation in microbial electrochemical cells, Biosens. Bioelectron. 26 (2011) 1908–1912.

Y. Guo, S. Guo, Y. Fang, S. Dong, Gold nanoparticle/carbon nanotube hybrids as an enhanced material for sensitive amperometric determination of tryptophan, Electrochimica Acta 55 (2010) 3927.

Y. Qiao, C.M. Lia, S.J. Bao, Q.L. Bao, Carbon nanotube/polyaniline composite as anode material for microbial fuel cells, Journal of Power Sources 170 (2007) 79.

Y. Roh, H. Gao, H. Vali, D.W. Kennedy, Z.K. Yang, W. Gao, A.C. Dohnalkova, R.D. Stapleton, J.W. Moon, T.J. Phelps, J.K. Fredrickson, J. Zhou, Metal reduction and iron biomineralization by a psychrotolerant Fe(III)-reducing bacterium, Shewanella sp. strain PV-4, Appl. Environ. Microbiol. 72 (2006) 3236–3244.

Y.R. He, X. Xiao, W.W. Li, G.P. Sheng, F.F. Yan, H.Q. Yu, H. Yuan, L.J. Wu, Enhanced electricity production from microbial fuel cells with plasma-modified carbon paper anode, Phys. Chem. Chem. Phys. 14 (2012) 9966–9971.

Z. Ren, L.M. Steinburg, J.M. Regan, Electricity production and microbial biofilm characterization in cellulose-fed microbial fuel cells, Water Science and Technology 58 (2008) 617.